Post-translationally Modified Glucocorticoid Receptors and Protein Tyrosine Kinase 6 Modulate Triple Negative Breast Cancer Phenotypes

A Dissertation
SUBMITTED TO THE FACULTY OF
UNIVERSITY OF MINNESOTA
BY

Carlos Jesús Pérez Kerkvliet

Advisor: Carol A. Lange

July 2020

IN PARTIAL FULFILLMENT OF THE REQUIREMENTS
FOR THE DEGREE OF
DOCTOR OF PHILOSOPHY

Advisor: Dr. Carol A. Lange

Acknowledgements

I would like to acknowledge Dr. Carol A. Lange for the incredible professional and scientific mentorship during my time at the University of Minnesota.

I would also like to acknowledge the contributions of my thesis committee members: Dr. Deepali Sachdev, Dr. Douglas Yee, Dr. Kaylee Schwertfeger, and Dr. Scott Dehm.

The work presented here was funded by NIH/NCI R01 CA192178, the Tickle Family Endowed Chair for Breast Cancer Research to Carol A. Lange, an NIH/NCI institutional T32 CA009138 predoctoral fellowship to Carlos Perez Kerkvliet, an NIH/NIGMS institutional T32 GM008244 predoctoral fellowship to Carlos Perez Kerkvliet, and a NIH/NCI National Research Service Award F30 CA228261 to Carlos Perez Kerkvliet.

Dedication

This dissertation is dedicated to my wife, my family, and the beautiful archipelago of Puerto Rico. I am eternally grateful to my wife, Stephanie, for the many times that she has encouraged me to keep going. I am grateful to my family, especially my mom, who taught me that hard work is extremely important and that I should always keep trying. I am grateful to have been born in Puerto Rico because its people have taught and demonstrated the importance of resiliency in times of adversity. These three components of my life have been the pillars of my work and have, in many ways, supported me through my scientific endeavors.

Abstract

Triple negative breast cancer (TNBC) is the most metastatic and deadly breast cancer subtype, accounting for 20-30% of all breast cancer cases. There is a critical need to identify molecular targets that could be exploited as new biomarkers of TNBC prognosis and for improving therapies. Although TNBC lacks estrogen and progesterone receptors, 15-40% of TNBC patients express the glucocorticoid receptor (GR). Women with TNBC that express high levels of GR have poor outcomes. We hypothesize that GR is a key mediator of advanced cancer phenotypes in TNBC. Altered signaling pathways typify breast cancer and serve as direct inputs to steroid hormone receptor "sensors." We previously reported that phospho-Ser134-GR (pS134-GR) species are elevated in TNBC and cooperate with hypoxia-inducible factors, providing a novel avenue for activation of GR in response to local or cellular stress. Specifically, we propose that GR acts as a "sensor" for stress signaling pathways commonly activated by soluble factors that are abundant within the tumor microenvironment (TME) of TNBC.

Herein, we show that in the absence of GR ligands, GR is transcriptionally activated via p38-dependent phosphorylation of Ser134 as a mechanism of homeostatic stress-sensing and regulated upon exposure of TNBC cells to TME-derived agents. The ligand-independent pS134-GR transcriptome encompasses Transforming Growth Factor β1 (TGFβ1) and Mitogen Activated Protein Kinase (MAPK) signaling gene sets associated with TNBC cell survival and

migration/invasion. Accordingly, pS134-GR was essential for TNBC cell anchorage-independent growth in soft-agar, migration, invasion, and tumorsphere formation, an *in vitro* readout of cancer stemness properties. Both pS134-GR and expression of the MAPK-scaffolding molecule 14-3-3ζ were essential for a functionally intact p38 MAPK signaling pathway downstream of MAP3K5/ASK1, indicative of a feed-forward signaling loop wherein self-perpetuated GR phosphorylation enables cancer cell autonomy. A 24-gene pS134-GR-dependent signature induced by TGFβ1 predicts shortened overall survival in breast cancer patients.

Additionally, GR is known to induce the expression of PTK6, a soluble protein tyrosine kinase important in mediating signaling in response to cellular stress. PTK6 is overexpressed in 86% of breast cancer patients, regardless of subtypes. Although GR is known to modulate PTK6 expression in TNBC, PTK6-driven signaling events in the context of TNBC are largely undefined. We sought to delineate the functions of downstream of PTK6. To do this, we created kinase-dead (KM) and kinase-intact domain structure mutants of PTK6 via in frame deletions of the N-terminal SH3 or SH2 domains. While the PTK6 kinase domain contributed to soft-agar colony formation, PTK6 kinase activity was entirely dispensable for cell migration. Specifically, TNBC models expressing a PTK6 variant lacking the SH2 domain (SH2-del PTK6) were unresponsive to growth factor-stimulated cell motility relative to SH3-del, KM or wild-type PTK6 controls. Reverse phase protein array revealed that the SH2 domain of PTK6 mediates

TNBC cell motility via activation of the RhoA and/or AhR signaling pathways. Inhibition of RhoA and/or AhR blocked TNBC cell migration as well as the branching/invasive morphology of PTK6+/AhR+ primary breast tumor tissue organoids. The combination of AhR and Rho inhibitors enhanced paclitaxel cytotoxicity in TNBC cells, including a taxane-refractory TNBC model.

In conclusion, our results identified pS134-GR as a critical downstream effector of p38 MAPK signaling and TNBC migration/invasion, survival, and stemness properties. Our studies define a ligand-independent role for GR as a homeostatic “sensor” of intrinsic stimuli as well as extrinsic factors rich within the TME (TGFβ1) that enables potent activation of the p38 MAPK stress-sensing pathway and nominate pS134-GR as a therapeutic target in aggressive TNBC. Additionally, we identified that PTK6 (SH2-domain), a downstream gene of GR, is a potent effector of advanced cancer phenotypes in TNBC. We identified both RhoA and AhR as novel therapeutic targets in PTK6+ breast tumors since these two proteins are downstream effectors of PTK6 functions in TNBC.

Table of Contents

List of Tables

List of Figures

Chapter 1 Introduction

Breast Cancer: An overview and current state of the field

Breast cancer affects up to 12.5% of American women in their lifespan (1). It is the second leading cause of cancer-associated deaths in women in the United States (1). Many years of research have significantly improved outcomes for breast cancer patients (2). Namely, the discovery of how steroid hormone receptors contribute to pathogenesis and disease progression have provided insightful information about how to target and decrease progression of different breast cancer subtypes. Clinicians mainly rely on the subtyping of breast cancer by identification of receptors that are targetable with Federal Drug Administration (FDA) approved agents. As of right now, treatment is mainly dictated by using the following breast cancer subtyping: hormone receptor (HR) positive/Human Epidermal Growth Factor Receptor 2 (HER2) amplification negative, HR+/HER2+, HR-/HER2+ and HR-/HER2- (3, 4). The HR-/HER2- cohort is often known as Triple Negative Breast Cancer (TNBC).

Approaches to breast cancer treatment are multidisciplinary and require the integration of surgery and different modalities of oncological therapies (i.e. hormone action regulation, cytotoxic chemotherapy, immunotherapy, and others). Breast cancer patients that are classified as HR+/HER2- are treated with agents that target and diminish the actions of the steroid HR called estrogen receptor (ER). Most recently, patients that are ER+ may receive CDK4/6 inhibitors in addition to ER modulators. Patients that are classified as HER2+ are treated with agents that target the actions of the HER2 such as trastuzumab or pertuzumab

(5). In contrast, treatment of HR-/HER2- cases is mainly limited to cytotoxic chemotherapeutic agents (anthracyclines, alkylators and taxane-based chemotherapy) (6-8). Recent reports have provided some insight about the use of immunotherapy (pembrolizumab), polyadenosine diphosphate-ribose polymerase (PARP) inhibitors and topoisomerases inhibitors (Sacituzumab) in the HR-/HER2- subtype (9-11). Although this provides, in part, a “way to fill” the gap-in-knowledge of how to treat TNBC more adequately, we are still far from closing the gap between relatively good prognosis for HR+ patients when compared to those with HR- disease. Interestingly, the nomenclature we use to classify HR- breast cancer patients is somewhat erroneous because we nominate these cancer patients as HR- based solely on the measurement of expression of either ER or progesterone receptor (PR). Few research projects have addressed the possible actions of other steroid hormone receptors in TNBC. However, exploring the actions of other steroid hormone receptors have proven to be fruitful. For example, the androgen receptor (AR) has been show to be expressed in breast cancer. Interestingly, AR was found to indicate good prognosis in some ER+ patients and worst prognosis for ER- patients (reviewed in (12)).Further studies are needed to better understand the role of AR in ER+ and ER- breast cancer. Identifying the roles of these other receptors in TNBC could be of great importance since there are existing therapeutics that can abrogate the actions of steroid HRs such as the glucocorticoid receptor (GR) or mineralocorticoid receptor (MR).

Glucocorticoid receptor: general introduction

The GR is a well-studied member the steroid hormone receptor superfamily (13, 14). Similar to other steroid hormone receptors, the structure of the GR is composed of: N-terminal transactivation domain (NTD), DNA binding domain (DBD) and ligand binding domain (LBD) in the C-terminus. In the absence of cortisol or agonist ligand, the GR mostly resides in the cytoplasm of the cell. There is an activating-function (AF1) motif in the NTD region which is essential for the binding of cofactors and other components that are required for transcription and translocation of GR to the nucleus (reviewed in (15)). In the presence of its natural ligand, cortisol, GR translocates to the nucleus of the cell and interacts with DNA to regulate the transcription of numerous gene sets important for cellular homeostasis such as reduction of inflammation, immunomodulation, and execution of the circadian rhythm (reviewed in (15, 16)). GR utilizes glucocorticoid response elements (GRE) in the DNA containing two pseudo-palindromic repeats of six bases: AGAACAnnnTGTCCG (17). However, the mechanism by which GR modulates gene transcription is complex and does not only depend on interacting directly with DNA. Recently, it was described that GR utilizes three main mechanisms to regulate the expression of genes: **(1)** it can bind to GR binding sites that have little agonist dependency for accessibility to chromatin (ligand-independent), **(2)** GRs also bind to sites occupied by pioneering factors, such as BRG1, and with either the presence or absence of agonist can bind to DNA, and **(3)** agonist treatment induces an extensive

chromatin remodeling event that allow GRs to bind and regulate gene expression (15, 18, 19).

Although the GR depends on agonist ligand for many of its activities, there is growing evidence indicating that the GR functions beyond agonist activation. GR can also signal through non-genomic signaling. Notably, GR has been shown to interact with c-SRC and influence its tyrosine kinase activity in the cytoplasm (20). It is likely that this happens with other proteins that reside in the cytoplasm. Ultimately, a combination of both non-genomic and genomic actions of GR may occur in cancer tissues.

Glucocorticoid receptor expression in breast cancer

The GR is a ubiquitous HR that is overexpressed in many types of cancer (21). Notably, GRs are highly expressed in endocrine-related neoplasia such as prostate, ovarian, pancreas and breast cancer (21). Much work is needed to better define the role of GR in these cancer types. However, there is substantial evidence that implicates GR in breast cancer prognosis. Importantly, GR has a dichotomous role in breast cancer depending on its subtype. Recent studies have suggested that expression of GR has a positive impact (i.e. predicts good outcome) on prognosis in breast cancer patients whose tumors are ER-positive (22). We hypothesized that in this context, GR may compete with ER at the genomic level for the expression of genes that fuel ER-positive breast cancer progression.

In contrast, overexpression of GR has a negative impact on prognosis in ER-negative breast cancer patients (22). GR-driven actions in the context of ER-negative breast cancer are poorly understood. Several reports have established that GR is essential for chemotherapy resistance and growth of triple negative breast tumors in the presence of chemotherapeutic agents such as paclitaxel (taxane-based chemotherapeutic agent) (23). Recently, an activated-GR gene signature was identified in ER-negative breast cancer patients. Interestingly, this GR gene signature modulated the expression of genes that are essential for processes such as invasion of tumors, cell survival, cell transformation, epithelial-mesenchymal transition of breast cell lines and metastasis of tumor cell lines (24). Thus, GR activation may modulate cancer metastasis in addition to chemotherapy resistance. In fact, a recent report has demonstrated that GR activation with the artificial ligand Dexamethasone (Dex) can increase metastasis in mouse models (25). Interestingly, these models also showed increased expression of kinases that may be involved in breast cancer progression (25). Another report demonstrated that Epithelial Mesenchymal Transition (EMT) is regulated by GR via suppressing the actions of the insulin-receptor substrate-1 (IRS1) and by increasing the oncogenic activity of the ERK2 Mitogen Activated Protein Kinase (MAPK) (26). Thus, it is clear that some actions of the GR in ER-negative breast cancer are mediated via the actions of protein kinases.

Another important report in ER-negative breast cancer has revealed interactions of GR with other steroid hormone receptors such as the androgen receptor (AR) (27). Interestingly, many ER-negative breast cancers express either the AR or the GR. Co-expression of these receptors correlate with improved overall and disease free survival in patients. However, high expression of GR and low expression of AR correlate with decreased overall survival in ER-negative patients. It is possible that when AR is present, GR is not able to influence the expression of genes relevant for cancer progression (i.e. EMT, invasion, chemoresistance, etc) in ER-negative breast cancer patients (27). This would be a similar process to the limitation (i.e. by competition) of ER functions by co-expressed GR in ER-positive breast cancer (mentioned above).

Post-translational modifications to the glucocorticoid receptor

One aspect of GR action that has not been clearly defined is the influence of post-translational modifications to GR in ER-negative breast cancer. Our studies have shown that phosphorylation of GR on S134 is elevated in the breast tumors of TNBC patients relative to other subtypes of breast cancer. Thus, it is possible that GR actions in TNBC are dictated by the presence or absence of post-translational modifications to GR (23). Mechanisms of GR activation are important to define in the context of breast cancer, given that other steroid hormone receptors actions in breast cancer have been shown to be modulated by post-translational modifications such as phosphorylation (reviewed in (28)).

GR is susceptible to many types of post-translational modifications. Importantly, post-translational modifications can influence the genomic activity of GR. Mainly, GR is modified by phosphorylation, ubiquitylation, sumoylation, acetylation and nitrosylation (reviewed in (15)). A few examples of how these post-translational modifications alter GR activity will be given in the following section.

Ubiquitylation mainly influences protein turnover. When liganded GR is ubiquitylated on Lys419, it is exported from the nucleus and tagged for degradation via the proteasomal degradation system. This process induces an accelerated ligand-dependent turnover of the GR (29). Sumoylation modifications are mainly responsible for decreasing the transcriptional activity of GR (reviewed in (15)). For example, sumoylation of GR on Lys293 leads to transrepression of the GR activity by inducing recruitment of corepressors such as the Silencing Mediator for Retinoid or Thyroid hormone receptor (SMRT) or the Nuclear receptor Corepressor 1 (NCoR1) (30). The acetylation status of the GR has been shown to alter GR sensitivity to agonists such as Dex. Histone Deacetylase 2 (HDAC2) is responsible for deacetylating GR. This deacetylation process induces its interaction with Nuclear Factor Kappa Beta (NFkB) and subsequently regulates gene expression (31). Ligand insensitivity can be caused by GR nitrosylation as well. Specifically, nitrosylation of GR can cause the Zinc molecules in the two zinc finger domains to displace. Consequently, this inhibits ligand interaction with GR (reviewed in (15)).

The most studied post-translational modification on GR is phosphorylation. Phosphorylation of GR has been reported in at least seven residues (S113, S134, S141, S203, S211, S226, and S404) (Figure 1.1). All of these residues are in the NTD region of the GR which may suggest that recruitment of cofactors may be mediated via phosphorylation of these residues. These cofactors may be responsible of the transcriptome defined by GR in different cellular contexts. In 1997, Cidlowski et al. showed that the transcriptional activity of mouse GR largely depends on these phosphorylation sites. More importantly, that same report showed that these sites influence the half-life of the GR (32).

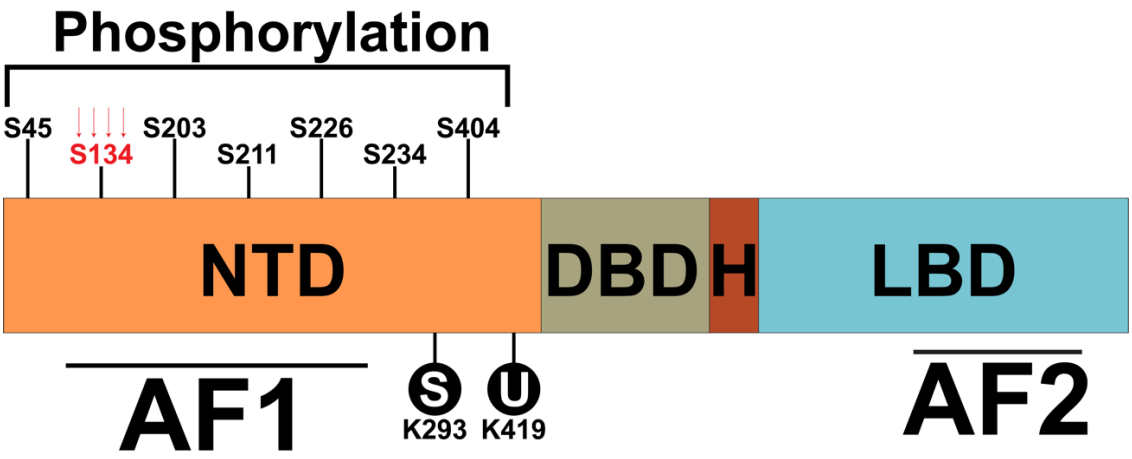

Figure 1.1 Glucocorticoid Receptor structure, domains and relevant post-translational modifications.

Cartoon image showing the different domains of the glucocorticoid receptor. To the left, we have the N-terminal domain and the associated AF-1 region. Depicted in this region are potential phosphorylation residues. Highlighted with arrows and in red is the residue S134 which is of seminal importance for the work presented in this dissertation because of the ability to be phosphorylated even in the absence of GR ligand. DNA binding domain is also depicted as DBD. The DBD has a double zinc-finger that assist with DNA interaction. The hinge region assists in conformational changes of the GR. Finally, the Ligand Binding Domain (LBD) is towards the C-terminal of the GR structure and as the name reflects it is important for ligand binding and possible transcriptional activation of GR. The post-translational modifications indicated alter many of the functions of the GR including its ability to interact with DNA or ligand. The “S” and the “U” stand for sumoylation and ubiquitination.

Diverse signaling inputs have been shown to be responsible for the phosphorylation of GR on multiple sites. Interestingly, most of these sites are not phosphorylated at low levels or in the absence of glucocorticoids. However, when glucocorticoids are present, these residues are highly phosphorylated (reviewed in (15)). An exception to this is the S134 residue. It was reported that phosphorylation on S134 occurs in the absence of GR agonists. More importantly, phosphorylation of GR on S134 is essential for its interaction with scaffolding proteins such as 14-3-3ζ (Figure 1.1) (33).

Interestingly, using a tissue microarray with 281 samples of primary breast cancer, it was identified that phosphorylated S134-GR (pS134-GR) is elevated in TNBC patients when compared to non-TNBC patients. More importantly, chemotherapy and other forms of cellular stress (hypoxia, radical oxygen species, nutrient deprivation) promote phosphorylation of GR on S134 in breast cancer tissue and cell lines (23).

Thus, it is critical to dissect the specific functions of pS134-GR in TNBC. It is possible that cellular stress mediators (i.e. chemotherapy, radical oxygen species – ROS) induce post-translational modifications on GR. More importantly, therapies that are often provided to patients to decrease tumor burden in TNBC, such as paclitaxel and other cytotoxic chemotherapeutic agents, may be able to increase GR phosphorylation. In fact, it is known that paclitaxel and 5-florouracil induce phosphorylation of GR on S134. Another form of cellular stress that

promotes pS134-GR is ultra-low attachment treatment (23). These findings point to the possibility that GR is phosphorylated on S134 in response to a diverse array of inducible inputs that are involved in cellular responses to stress and relevant to cancer processes such as EMT, formation of stem cells, metabolism and ultimately metastasis.

Finally, phosphorylation of GR enhances recruitment of co-factors and ultimately modulates the transcription of genes. Importantly, two co-factors are known to interact with GR when phosphorylated on S134. The first co-factor that was identified to bind pS134-GR was 14-3-3ζ. The 14-3-3 family of proteins mainly act as molecular chaperones and are known to bind numerous proteins that modulate cellular signaling (33). Often, these proteins are essential for survival and importantly they are known to modulate the action of MAPKs. Notably, 14-3-3 proteins have been implicated in breast cancer progression. Specifically, studies nominate 14-3-3ζ as an important promoter of early stage progression of breast cancer. 14-3-3ζ has been found to modulate and promote anchorage independent growth and halts apoptosis in human breast cancer (34). Additionally, 14-3-3ζ is an important mediator of Transforming Growth Factor β1(TGFβ1) signaling in breast cancer. It has been shown that TGFβ1 in cooperation with 14-3-3ζ stabilized GLi2, and in turn promoted the action of SMAD partners via direct binding to drive metastasis from breast tissue to bone in response to TGFβ (35).

Target genes of the glucocorticoid receptor

Several genes have been identified as influential and key for actions of GR in TNBC. Many of these genes are important for cancer processes associated to chemotherapeutic resistance. SGK-1 and MKP-1 have been identified as Dex-responsive genes that are important in resistance to chemotherapy. Ectopic expression of either SGK-1 or MKP-1 enables resistance to paclitaxel (taxane-based chemotherapy) or doxorubicin in different breast cancer cell lines. Specifically, both SGK-1 and MKP-1 are important for inhibiting apoptosis when cancer cells are exposed to chemotherapeutic agents (36). Notably, both of these proteins are tightly involved with the MAPK family of proteins. SGK-1 is a serine/threonine kinase that is a downstream target of the PI3K pathway. The PI3K pathway has been shown to modulate the action of MAPKs modules (reviewed in (37)). Additionally, recent data indicate that GRs mediate metastasis via the expression of ROR1. ROR1 is a transmembrane protein tyrosine kinase that modulates cellular growth, especially in the central nervous system. However, in the context of breast cancer, it was found that GR is activated with Dex ligand and in turn GR increases the expression of ROR1 in TNBC *in vivo*. Interestingly, it was also found that ROR1 correlated with decreased survival when amplified (25).

Evidently, the work that has been done in elucidating the role of GR in TNBC has led to the discovery of many kinases that may be involved in breast cancer progression. Importantly, many of these kinases have been highlighted as

essential proteins to respond to cellular stress. Another kinase that has been implicated in GR signaling of TNBC is the Protein Tyrosine Kinase 6 (PTK6). PTK6 is an intracellular soluble tyrosine kinase that promotes phosphorylation of signaling molecules as well as factors involved in both transcription and RNA splicing. PTK6 has both cytoplasmic and nuclear actions and its structure is closely related to the c-Src kinase family (38). Interestingly, PTK6 is key for mediating chemotherapeutic resistance in TNBC. Recently, it was demonstrated that when paclitaxel or 5-FU promotes phosphorylation of GR on S134, GR is able to induce the expression of PTK6 (23).

Another way that GR induces PTK6 expression is via direct or indirect interaction with the Hypoxia Inducible Factor 1 (HIF1), Hypoxia Inducible Factor 2 (HIF2) and Aryl Hydrocarbon Receptor (AhR) (23, 39). Specifically, when cell lines are treated with either hypoxia or Dex, GR and HIFs protein interactions ensue and cooperate to induce the transcription of PTK6 (39). On the other hand, GR preferentially interacts with AhR to promote its activity in TNBC when phosphorylated on S134, specifically when treated with chemotherapeutic agents (i.e. paclitaxel) (23). Surprisingly, although it is known that PTK6 is a kinase and has a significant role in breast cancer progression, very little research has been done to dissect the specific role of PTK6 protein domains in TNBC.

PTK6 expression in breast cancer and its structure

PTK6 is expressed in normal breast tissue but in relatively low levels (40). However, moderate to high expression in breast cancer tissue has been shown relative to normal tissue. It has been reported that up to 86% of all breast cancer tumors overexpress PTK6 (41). Notably, PTK6 is localized in close proximity to the plasma membrane in mammary cancer cells when compared to normal human mammary models. It is important to note, that in some cases PTK6 is present in the nucleus as well (42). Thus, it is possible that PTK6 influences the activity of different transcription factors or GR itself in the context of TNBC. Further research is needed to better understand this. Finally, PTK6 expression correlated with higher histological grade (41). Because of this, it is important to dissect the specific role and the signaling context of PTK6 in TNBC.

As stated above, PTK6 is closely related to SRC family kinases. Similar to c-SRC, it contains a Src homology (SH) domain 2, an SH3 domain and a kinase domain. However, contrary to c-SRC, PTK6 is not myristolated or palmitolated to anchor it in the plasma membrane region of cells (Figure 1.2) (38). In addition, PTK6 diverges in the SH2 domain. Contrary to c-SRC, which can assume an inhibited or “closed” structure via internal SH2/p-Tyr interactions, the SH2 domain of PTK6 does not have high affinity for the autoinhibition tyrosine of PTK6 itself (Y447) (43). Another important protein residue for PTK6 activity is found in the kinase domain, Y342. This residue promotes kinase activation via conformational changes that depend on autophosphorylation of Y342 (44). In addition, although PTK6 is a kinase, its kinase domain is dispensable for many of its actions in

Figure 1.2 PTK6 protein domain organization.

In the N-terminal region, there is a Src homology 3 (SH3) domain that is known to mediate the interactions of PTK6 with proline-rich proteins. The SH2 domain may bind Y447 and can cause auto-inhibition. Auto-phosphorylation of Y342 located in the kinase domain can cause a conformational change that could lead to activation of the kinase domain.

cancer progression. Somatic mutations to the *PTK6* gene have been reported in renal cell carcinoma and gastric cancers. These mutations are not limited to the kinase domain but include the SH2 and SH3 domains as well. These mutations have been reported to have profound effects in substrate recognition and enzymatic activity (45). Similar reports have been found in colorectal cancer (46).

In support of the conclusion that the kinase domain of PTK6 is dispensable, breast cancer cells expressing kinase-dead PTK6 were still equally able to migrate when compared to cells expressing the wild-type version of PTK6. These data suggest that PTK6 largely depends on its scaffolding actions (i.e. SH2 and SH3) for enhancing progression in breast cancer. In addition to migration, PTK6 was found to be essential in mediating survival of cells and promoting anchorage-independent growth in non-cancerous mammary cells (47, 48). Taken together, these data clearly suggest that PKT6 depends on its SH2 and SH3 domains for its oncogenic activity in breast cancer.

PTK6 signaling and biology in breast cancer

PTK6 is an important mediator of many signaling pathways. It is upstream of proteins such as Rac1, CrkII and paxillin and its kinase domain is essential for its effects in these proteins (49). Similarly, PTK6 activates the stress-related p38 MAPK. In fact, there is a strong relationship between cellular stress and PTK6 expression. Different inputs to the tumor (intrinsic or extrinsic) may increase cellular stress signaling and subsequently induce the transcriptional activity of

HIFs and GR, which are both highly dependent on cellular stress, with the final product of inducing expression of PTK6 (39, 40).

PTK6 is known to be activated by epidermal-growth factor (EGF), hepatocyte growth factor (HGF), and Heregulin. In turn, activation of PTK6 increases ERK5 and p38 MAPK activity in breast cancer. Ultimately, the increase in activity of this signaling axis causes an increase in the expression of cyclin D1 and these events lead to breast cancer cell survival in both non-TNBC and TNBC cell lines (41). Importantly, Castro and Lange reported in 2012, that HGF induces activation of PTK6 and ERK5 via the Met receptor (HGF receptor) in both TNBC cellular models (MDA-MB-231) and non-TNBC cellular models (T47D). This activation event is essential for cellular migration (50). Similarly, p38 MAPK is a key regulator of the expression of cyclin D1. Specifically, inhibition of breast cancer cells with SB203580, halts the induction of cyclin D1 by more than half. Additionally, when activated by Heregulin, migration is inhibited if PTK6 expression is diminished via siRNAs. In a similar fashion, Heregulin-mediated migration is highly dependent on p38 MAPK activation (as measured via phosphorylation of active site residues) (41).

PTK6 is also relevant in the context of HER2+ breast cancer. Recent discoveries have shown that when crossing PTK6-/- mice with mice expressing an activated version of ERBB2, ERBB2-driven tumor formation was halted (51). The mechanism of this is based in the PTK6-dependent activation of the Signal

Transducer and Activator of Transcription 3 (STAT3). In fact, proliferation of pre-tumorigenic tissue was dependent on PTK6 in these mouse models (51). Taken together, it is clear that PTK6 is essential for both survival and migration of different breast cancer subtypes. More importantly, this leads to the hypothesis that PTK6 assists in the metastatic cascade by promoting both of migration and survival of cancer cells.

Recent studies have demonstrated that PTK6 expression is in part dependent on AhR (23). The AhR is a ligand activated transcription factor that is part of the basic Helix-Loop-Helix/Per-ARNT-Sim (bHLH/PAS) subfamily of transcription factors (52). The ligands for the AhR can be various but most of them fall under the category of Polycyclic Aromatic Hydrocarbons (PAH). Once liganded, the AhR will dimerize and act as a transcription factor. Interestingly, AhR has been shown to be relevant in embryogenesis and early proliferation of cells (53, 54). Both of these processes overlap with hallmarks of cancer (55). More importantly, this receptor has been found to be essential for the development of the mammary gland (56, 57). The AhR has recently been established as a novel mediator of cancer cell survival. Recent studies demonstrated that AhR binds directly to the GR in response to chemotherapeutic treatment (paclitaxel) and this interaction is likely needed for the transcriptional functions that AhR exerts in target genes such as CYP1B1 and CYP1A (23).

Similarly, to HIFs, GR, PTK6 and p38 MAPK, AhR is tightly involved in cellular stress. For example, AhR is known to generate ROS because it

modulates the expression of monooxygenases and xanthine oxidase/xanthine dehydrogenase. In turn, this action decreases the activity of glutathione peroxidases, which subsequently increases the availability of hydrogen peroxide (H_2O_2) (58). In normal physiology, this would help to induce inflammation in the case of local injury or presumed infection. In the context of cancer signaling, H_2O_2 can increase the activity of kinases that are key for cellular stress such as p38 MAPK. In fact, ROS increases invasion and migration through p38 MAPK in breast cancer (59).

Inhibition of GR or PTK6 and its potential actions in halting disease progression

Pharmacological targeting of PTK6 and GR (and other key players of their actions) may be of importance in TNBC. GR inhibition with mifepristone (RU486) in the context of TNBC is already being tested in clinical trials. A phase I clinical trial had nine women that were treated with mifepristone. All of these women had either metastatic or locally advanced breast cancer. In this cohort both HR+ and HR- breast cancer patients were included. HR+ criteria established that the patients must have progressed even if treated with hormonal therapy. Some tumors showed response in this phase I clinical trial. There were two patients with a complete response, three patients with partial response, one patient with stable disease and three with progression of disease. Although these are preliminary results, Conzen and colleagues discuss encouraging findings in that the response for the TNBC patients were all either complete or partial responses.

No progression of disease was found in TNBC patients. Also, patients that had either complete or partial responses were strongly GR-positive when evaluated for the presence of GR using immunohistochemistry. Neutropenia was the most significant side effect (60). Other encouraging results that support the use of mifepristone in the clinic, is that mifepristone was found to decrease migration and invasion of cancer cells. The latter is not limited to breast cancer cell lines but also includes prostate cancer cell lines (61).

On the contrary, PTK6 (downstream of GR) inhibition has been more challenging. Many studies have tried to identify if inhibition of the kinase domain is effective against cancer progression. Small molecule inhibitors of the PTK6 kinase domain decreased tumor cell growth without inhibiting PTK6 kinase activity. Thus, these small molecule inhibitors of PTK6 decreased tumor cell growth independently of their activity in the kinase domain of PTK6 (62). To our knowledge, no inhibitors of PTK6 have been utilized in clinical trials yet.

Stress in the context of cellular cancer signaling

Physiological stress and the circadian rhythm regulate the GR via the hypothalamus-pituitary-adrenal axis. Cortisol is synthesized in response to both stress and the circadian rhythm. The Adrenocorticotropic Hormone (ACTH) is synthesized in the anterior pituitary and travels via bloodstream to the adrenal glands where cortisol is produced (adrenal cortex). Response to cortisol is tissue-specific and it is possibly determined by cofactors and post-translational

modifications that alter GR activity (as explained above). Aberrant changes to this tightly regulated homeostatic machinery can induce pathogenesis. Cancer cell signaling parallels with cellular stress signaling for many of the pathways that are important in cancer progression. Glucocorticoid receptor mediates in part the regulation of how cells and the body respond to stress. Thus, it could act as a sensor and linker between physiologic stress and cellular stress. In the context of cancer, this could have impactful implications. Cellular stress is regulated by many factors that contribute to cancer progression such as solid tumor core necrosis, angiogenesis, oxygen tension, metabolism and the presence of multiple cytokines that contribute to activation of cellular stress pathways (63). Interestingly, p38 MAPK and JNK MAPK are activated in many cancer subtypes including breast cancer (59, 64, 65). These two kinases are often termed stress-activated protein kinases (SAPKs). They are also important in immunological process and can respond to many cytokines that are available in the tumor milieu (reviewed in (66)). Additionally, they have been shown to modulate the activity of the GR (33, 67). Ultimately, cellular stress sensing could be activating GR transcriptional activity and/or modulating GR promoter selection, thus increasing the expression of PTK6 which is also associated to cellular response to stress.

One way that external stimuli could promote rapid GR responses is possibly via post-translational modifications. To date, very little is known about how post-translational modifications affect GR functions in the context of cellular stress or altered signaling in the context of cancer. Improved understanding of

how cellular stress modulates GR could have potential implications in the way we treat breast cancer. Dex is widely used to alleviate gastrointestinal-related symptoms that patients under cytotoxic chemotherapeutic regimen (another form of cellular stress) suffer from (68). Activation of GR via Dex may inadvertently contribute to disease progression in a subset of TNBC patients (and possibly other solid neoplasia). There is an urgent need to investigate how different signaling inputs impact GR activity in TNBC so that better treatments may be developed and deployed.

Chapter 2 Materials and Methods

Cell lines and culture conditions

Parental (unmodified) MDA-MB-231 cells are a gift from Dr. Ronald Wegener and were maintained in 10% FBS and 1% P/S. Cells that were used for generation of CRISPR/Cas cell line were authenticated on April 27, 2017 by the University of Arizona Genetics Core and were compared to the ATCC short-tandem repeat (STR) database. Additionally, cells tested negative for Mycoplasma. U2OS cell lines were obtained from Dr. John Cidlowski. These cells were maintained in 10% FBS, 1% P/S, 1% glutamax, .2mg/mL Hygromycin, and 200µg G418. The TNBC cell lines: Hs578T, MDA-MB-468 and HCI-10 cells were maintained in 10% FBS and 1% P/S.

MDA-MB-231 PTK6 clone 27 knockout (KO) cells were generated as described previously and were cultured in DMEM (HyClone Thermo Fisher Scientific (Waltham, MA USA) supplemented with 10% FBS (Gibco, Invitrogen (Carlsbad, CA USA)), 1% penicillin/streptomycin and 4 µg/mL puromycin (Fisher Scientific (Hampton, NH USA)) (23). The PTK6 KO admixture was generated by co-transfecting MDA-MB-231 cells with a gRNA to PTK6 (#CM-003166-01-0002) or to a non-targeting control (NTC; # U-007503-01-05), a Cas9-expressing plasmid (#U-005300) and transfection reagent (DharmaFECT Duo) using the manufacturer's recommendations (Dharmacon Inc. (Lafayette, CO USA)). Seventy-two h post-transfection, cells were selected with 1 µg/mL of puromycin and then maintained with 0.3 µg/mL of puromycin. To generate the clone admixture, 3 individual PTK6 KO clones with the highest deletion frequency of

PTK6 were admixed 1:1:1 with each other and expanded for fewer than 4 passages before use *in vitro* or *in vivo*. cHCI-10 Luc2+ cells (abbreviated cHCI-10) were cultured in modified M87 media as described in (69): DMEM/F12, 2% FBS, 1% antibiotic/antimycotic (Sigma), 1x insulin-transferrin-selenium (ITS, Corning (Corning, NY USA)), 5 ng/mL EGF (Life Technologies), 0.3 µg/mL hydrocortisone (Sigma), 0.5 ng/mL cholera toxin (Sigma), 5 nM 3,3',5-Triiodo-L-thyronine (T3, Sigma), 0.5 µM (±)-Isoproterenol hydrochloride (Sigma), 50 nM ethanolamine (Sigma), and 50 nM *O*-phosphorylethanolamine (Sigma). Hs578T cells were maintained in DMEM with 10% FBS and 1% penicillin/streptomycin. Cells were authenticated by short-tandem repeat (STR) profiling in December 2015 (ATCC) and in 2017 (Arizona Genetics Core), or by comparing gene expression profiles of the cHCI-10 primary cell line to the original HCI-10 PDX tumor material at the Huntsman Cancer Institute (HCI).

In the case of the generation of the stable cell lines for PTK6 domain mutants, re-expression of different mutants of PTK6 was done by transfecting MDA-MB-231 PTK6-KO (clone 27) cells with pFB-neo vector containing FLAG-tagged wild-type (WT) PTK6, truncated PTK6 missing N-terminal domain (SH3-del PTK6), PTK6 with SH2-domain deleted (SH2-del PTK6, kinase-inactive (KM-PTK6) or constitutively active PTK6 containing point mutation at Tyr447 (YF-PTK6) using FuGENE HD (Roche Applied Sciences (Basel, Switzerland)). Stable pool populations were selected in and maintained as described above with 0.2 mg/mL G418 sulfate (Thermo Fisher Scientific). HIF-1/HIF-2 double knockout (DKO) cells

created by CRISPR/Cas9n-mediated deletion were created and propagated as described in Regan Anderson et al. 2018 (23).To generate wild type PTK6 over-expressing cells, MDA-MB-231 parent cells or HIF DKO cells were transduced with lentiviruses expressing either empty vector (pFB-neo) or pFB-PTK6; cells were then selected with 2 mg/mL of G418 and maintained with 1 mg/mL G418. All cell lines tested negative for mycoplasma before use in experiments.

Materials and Reagents

Name	**Source or reference**	**Distributors and versions used**
DESeq2	PMID:25516281	v. 1.22.2
Pheatmap	https://cran.r-project.org/web/packages/pheatmap/index.html	v 1.0.12
FastQC	https://www.bioinformatics.babraham.ac.uk/projects/fastqc/	v 0.11.7
HISAT2	PMID:25751142	v 2.1.0
Subread	https://bioconductor.org/packages/release/bioc/html/Rsubread.html	
fgsea	https://bioconductor.org/packages/release/bioc/html/fgsea.html	v 1.8.0
R Studio	https://www.rstudio.com	v 3.5.2
R	https://cran.r-project.org	v3.5
Adobe Illustrator	Adobe	v23.0.5
PRISM	GraphPad	v7/v8
pGR	Custom made - Pierce Biotechnology PMID: 26825173	Custom made - Pierce Biotechnology

		PMID: 26825173
GR	Cell Signaling Technology, Danvers, MA Sigma Aldrich	4511p sc-1003
p-p38	Cell Signaling Technology, Danvers, MA	9211S
p38	Cell Signaling Technology, Danvers, MA	9212S
YWHAZ (14-3-3ζ)	Millipore, St. Louis, MO	AB9746
ASK1 (MAP3K5)	Santa Cruz	sc5294
pERK1/2	Cell Signaling Technology, Danvers, MA	9101S
ERK1/2	Cell Signaling Technology, Danvers, MA	9102S
pJNK	Cell Signaling Technology, Danvers, MA	9251S
JNK	Cell Signaling Technology, Danvers, MA	9252S
FLAG	Sigma Aldrich	F1804
PTK6 D-6	Santa Cruz	sc166243
GAPDH	Santa Cruz	sc0411
RhoA	Cytoskeleton Inc	ARH04
AhR	Cell Signaling Technology, Danvers, MA	83200
goat anti-rabbit IgG-HRP	BioRad	
goat anti-mouse IgG-HRP	BioRad	
SB203580	Calbiochem	559389
LY294002	Millipore Sigma	440202
UO126	Millipore Sigma	662009
SB202190	Cell Signaling Technology, Danvers, MA	8158S
Selonsertib	Thermo Fisher, Waltham, MA	501365910
Puromycin	VWR International	AC22742-0100
G418	Corning, Corning NY	61-234-RG
Glutamax	Fisher Scientific, Waltham, MA	35050061
Hygromycin B	Thermo Fisher, Waltham, MA	10687010
mini tablet protease inhibitors	Roche	11836153001
PhosStop	Roche	4906837001
Agarose	Invitrogen	16500500
Dexamethasone	Sigma Aldrich, St. Louis, MO	D4902
MTT	Sigma Aldrich, St. Louis, MO	M2128

TGFβ1	R&D	240B010 R&D
HGF	Sigma Aldrich, St. Louis, MO	H9661
MDA-MB-231	PMID:23928995	
Hs578T	PMID:23928995	
U2OS models	PMID: 21930780	
HCI-10 PDX models	PMID:26825173	
sh14-3-3ζ	TRCN0000029404	CMV-Neo lentiviral vectors
sh14-3-3ζ	TRCN0000029406	CMV-Neo lentiviral vectors
8μm transwell inserts	Corning, Corning NY	353097
IMEM	Fisher Scientific, Waltham, MA	A1048901
DMEM	Fisher Scientific, Waltham, MA	10-013-CV
CT04	Cytoskeleton Inc.	CT04-A
CH223191	Stem Cell Technologies	72732
HGF	Millipore and Life Technologies	
FuGENE HD	Roche Applied Sciences, Basel, Switzerland	??

Table 2.1 Material and Reagents used for this dissertation.

Generation of MDA-MB-231 NR3C1 (GR) S134A knock-in cells (CRISPR).

Generation of Customized Guide RNA Expression Construct. In order to genetically modify MDA-MB-231 cells to express NR3C1 containing an S134A mutation, CRISPR/Cas9 mediated gene targeting was implemented. This was accomplished using an HDR donor vector along with a CRISPR/Cas9-GFP expression vector; an anti-sense gRNA sequence (NR3C1-S134A-AS1-sgRNA) targeting the coding sequence of NR3C1 was cloned into a CRISPR/Cas9-GFP expression vector (PX458). For the generation of the CRIPSR/Cas9-GFP vector, a sense oligo 5'-CACCGCTTGGGGTTCTCTGGAACAC-3' and an anti-sense

oligo 5'-AAACGTGTTCCAGAGAACCCCAAGC-3', containing four base-pair overhangs compatible with PX458 BbsI restriction enzyme digestion sites, were annealed and ligated into PX458. In addition, a second anti-sense sgRNA sequence (NR3C1-S134A-AS2-sgRNA) 5'-CAGTGGATGCTGAACTCTTG-3' was incorporated in an identical way into a separate PX458 plasmid. Correct incorporation of both sgRNA sequences was confirmed by Sanger sequencing (Genewiz).

Generation of a dsDNA Plasmid Donor for the Incorporation of S134A Mutation in the Coding Sequence of *NR3C1.* The donor vector used to incorporate the S134A mutation into the *NR3C1* (Glucocorticoid Receptor) coding region was generated using a golden-gate strategy. Briefly, pAAV-GG-MCS-SEPT-Neo, a kind gift from the Hendrickson Laboratory at the University of Minnesota, was used to incorporate a 2100 bp sequence that spans the coding sequence of NR3C1 and contains the S134A (AGT – GCT) mutation as well as a single silent mutation within the sgRNA sequence to interrupt the protospacer adjacent motif (PAM) for both sgRNAs (i.e. to prevent repeated Cas9 cleavage after successful incorporation of the donor by homology directed repair). Conveniently, the AGT to GCT S134A mutation also generates a unique PvuII restriction enzyme site (CAGCTG) that was used for screening for desired clones. The left homology arm was generated using primers LArmF 5'-GACGCTCTTCACCGGGCACATCCAGTCAGAAGTATGGGT-3' and LArmR 5'-GACGCTCTTCTCTCTGGAACAgctGTCGACCTATTGAG-3' while the right

homology arm was generated using primers RArmF 5'-GACGCTCTTCCGAGAAtCCCAAGAGTTCAGCATCCAC and RArmR 5'-GACGCTCTTCGATGAATAAAATCCTCACCGTTGGCCAATGG-3'. The left and right homology arms were cloned into pAAV-GG-MCS-SEPT-Neo using BspQI golden gate cloning.

MDA-MB-231 Transfections and Screening for *NR3C1* S134A Knockin Clones.

The PX458-NR3C1-S134A-AS1-sgRNA or PX458-NR3C1-S134A-AS2-sgRNA plasmids along with the pAAV-GG-NR3C1-S134A donor vector were transfected into MDA-MB-231 cells using Lipofectamine 3000 (Invitrogen), and allowed to recover for at least two days. GFP positive cells were then collected by FACS sorting, expanded and sub-cloned by limited dilution into 96 well plates. Single cell clones were identified and expanded further into 24 well plates for genomic DNA collection and PCR screening. In order to identify CRISPR/Cas9 edited cells, two primers that span the CRISPR/Cas9 cut sites for NR3C1 S134A AS1 and AS2 NR3C1_S134A_ScrF2 5'- GGCTGTCGCTTCTCAATCA-3' and NR3C1_S134A_ScrR2 5'- GGACTCTCATTCGTCTCTTTACC-3' were used to produce a 492 bp amplicon by PCR. Clones that had correctly incorporated the S134A mutation were identified by performing PvuII restriction enzyme digestion on the resulting amplicons. Amplicons that exhibited PvuII cleavage by gel electrophoresis were sequenced using the NR3C1_S134A_ScrF2 primer.

Two independent clones were identified as having incorporated the intended S134A mutation as well as the PAM mutation in a bi-allelic fashion. To control for off target cutting by CRISPR/Cas9 during the generation of these clones a non-targeted clone, 34A was also recovered from the population (wt-GR cells).

Generation of MDA-MB-231 shcontrol and sh14-3-3ζ cells

Stable sh14-3-3ζ (TRCN0000029404 and TRCN0000029406) were generated by transducing MDA-MB-231 models with CMV-Neo lentiviral vectors containing target gene shRNA sequences (MISSION TRC library - Sigma). Pools were selected and maintained through culture with .75 mg/mL of G418 sulfate (Corning).

Scratch wound migration assay

Cells were plated in a 6-well plate at a density of $1.5x10^5$ cells to achieve monolayer growth at 100% confluency. Pre-treatment (hormone, growth-factor) was performed at various times before the scratch was created, as indicated. Experiments that required hormone (Dex), growth factor (Hepatocyte Growth Factor - HGF) or cytokine (Transforming Growth Factor Beta β1 – TGFβ1) treatment, cells were starved for 18-24 hrs in Modified Improved Minimum Essential Media (IMEM) containing 1% DCC. A 200μL sterile pipette tip was used to create each scratch. After scratching was performed, cells were maintained in 37°C, 5% CO2 with their respective treatments (see legends). Three independent wells per group were imaged by taking three images of each well at 10X

magnification. Image J was used for quantification of the area of the wound and three biological replicates were used per cell line. Data are shown as a representative of three experimental replicates.

Cell proliferation assay

Proliferation assays were measured via MTT ((3-[4,5-dimethylthiazol-2-yl]-2,5-diphenyltetrazolium bromide). Using 24-well plates, $2.5x10^4$ cells/well were plated. At days 0, 1, 3 and 7 cell proliferation were determined. Sixty microliters of MTT was added per well for a final concentration of 5mg/mL. Plate was incubated at 37°C for 3 hrs. At this point, the medium was removed and solubilization solution (90% v/v dimethyl sulfoxide (DMSO)/PBS) was added to lyse the cells. Absorbance was measured in plate reader at 650 and 570nm. The 650nm measurements were subtracted from the 570nm measurements. Sample means were normalized to day zero and plot ± Standard Deviation (SD) using a linear plot.

Western blot

Cells were plated and for experiments that required hormone (Dex), growth factor (HGF) or cytokine (TGFβ1) treatment, cells were starved for 18-24 hrs in Modified Improved Minimum Essential Media (IMEM) containing 1% DCC. Whole cell lysates were prepared using RIPA lite supplemented with 1 mmol/L PMSF, 5 mmol/L NaF, 0.05 mmol/L Na_3VO_4, 25 mmol/L beta glycerophosphate (BGP), 20 µg/mL aprotinin. 1 complete mini tablet protease inhibitors (Roche)

and 1 tablet of PhosSTOP (Roche). Electrophoresis in an SDS page gel was used to resolve and separate the proteins. 50µg of protein per lane was loaded. After electrophoresis, proteins were transferred to polyvinylidene difluoride membranes and probed with the following antibodies: pGR (1:750 - custom made, Pierce Biotechnology), GR (1:1000 - Santa Cruz Biotechnology, sc-1003), p-p38 (1:1000 - Cell Signaling Technology, 4511p), p38 (1:1000 - Cell Signaling Technology, 9212), YWHAZ (14-3-3ζ – 1:3000 – Millipore, AB9746), MAP3K5/ASK1 (1:1000 – Santa Cruz Biotechnology, sc5294), pERK1/2 (1:1000 – Cell Signaling Technology, 9101S), ERK1/2 (1:1000 – Cell Signaling Technology, 9102S), pJNK (1:1000 – Cell Signaling Technology, 9251S), JNK (1:1000 – Cell Signaling Technology, 9252S), FLAG (Sigma #F1804), PTK6 (D-6; 1:1000 - Santa Cruz Biotechnology, sc166243), GAPDH (1:5000 - Santa Cruz Biotechnology sc0411), RhoA (Cytoskeleton Inc #ARH04), AhR (D5S6H; Cell Signaling Technology #83200), goat anti-rabbit IgG-HRP (BioRad), and goat anti-mouse IgG-HRP (BioRad). Blots were developed using an ECL reagent (Super Signal West Pico PLUS; Thermo Fisher Scientific) and imaged by film. For densitometric calculations, Fiji software version 2.0 was used to quantify bands representing total and phosphorylated proteins. All samples were normalized to respective controls and fold-change calculated relative to the vehicle condition. Densitometric data were collected for at least 2-3 independent experiments and relative values were plotted as the mean ± SEM; the one-way ANOVA post-hoc Fisher test was utilized to assess statistical significance.

Cell migration and invasion transwell assays

Cell migration was measured using 8 μm transwell Boyden Chamber inserts (Corning). Cells were pre-treated as indicated by the figure legends. After pre-treatment, cells were trypsinized and plated at a density of $5x10^4$ cells in the upper chamber of the transwell system in IMEM media. Chemoattractant agents that were added to the lower-well are indicated in the figure legends in addition to 1% DCC. Cells were incubated for the time indicated in figure legends and maintained in 37°C, 5% CO2. Cellular invasion assays were done in a similar fashion with the exception that Matrigel (Corning) transwell inserts were utilized; Matrigel inserts were placed for at least 2 hours in the incubator before plating the cells. Transwell inserts were imaged using a light microscope. Four pictures per transwell were taken at 10X magnification. Cells were allowed to migrate for 6-18 hrs (MDA-MB-231) or 24hrs (cHCI-10) before fixation with 4% paraformaldehyde (Sigma Aldrich (St. Louis, MO USA)) or methanol and staining with 0.5% crystal violet (Sigma Aldrich). The number of migrated cells was counted for 4 representative fields per sample at 10X magnification, and results were normalized to the number of migrated control cells.

Colony formation assay

Six-well plates were prepared, and a base agarose layer (Invitrogen) was created in the surface of the wells. Cells were trypsinized, counted, and $4x10^4$ cells were plated in the top agarose layer in triplicate per treatment condition (indicated in figure legends). Plates were kept at 4°C for 10 mins to allow the

agar to solidify. Incubation of plates occurred at 37°C and 5% CO2 for 15 days. To quantify colonies, 1mL of PBS containing 4% formaldehyde and .005% crystal violet was added to each well. Cells were incubated for 1hr at room temperature. Four images were taken in each well. Results are reported as colonies counted per field and using mean ± SD.

Co-immunoprecipitation assays

Cells were lysed in ELB lysis buffer containing the following: 50 mmol/L HEPES, 0.1% nonidet P-40 (NP-40), 250 mmol/L NaCl, 5 mmol/L EDTA, 1× complete protease inhibitors (Roche), 1× PhosSTOP (Roche), 1 mmol/L PMSF, 1mmol/L NaF, 0.5 mmol/L Na_3PO_4, 25 mmol/L BGP, and 20 μg/mL aprotinin]. 1000μg of lysate was incubated with 1μg of specific antibodies overnight at 4°C in a rotator. Protein G agarose was used to isolate the complexes for 1 hour at 4°C. SDS-Page and western blot analysis were used to analyze the immunocomplexes.

Tumorsphere Assay

A single cell solution was obtained after enzymatic dissociation in 0.25% trypsin-EDTA and strained through a 40 μm sieve (BD Falcon). Cells were plated in ultra-low attachment plates (Corning) at $1x10^3$ cells per well and grown in a serum-free DMEM/F12 phenol-free medium (Corning) containing 1% methylcellulose (Sigma Aldrich), 1% B27 proprietary supplement (Invitrogen), 1% penicillin-streptomycin, 20 ng/ml EGF (Sigma Aldrich), 20 ng/ml basic-FGF

(Gibco), and 10 µg/ml Heparin (Sigma Aldrich). After 5-7 days, generate secondary tumorspheres were generated; primary spheres were collected and dissociated enzymatically in 0.25% trypsin-EDTA. Single cells were plated as described in conditioned media, which consisted of a 1:1 mixture of DMEM/F12 tumorsphere media (as above) and media from cultured parental cells. The tumorspheres were allowed to grow for 5-7 days before manual counting. Data are presented as the average ± SD of two or three independent measurements.

RNA expression analysis for METABRIC samples.

Molecular Taxonomy of Breast Cancer International Consortium (METABRIC) data (via cBioPortal – http://www.cbioportal.org/) were obtained for patients who had the 3-gene classifier and microarray data available for MAP3K5 and 14-3-3ζ (70-72). After that, we log2 transformed all of the mRNA expression values. Boxplot was utilized to plot the data and compare the expression across groups. Statistical significance was calculated based on one-way ANOVA and Tukey post-hoc.

RNA library preparation and sequencing

MDA-MB-231 expressing either wt-GR or S134A-GR were serum starved in IMEM containing 1% DCC for 18 hrs. Cells were treated with vehicle treatment, 10 ng/mL of TGFβ, or 1µM Dex for 6 hrs. Total RNA was extracted using the Qiagen RNAeasy kit. RNA quality and concentration were assessed by nanodrop. A TruSeq RNA kit was utilized to prepare and generate the mRNA

libraries that were sequenced at the National Institute of Environmental Health Sciences on the Illumina HiSeq2500 in a 75-base paired-end mode. Forty million reads were sequenced on average per sample.

RNA-seq data processing

Quality of raw RNA-seq sequences for each sample was assessed with FastQC. Trimmommatic was used to remove low quality bases and trim adapters. FastQC was used again on each filtered FASTQ files to generate a sequence quality plot. Alignment to the hg38 genome was performed using HISAT2 (73). Abundance of transcript was estimated with the featureCounts program in the SubRead package. DESeq2 (Version 1.22.2) was used to evaluate differential expression across groups and generate Principal Component Analysis (PCA) plots (74). For analyses of data using the generalized linear model framework we utilized the EdgeR package (v3.26.8). Generation of heatmaps was performed with the pheatmap package (Version 1.0.12) using log2 normalized read counts from DESeq2 analysis. The package that was used to perform the gene set enrichment analysis was fgsea (Version 1.8.0). Ingenuity Pathway Analysis was also used to evaluate pathway significance. To do this, we uploaded the differential expression gene analysis obtained from the DESeq2 and EdgeR (Generalize Linear Model) analysis. All packages were used in the R environment (Version 3.5.2) and through R Studio (Version 1.1.383). In general, the cutoff for differential expression were an

absolute log2 fold-change of 1.5 and a Benjamini-Hochberg p-adjusted value of 0.05. Figure legends include the criteria for gene selection.

Quantitative RT-PCR

Quantitative real-time PCR (qRT-PCR) experiments were conducted as previously described (40). The cDNA was generated from total RNA extracted from cell lines indicated in figure legends. Cells were plated at $5x10^4$ cells/well in 6-well plates. After their respective treatments, media was removed, and cells were washed twice with cold 1X PBS. RNA was isolated with trizol, as per the manufacturer's protocol. The cycling conditions by qPCR were as followed: 10 mins of initial denaturation at 95°C, 10 seconds denaturation at 95°C, 10 seconds at 60°C for annealing of primers and extension at 72°C for 5 seconds for 45 cycles. Relative target gene expression was normalized to the expression of internal control genes, either TATA-binding protein (*TBP*), Actin (beta-actin*)*, or *18S rRNA* and they are shown as the mean value of three biological replicates ± SD. The primers used were MAP3K5-F 5'-AGGTGGTACTCTTTGGTTTTCAAG-3' and MAP3K5-R 5'-GATACTGTCTAAGGCAAACATCCAG-3'; LEFTY2-F 5'-CTGGACCTCAGGGACTATGG-3' and LEFTY2-R 5'-TCCCCTGCAGGTCAATGTAC3'; PIK3IP1-F 5'-CCTGGTGCTACGTCAGTGG-3' and PIK3IP1-R 5'-TCCTGGATTTCTGTCGTGAAG-3', AhR-F 5'-ATATGTCGTCTAAGGTGTCTGCTG-3', AhR-R 5'-AGTATTGATCCATCTTTCCCTTTC-3', CYP1A1-F 5'-GCTGACTTCATCCCTATTCTTCG-3', CYP1A1-R 5'-

TTTTGTAGTGCTCCTTGACCATCT-3', CYP1B1-F 5'-GGCATTAGAGTCAACTACACAAAGC-3', CYP1B1-R 5'-GAATGGCAAGTGCCAAAAA-3', PTK6-F 5'-GGACCCCGTGTACATCATCAC-3', PTK6-F 5'-ACGGGCAGGACTTTCTCATC-3'.

Correlation of GR (*NR3C1)* and MAP3K5 in TNBC patients

RNA-Seq data available as RSEM was downloaded for patients with negative status for ER, PR and HER2 for the TCGA breast cancer provisional dataset using cBioPortal (70, 71). All expression data were log2 transformed for both genes. PRISM (Graphpad) was employed to plot each value and to execute the Pearson analysis of correlation.

Chromatin Immunoprecipitation Assay (ChIP)

ChIP assays were performed as per manufacturer instruction (ChIP-IT express – Active Motif). Following respective treatments as indicated in figure legends, 37% formaldehyde was used for fixation (5 mins) and sonication was utilized to shear chromatin for 30 mins. Lysates were immunoprecipitated for 4hrs with the following antibodies: 2µL of GR (sc-1003), 2µL of AhR, and equal amount of rabbit IgG. QPCR was used to analyze the resulting DNA and the data is represented as a percentage of input DNA. The primers used were LEFTY2 ChIP F 5'-CCCTCTAGTGGTTACAGGAAGACTC-3' and LEFTY2 ChIP R 5'-AAAATCTGAGAGCAACTGAAGTGAG-3'; PIK3IP1 CHIP F 5'-GTACAAGTGCCCTGATAGGATTG-3' and PIK3IP1 CHIP R 5'-CACTTCCCAGAACTGTTTTCAAC-3'. These primers were designed based on

previous ChIP-Seq studies that focus on bindings sites of the GR (75, 76). In the case of the ChIP primers for CY1B1, the primers used were: CY1B1 CHIP F 5'-TTATCGGGT TGAAGTTTCTGC-3' and CY1B1 CHIP R 5'-ATATGACTGGAGCCGACTTTC-3'.

Survival analysis for METABRIC and TCGA (SurvExpress) samples.

The METABRIC microarray expression data and survival data were downloaded for the following genes via cBioPortal – http://www.cbioportal.org/: *YWHAZ*(14-3-3ζ)*, DLEU7, JUNB, LBH, SNAI1, C1orf106, CCL20, NRP2, PIK3IP1, SYT8, KRT16, NLRC3, LEFTY1, NKD1, KPNA7, LTBP3, MDFI, SYN1, LEFTY2, MYOZ1, GPR183, MATK, STK19, HRAS*, and *COL8A2* as available for subjects. First, we log2 transformed all of the mRNA expression values. In the case of the survival analysis for 14-3-3ζ (Figure 3.7B), we classified patients into upper 50th percentile and bottom 50th percentile based on the median cutoff for the log2 mRNA expression of 14-3-3ζ across all patients. For our gene-signature, R programming was used to calculate the average gene expression of all genes from each patient and stratify groups based on the median of the average expression into upper 50th percentile or bottom 50th percentile. Kaplan-Meier plots and logrank test was used to assess the differences in overall survival between the cohorts using PRISM (Graphpad).

SurvExpress was used to analyze survival data for the TCGA cohort. The 24 TGFβ-induced pS134-GR-dependent gene signature (*DLEU7, JUNB, LBH,*

SNAI1, C1orf106, CCL20, NRP2, PIK3IP1, SYT8, KRT16, NLRC3, LEFTY1, NKD1, KPNA7, LTBP3, MDFI, SYN1, LEFTY2, MYOZ1, GPR183, MATK, STK19, HRAS, and *COL8A2*) was utilized for the SurvExpress analysis. Data was downloaded and analyzed locally in R. PRISM (Graphpad) was used to generate the Kaplan-Meier plots. Logrank test was used to assess the differences in survival between expression cohorts.

IncuCyte S3 Live Cell Imager Wound Healing Assays.

MDA-MD-231 cells were plated into 96-well format ImageLock microplates (Essen BioScience (Ann Arbor, MI USA)) at a density of either 4.5 x 10^4 cells/well or 6 x 10^4 cells/well (HIF DKO), such that cells would be at 100% confluence 18 hrs after plating. The WoundMaker tool was used to create a uniform 800 µm scratch/well, the wounds were gently washed and growth media re-applied. Cells were cultured up to 50 additional hours. Images were obtained every 2 h and data analyzed using the IncuCyte total wound area algorithm.

Public Data Mining for PTK6, AhR and NR3C1.

Datasets were analyzed using KM Plotter (77) and SurvExpress (78). For TCGA survival analysis (KM plotter - http://kmplot.com/), overall survival was stratified by PTK6 mRNA expression in ER- patients (downloaded October 2018). SurvExpress (http://bioinformatica.mty.itesm.mx:8080/Biomatec/SurvivaX.jsp) analysis of

grouped PTK6, AHR and NR3C1 (GR) expression was performed on the TCGA breast cancer recurrence database and includes all patients (ER+ and ER-).

Tail Vein Assay

To study gain of PTK6 function, 8-10-week old female Nod/Scid/Gamma (NGS) mice were injected via the tail vein with MDA-MB-231 +Vector or +PTK6 cells (2.5 x 10^5) or HIF DKO +Vector or HIF DKO +PTK6 cells (5 x 10^5 cells); more HIF DKO cells were injected due to the reduced metastatic potential of MDA-MB-231 cells lacking both HIF transcription factors (9). All animals were harvested at day 28 post-injection. To determine the effects of PTK6 KO, MDA-MB-231 parent, NTC or PTK6 KO admixture cells (200,000) were injected. All animals were harvested at day 19 post injection. The lungs were inflated with formalin and post-fixed with formalin. Paraffin sections were stained with an anti-human specific mitochondrial marker ((AbCAM #ab92824) as in El Ayachi, et al. 2012 (79)). Whole stained slides were digitally scanned at high resolution with a 3DHISTECH PANORAMIC slide digitizer and the staining intensity analyzed by pixel counts using the densitometry algorithm, leading to generation of a percent "positive area" of metastasis score for each slide. Digital images of whole lungs representative of the mean value of each genotype are also shown.

Mammary fat pad transplantation

All animal studies were carried out in adherence to the NIH Principles of Laboratory Animal Care and protocols approved by the Institutional Animal Care

and Use Committee at the University of Tennessee Health Science Center (protocol 18-045). Approximately 5-6-week old female NSG mice were surgically inoculated via the left and right inguinal mammary gland fat pads with tumor cells (250,000) suspended in 10 µl of HBSS. Tumor size was measured twice a week using digital calipers and the body weight of the mice was recorded at the same time. The tumor volume was calculated as ($width^2$ x length)/2. All mice were necropsied at day 30 post-inoculation, tumors were excised and measured ex vivo via calipers, and weighed.

Reverse Phase Protein Array

Cells were stimulated with HGF (50 ng/mL) for 30 min and then lysed with RPPA lysis buffer (1% Triton X-100, 50mM HEPES, pH 7.4, 150mM NaCl, 1.5mM $MgCl_2$, 1mM EGTA, 100mM NaF, 10mM Na pyrophosphate, 1mM Na_3VO_4, 10% glycerol, freshly added protease and phosphatase inhibitors from Roche Applied Sciences #05056489001 and 04906837001, respectively). After clearing by centrifugation, lysates were denatured in Sample Buffer (40% Glycerol, 8% SDS, 0.25M Tris-HCl, pH 6.8, beta-mercaptoethanol at 1/10 volume). RPPA was performed by MD Anderson RPPA Core. Briefly, lysates were manually serial-diluted in 5 two-fold dilutions with lysis buffer and printed on nitrocellulose-coated slides (Grace Bio-Labs (Bend, OR USA)) using Aushon 2470 Arrayer (Aushon BioSystems (Billerica, MSA USA)). Slides were probed with validated primary antibodies followed by detection with appropriate Biotinylated secondary antibodies (Goat anti-rabbit IgG, Goat anti-Mouse IgG, or

Rabbit anti-Goat IgG). Only antibodies with a Pearson correlation coefficient between RPPA and western blotting of greater than 0.7 were used for RPPA. The signal obtained was amplified using a Dako Cytomation-Catalyzed system and visualized by DAB colorimetric reaction. The slides were scanned, analyzed and quantified using a customized software to generate spot intensity. Dilution curves were fitted with a logistical model ("Supercurve Fitting" developed by the Department of Bioinformatics and Computational Biology in MD Anderson Cancer Center, http://bioinformatics.mdanderson.org/OOMPA). This fits a single curve using all the samples on a slide with the signal intensity as the response variable. The fitted curve was plotted with signal intensities on the y-axis and the log2-concentration of proteins on the x-axis. The concentrations of each set of slides were then normalized for protein loading. Correction factor was calculated by both median-centering across samples of all antibody experiments, and median-centering across antibodies for each sample.

Rho activation assay

Activated Rho assays were performed according to the manufacturer's instructions (Cytoskeleton Inc). Briefly, sub-confluent cell cultures were starved for 16 h in IMEM (10% DCC, 1% P/S) and then stimulated with HGF (50 ng/mL) for 30 min before rinsing with ice-cold PBS and lysing in 200 µl lysis buffer. Equal volumes of supernatant were incubated with GST-Rhotekin-RBD affinity beads for 1 h at 4°C, followed by two washes in 25 mM Tris pH 7.5, 30 mM $MgCl_2$, 40

mM NaCl. Bound proteins were eluted in sample buffer and examined by SDS-PAGE in a 7.5% gel and western blotting.

Patient sample processing

De-identified tumor samples and normal adjacent tissue samples in excess of diagnostic requirements were obtained from University of Minnesota's Biorepository and Laboratory Services program (IRB approval protocol #0305M47681). The organoid procedure was initiated within hours of surgery. Briefly, sliced pieces of tissue were incubated at 100 rpm for 30 min at 37°C in Collagenase A solution (Advanced DMEM/F12 [Gibco; Thermo Fisher Scientific] supplemented with 1x GlutaMax [Gibco; Thermo Fisher Scientific], 1X HEPES [Gibco; Thermo Fisher Scientific], 1% penicillin/streptomycin [Life Technologies]; AdDF+++, and 2 mg/mL Collagenase type IV [Gibco; Thermo Fisher Scientific] for tumor samples or 1 mg/mL Collagenase for normal breast tissue). The digested tissue suspension was sequentially sheared using 10 mL, 5 mL and flamed glass Pasteur pipettes. After every shearing step the suspension was strained over a 100 μm filter with retained tissue pieces entering a subsequent shear step. 2% FBS was added to the strained suspension before centrifugation at 2,000 rpm. The pellet was resuspended in 10 mL AdF+++ and centrifuged again, then seeded for organoid culture.

Organoid culture

Neutralized rat tail Collagen I (Fisher Scientific #CB354249) was used to make a thin underlay on 24 or 96-well ultra-low attachment plates (Corning), which was allowed to solidify at 37°C until ready for plating. The tissue pellet was resuspended in a mixture of 3:7 Matrigel (Fisher Scientific #08774552) to Collagen I, and the desired amount of matrix/organoid suspension was plated on top of the pre-prepared underlay. Plated organoids were incubated at 37°C, 5% CO_2 for 45-60 min. After gelation, pre-warmed AdF+++ supplemented with R-Spondin 3 (250 ng/mL; PeproTech (Rocky Hill, NJ USA)), Neuregulin (5 nM; PeproTech), EGF (5 ng/mL PeproTech), Noggin (100 ng/mL; PeproTech), and 1% B27 (Invitrogen) was added to the wells. Sterile PBS was added to empty wells to prevent desiccation. Organoid morphology was examined under phase contrast after 10 d, and the number of branching organoids counted. For qPCR analysis, organoids were collected from Matrigel/Collagen by addition of ice-cold AdF+++ and mixing with Pasteur pipettes. After collection by centrifugation, organoids were resuspended in TriPure Isolation Reagent (Roche Applied Sciences) and processed for qRT-PCR as described above.

Growth inhibition assays following chemotherapy treatment using the IncuCyte S3 live cell imager

To compare cell growth inhibition curves, cHCI-10 (1.5×10^4) or MDA-MB-231 (5×10^3) cells were seeded per well in a flat-bottom 96-well plate and allowed to adhere for 24 h. Appropriate working dilutions of paclitaxel (Sigma),

CT04 or CH223191 were prepared in M87 (cHCI-10) or DMEM-Hi (MDA-MB-231) growth media containing the fluorescent nuclear marker Miami Green to enumerate cells (Kerafast (Boston, MA USA), 1 μM final concentration). A dose range was tested for each individual drug to determine the IC_{30}, IC_{50} and IC_{70} values (CT04: 0.01 μg/mL to 1 μg/mL, ~ equivalent to 0.4 nM to 40 nM, or CH223191: 1 μM to 7575 μM for cHCI-10 and 100 nM to 50 μM for MDA-MB-231). Paclitaxel was added in combination with the approximate IC_{30} dose of either CT04 for cHCI-10 cells (0.1 μg/mL) or the dose used in transwell assays for MDA-MB-231 cells (1 μg/mL) or paired with CH223191 (8 μM, cHCI-10; 2.5 μM, MDA-MB-231). Each drug dose/condition was tested in triplicate, including untreated controls or vehicle-only controls. After addition of fresh growth medium containing each concentration of each drug to the cells, all bubbles were removed, and the plate incubated in the Incucyte S3 live-cell imager for a minimum of 48-96 h. Wells were scanned every 2-4 h to report cell density as measured by phase contrast and by green nuclear signal to enumerate cell number. The media was not changed over the course of the experiment. All data were normalized well-to-well to corresponding individual initial t=0 images and re-expressed as the mean ratio in the change of growth over time ± SEM. Data were exported and input into Prism 8 (GraphPad) and the non-linear regression algorithm with sigmodal graphing used to generate representative dose curves. The reported IC_{50} values are the mean ± SEM of three independent biological replicate experiments. Combination indices were calculated in Excel using the

isobole method in Excel; values for the combination index (CI) < 1.0 indicate drug synergy.

Statistics

All statistic information is disclosed in the legends. In general, for experiments that involve two groups, one-paired Student's t-test was performed. For experiments that involved more than two groups, one-way or two-way ANOVA were utilized. Post-hoc tests within the vehicle or control treatment was performed using Dunnett's statistical testing. However, if comparison within different groups was required, Tukey's post-hoc test was utilized. For densitometric analysis, one-way ANOVA and Fisher Least Significant Difference (LSD) post-hoc. Statistical tests were performed using either PRISM v7/v8 and R v3.5.

Chapter 3 Glucocorticoid Receptors are Required Effectors of TGFβ1-Induced p38 MAPK Signaling to Advanced Cancer Phenotypes in Triple Negative Breast Cancer

Introduction

Although TNBC is intensely studied, molecular targeted-therapies are still largely unavailable for TNBC patients, who suffer from higher disease recurrence, more frequent metastasis, and a worse prognosis relative to patients with other breast cancer (BC) subtypes (80). Appropriate biomarkers of driver pathways and new therapeutic targets are urgently needed. Approximately, up to 40% of TNBC tumors express elevated GR levels (22, 36, 81-83). Recently, a GR gene-signature was employed to stratify patients by prognosis; patients who expressed high/low levels of the 74 GR-target gene mRNAs experienced shortened disease-free survival (24). As with other HRs, GR is subject to posttranslational modifications that impact its function. Similar to ER (84) and both PR isoforms (85), phosphorylation events dramatically alter GR target gene selection (33). Previously, it was shown that phosphorylation of GR on serine 134 is elevated in TNBC relative to other breast cancer subtypes (86); this p38 MAPK-dependent event was insensitive to GR ligands, but induced in response to cellular stress, including ROS/H_2O_2, hypoxia and nutrient starvation (39), as well as loss of attachment (i.e. cell suspension) and stress-inducing chemotherapies (86) such as paclitaxel (paclitaxel), a taxane microtubule stabilizing drug routinely used as adjuvant or neoadjuvant chemotherapy in TNBC patients (86, 87). Upon ligand (i.e. Dex, cortisol) binding, pS134-GR upregulated HIF2, AhR, and PTK6. These ligand-dependent pS134-GR-target genes are known mediators of pro-survival and metastasis in TNBC (39, 86).

The metastatic cascade is a multi-step process that is regulated by both intrinsic and extrinsic factors (55, 88, 89). Cancer cells must detach from the primary tumor mass, migrate and invade through surrounding local tissues, intravasate to the lymph or blood vessels, survive in the circulation as individual cells or as collective cell clusters, and extravasate from the vessels to the target tissue in order to finally colonize a new metastatic lesion (89). The tumor microenvironment (TME) contributes to many of these steps (90). Stromal cells within the primary tumor express cytokines and growth factors that modulate the invasive potential of breast epithelial carcinoma cells. Notably, TGFβ1 promotes cancer cell migration/invasion and is associated with poor outcome in TNBC patients (91). Inhibition of TGFβ signaling in pre-clinical models attenuated cell migration and blocked EMT in TNBC (92, 93). TGFβ1 activates the TGFβ Ser/Thr kinase receptors (types I and II), resulting in phosphorylation and activation of SMAD transcription factors (94). Phospho-SMADs enter the nucleus and induce the expression of genes that promote both migration and invasion (94). Importantly, SMAD-independent pathways are also regulated by TGFβ; stress-activated protein kinases, including p38 MAPKs are rapidly activated downstream of TGFβ receptors (95). Emerging data support a role for p38 MAPK signaling in advanced breast cancer biology. For example, p38 MAPK is essential for promoting lung metastasis in response to TGFβ (96). Namely, HRs, including GR, PR, and androgen receptor (AR), are important substrates for MAPKs (39, 97, 98).

Herein, we sought to determine the intersection of GR-driven actions with the TGFβ1 signaling pathway in TNBC. Although molecular cooperation between GR and TGFβ1 has been studied in other fields, its relevance to TNBC is under-explored. We show that TGFβ1 induces robust p38 MAPK-dependent GR S134 phosphorylation; this event is critical for TGFβ1-induced TNBC cell anchorage independent growth and migration. TGFβ1-mediated migration requires pS134-GR, but not exogenously added GR ligands and is blocked by GR antagonists. Remarkably, we find that pS134-GR is essential for the expression of MAP3K5, a key upstream regulator of MEK3/6 and p38 MAPK required for pathway activation. Finally, a novel gene signature composed of 24 pS134-GR-regulated transcripts predicts rapid disease progression in BC patients. We conclude that pS134-GR is both a major effector of the p38 MAPK signaling pathway downstream of the TME-derived factor TGFβ1 and required for a functionally intact p38 MAPK module (i.e. MAP3K5 - MEK3/6 - p38 MAPK). The amplification of p38 MAPK signaling by pS134-GR represents a feed-forward signaling loop that may be disrupted to halt TNBC progression. Phospho-GR species represent novel biomarkers for co-targeting GR and p38 MAPK in TNBC.

Results

Dexamethasone promotes biphasic migration in TNBC models

Previous studies demonstrated that GR activation has anti-migratory effects (99). Conversely, West and colleagues recently reported that GR induces the expression of genes that are essential for migration and invasion (24, 25).

Similar to other steroid hormone receptors, signaling context and the hormonal milieu (i.e. time and concentration of exposure to either agonist or antagonist) may dictate distinct receptor actions in the same biological system (100). We tested whether GR differentially responds to acute and chronic effects of Dex by exposing GR+ MDA-MB-231 TNBC cells to a range of pharmacologically relevant Dex concentrations at two different time points: 15 mins (“acute”) and 6 hrs (“chronic”) (Figure 3.1A). Our data demonstrate that when cells are pre-treated with Dex in charcoal-stripped serum-containing media (i.e. steroid hormone free, but growth factor rich) for 15 mins and then subjected to scratch wound assays, subsequent Dex-induced migration is inhibited (Figure 3.1B). Conversely, when the same cells are instead pre-treated with Dex for 6 hrs in charcoal-stripped serum-containing media, subsequent treatment with Dex stimulates migration (Figure 3.1C). A biphasic response of acute vs. chronic Dex treatment was also observed in Hs578T cells (Figure 3.2A-C).

To explore signaling pathways that may be altered upon chronic (i.e. 6 hrs) Dex treatment in TNBC cells, we probed existing microarray data from the GSE113571, in which MDA-MB-231 cells were treated with 100nM Dex for 4 hrs (24). Ingenuity Pathway Analysis was used to determine which pathways were significantly upregulated or downregulated by liganded GR. Notably, the TGFβ1 pathway was among the most significantly upregulated (Figure 3.1D). We thus evaluated the requirement for GR in TGFβ1-induced MDA-MB-231 cell migration. Cells were pretreated for 18 hrs with vehicle, RU486 (i.e. a GR antagonist) alone,

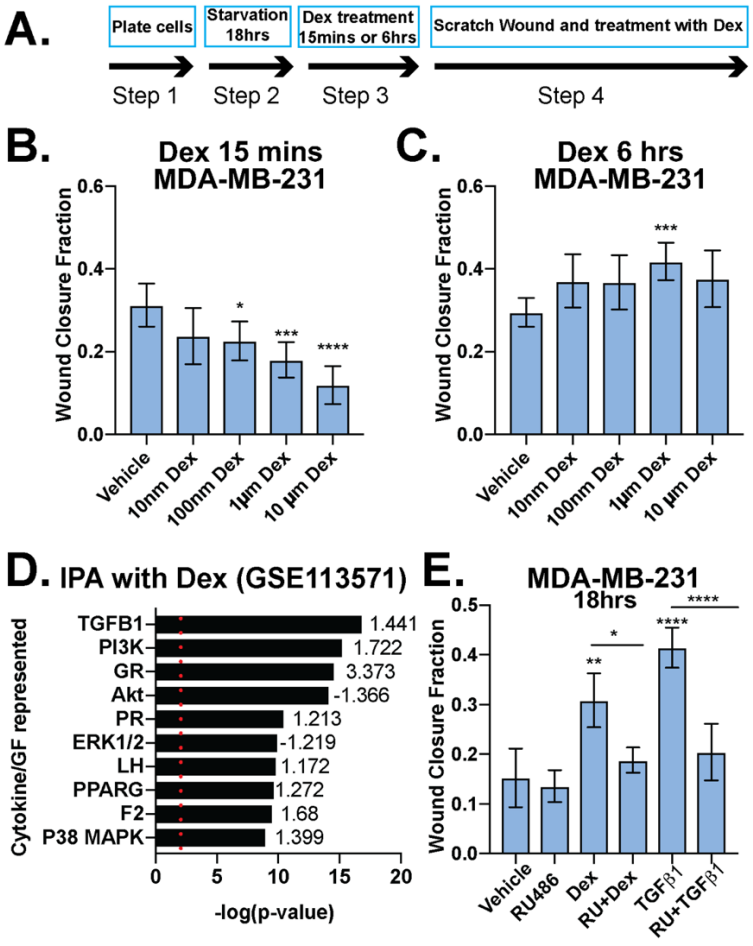

Figure 3.1 Dexamethasone either inhibits or promotes breast cancer cell migration in a time-dependent manner.

(A) Schematic of protocol used for B and C. MDA-MB-231 cells were pretreated with increasing doses of Dex for either 15 mins **(B)** or 6 hrs **(C)** and Dex-induced cell migration was measured by the degree of scratch-wound closure at 18 hrs. The mean of three field images from each of the three biological replicates experiments is shown ± standard deviation (SD). Fraction of wound area closure of MDA-MB-231 cells was determined image J. Statistical significance was assessed by One-way ANOVA and Dunnett's post-hoc for comparison within groups vs. vehicle treatment. (*, $P < 0.05$; **, $P < 0.01$; ***, $P < 0.001$; ****, $P < 0.0001$). **(D)** Ingenuity Pathway Analysis (IPA) for MDA-MB-231 cells treated with 100nM Dex from GSE113571 (24). P-value plot shows GR-mediated activation of cancer-relevant signaling pathways and their respective z-scores of activation/inhibition, including the TGFβ1 and p38 MAPK pathways. The top 10 most significant pathways for cytokine/growth factor (GF) signaling are shown. Red dotted line indicates the significance value of 1.3 ($P < .05$). **(E)** Fraction of wound area closure of MDA-MB-231 cells treated (18 hrs) with vehicle control, TGFβ1 (10 ng/mL), Dex (1µM), TGFβ1+Dex, RU486 (1µM), RU486+TGFβ1 or RU486+Dex. The mean of three fields from each of the three biological replicates experiments is shown ± SD. Statistical significance was assessed by One-way ANOVA and Tukey post-hoc for comparison within groups. (*, $P < 0.05$, **, $P < 0.01$, ****, $P < 0.0001$).

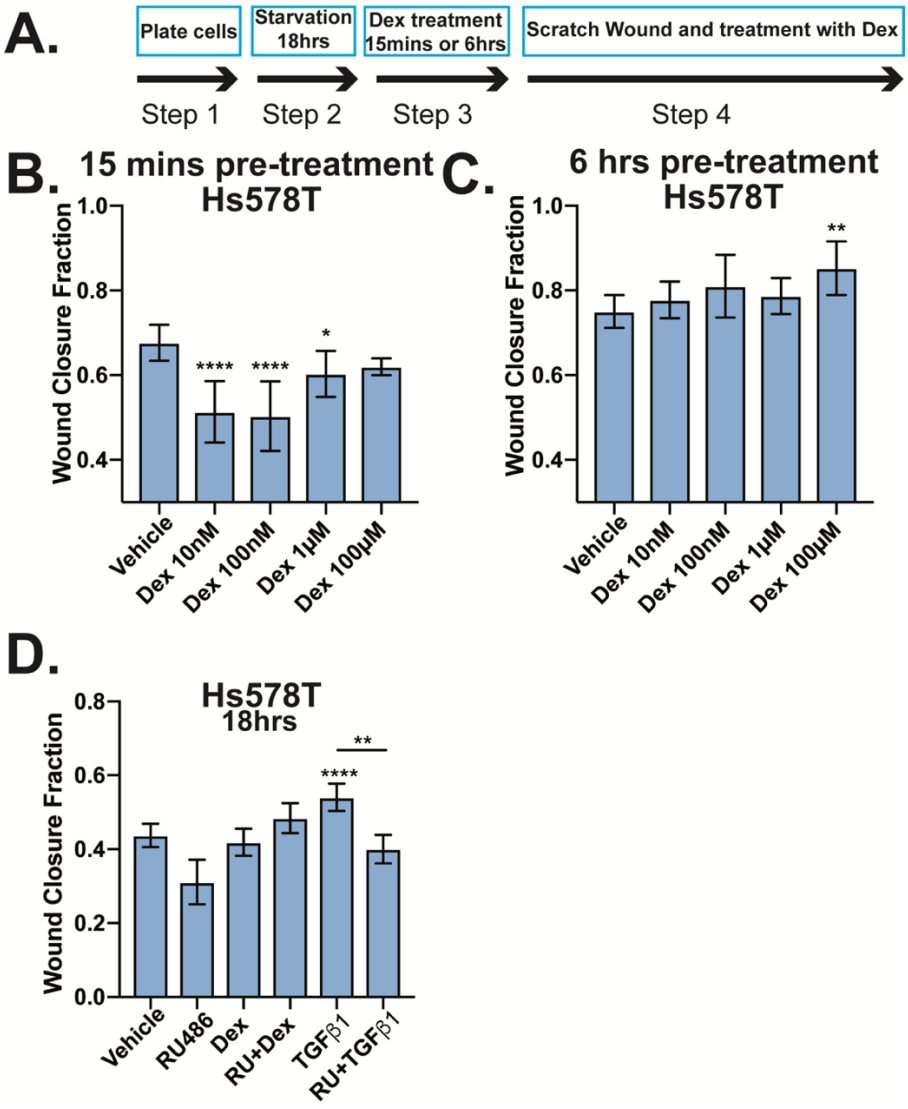

Figure 3.2 Dexamethasone either inhibits or promotes HS578T breast cancer cell migration in a time-dependent manner.

(A) Schematic of protocol used for B and C. Hs578T cells were pretreated with increasing doses of Dex for either 15 mins **(B)** or 6 hrs **(C)** and cell migration was analyzed by measuring scratch-wound closure at 18 hrs in the presence of their respective treatments. The mean of three field images from each of the three biological replicates is shown ± SD. Fraction of wound area closure of MDA-MB-231 cells was determined using ImageJ. Statistical significance was assessed by One-way ANOVA and Dunnett's post-hoc for comparison within groups vs. vehicle treatment (*, $P < 0.05$, **, $P < 0.01$ ****, $P < 0.0001$). **(D)** Fraction of wound area closure of Hs578T cells treated with vehicle control, TGFβ1 (10 ng/mL), Dex (1μM), TGFβ1+Dex, RU486 (RU; 1μM), RU+TGFβ1 or RU+Dex. The mean of three field images from each of the three biological replicates is shown ± SD. Statistical significance was assessed by One-way ANOVA and Tukey post-hoc for comparison within groups (**, $P < 0.01$, ****, $P < 0.0001$).

Dex alone, TGFβ1 alone, or either agent (Dex or TGFβ1) in combination with RU486. Cells were then subjected to scratch wound assays in the presence of the respective treatments. As expected, we observed pro-migratory effects on cells that were chronically treated with 1μM Dex (18 hrs). Cells that were treated for 18 hrs with 10 ng/mL of TGFβ1 were also more migratory relative to vehicle controls. Surprisingly, RU486 abrogated the pro-migratory effects of either Dex or TGFβ1 (Figure 3.1E). Similar results were observed in Hs578T TNBC cells (Figure 3.2D). Our results suggest that TGFβ1-induced TNBC cell migration is mediated by GR. Notably, TGFβ1-induced cell migration occurred in steroid hormone-free conditions in the absence of exogenously added GR ligands.

TGFβ1 induces TNBC cell migration via phosphorylation of GR S134

Previously, we reported that cellular stress (i.e. H_2O_2, hypoxia, nutrient starvation) and stressful growth conditions such as growth in low attachment/suspension and chemotherapeutic agents (i.e. Paclitaxel) increase phosphorylation of GR on S134, leading to the increased ligand-induced expression of selected GR target genes (e.g. BRK, HIF2, AhR) that are essential for advanced cancer phenotypes in TNBC (39, 86). Additionally, we reported that pS134-GR species are elevated in TNBC relative to luminal breast cancer subtypes (86). Since TGFβ1 expression is also elevated in TNBC and associated with poor outcome, we predicted tight linkage between TGFβ1 signaling and phosphorylation of GR S134 (101, 102). MDA-MB-231 cells were treated with 10 ng/mL TGFβ1 for 30 mins, 1 hr, and 2 hrs; phosphorylation of GR S134 was

induced by TGFβ1 at 1 hr and 2 hrs. Additionally, p38 MAPK activity, as measured by active site phosphorylation, was also elevated at these timepoints (Figure 3.3A and see densitometric analyses of aggregated data from multiple repeats in Figure 3.4A). Dose-response curves demonstrated robust GR S134 phosphorylation over a wide range of TGFβ doses (0.1-10 ng/ml) (Figure 3.3B and see densitometric analyses of aggregated data from multiple repeats in Figure 3.4B). We then tested the requirement for p38 MAPK in GR S134 phosphorylation in TNBC models; MDA-MB-231 cells were pre-treated with either vehicle control (DMSO) or SB203580 (p38 inhibitor) for 30 mins prior to TGFβ1 exposure for 1 hr. While basal levels of p38 MAPK activity remained somewhat elevated, inhibition of p38 MAPK completely blocked TGFβ1 dependent phosphorylation of GR S134 (Figure 3.3C and see densitometric analyses of aggregated data from multiple repeats in Figure 3.4C). The specificity of GR S134 phosphorylation by p38 MAPK was further explored using SB203580 and SB202190 (p38 inhibitors), LY294002 (Akt inhibitor), or UO-126 (MEK1/2 inhibitor). MDA-MB-231 and Hs578T TNBC cells were pre-treated for 30 minutes with each kinase inhibitor prior to TGFβ1 treatment; TGFβ1-induced GR phosphorylation was exclusively blocked upon inhibition of p38 MAPK, while inhibition of either AKT or ERK1/2 was without effect (Figure 3.4D and 3.4E). Similar to MDA-MB-231 and Hs578T cells, TGFβ1 induced robust phosphorylation of GR S134 in a TNBC Patient-Derived Xenograft (PDX) model (HCI-10) (Figure 3.3D).

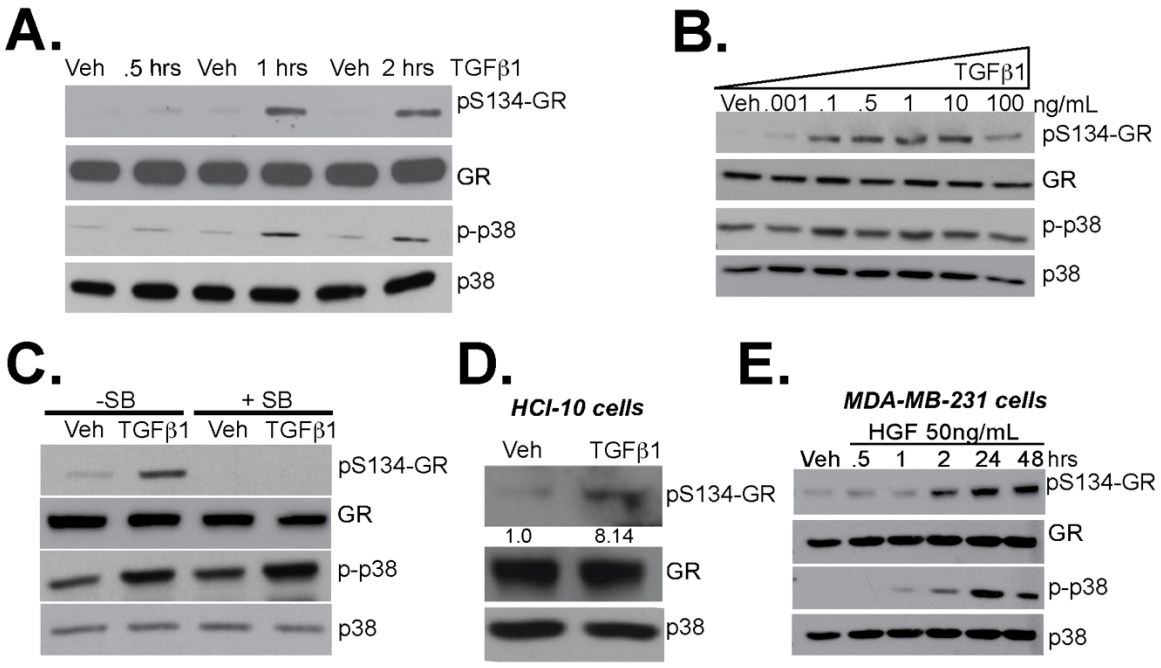

Figure 3.3 TGFβ1 induces p38 MAPK-dependent phosphorylation of GR S134.

(A) Representative Western blot analysis of phosphorylated GR (pS134-GR), total GR, phosphorylated p38 MAPK (p-p38 MAPK), and total p38 MAPK protein levels in MDA-MB-231 cells treated with either vehicle control or 10 ng/mL TGFβ1 for 0.5, 1, or 2 hrs. Representative images of at least three independent experiments is shown (Densitometry of aggregated data from multiple experiments is shown in Figure 3.4); total p38 serves as a loading control. **(B)** MDA-MB-231 cells were treated with increasing concentrations of TGFβ1 for 1hr. Western blot analysis shows pS134-GR, total GR, p-p38, and total p38 protein levels (Densitometry of aggregated data from multiple experiments is shown in Figure 3.4). **(C)** Representative Western blot analysis of pS134-GR, total GR, p-p38, and total p38 in MDA-MB-231 cells pre-treated with either 10μM SB203580 (p38 inhibitor) or DMSO control for 30 mins followed by either vehicle control or 10 ng/mL of TGF for 1hr. Representative images of at least two independent repeats are shown (Densitometry of aggregated data from multiple experiments is shown in Figure 3.4); total p38 serves as a loading control. **(D)** Patient-derive xenograft (PDX) HCI-10 cell line and were treated with 10 ng/mL of TGFβ1 and evaluated for expression of pS134-GR, total GR and total p38 (loading control) by Western blotting. Densitometry for pS134-GR levels are shown relative to vehicle-control. **(E)** Western blot analysis of pS134-GR, total GR, p-p38 MAPK, and total p38 MAPK protein levels in MDA-MB-231 cells treated with either vehicle control or HGF (50ng/mL) for 0.5, 1, 2, 24 and 48 hrs. Equal amounts of protein were loaded (Densitometry of aggregated data from multiple experiments is shown in Figure 3.4); total p38 serves as a loading control.

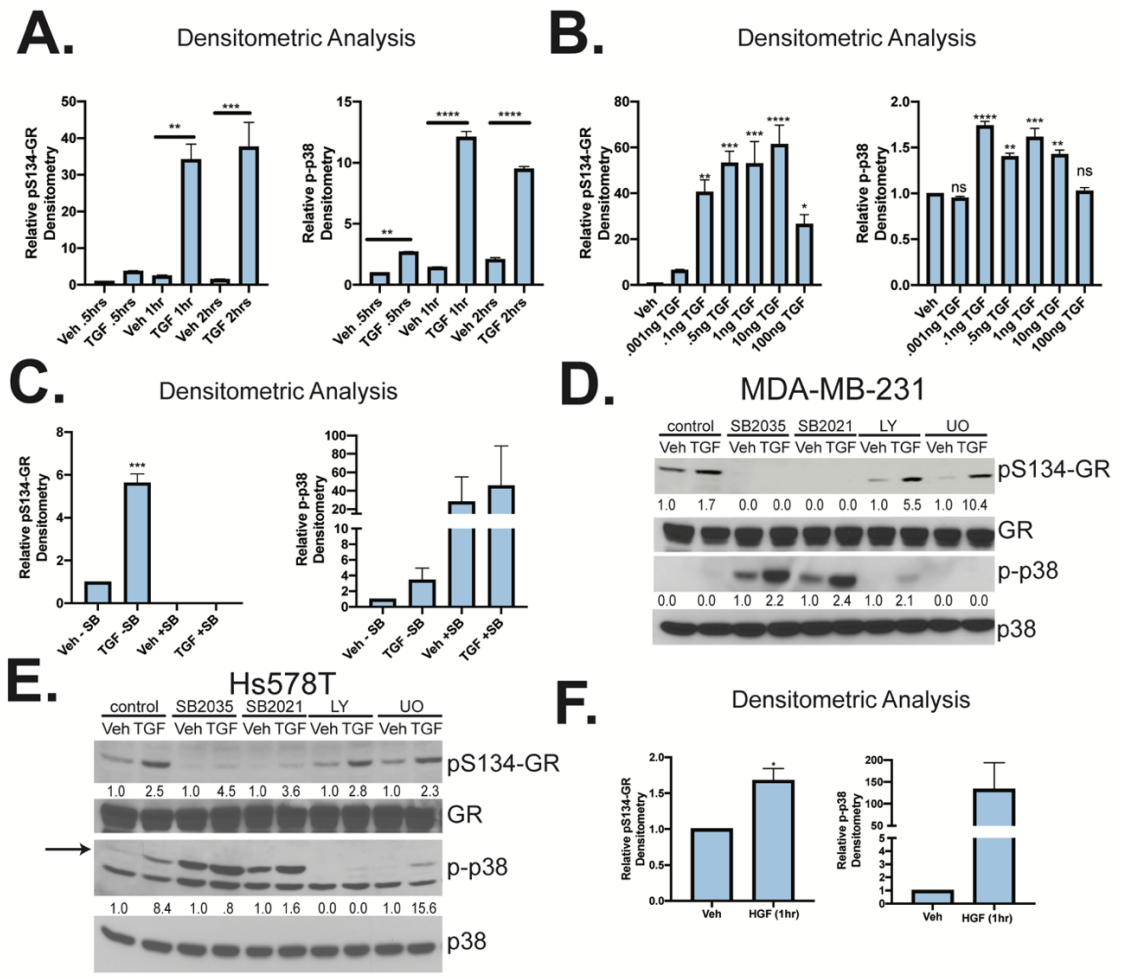

Figure 3.4 Phosphorylation of pS134-GR in TNBC models.

(A) Densitometric analysis for pS134-GR levels and p-p38 levels of two independents experiments representative of Figure 3.3A. Values are relative to the vehicle-control of the wt-GR group and are presented as the mean ± SEM. One-way ANOVA and Fisher's LSD test posthoc were used to evaluate statistical significance (**, $P < 0.01$,*** $P < 0.001$, ****, $P < 0.0001$). **(B)** Densitometric analysis for pS134-GR levels and p-p38 levels of two independents experiments representative of Figure 3.3B. Values are relative to the vehicle-control and are presented as the mean ± SEM. One-way ANOVA and Fisher's LSD test posthoc were used to evaluate statistical significance (*, $P < 0.05$, **, $P < 0.01$,*** $P < 0.001$, ****, $P < 0.0001$). **(C)** Densitometric analysis for pS134-GR levels and p-p38 levels of two independents experiments representative of Figure 3.3C. Values are relative to the vehicle-control and are presented as the mean ± SEM. One-way ANOVA and Fisher's LSD test posthoc were used to evaluate statistical significance (***, $P <$ 0.001). The difference in the levels of p-p38 did not reach statistical significance but an upward trend was observed. **(D)** Representative Western blot analysis of pS134-GR, total GR, p-p38, and total p38 in MDA-MB-231 cells pre-treated with either 10μM SB203580 (p38 inhibitor) SB203580 (p38 inhibitor), SB202190 (p38 inhibitor), LY294002 (Akt inhibitor), and UO-126 (MEK1/2), or DMSO control for 30 mins followed by either vehicle control or 10 ng/mL of TGF for 1hr. Densitometric analysis is shown with the values of either pS134-GR or p-p38 MAPK relative to vehicle-control of each inhibitor. **(E)** A similar approach was taken using Hs578T cells. **(F)** Densitometric analysis for pS134-GR levels and p-p38 levels of two independents experiments (1 hr) representative of Figure 3.3E. Values are relative to the vehicle-control and are presented as

the mean ± SEM. One-way ANOVA and Fisher's LSD test posthoc were used to evaluate statistical significance (*, $P < 0.05$).

In addition to TGFβ1, Hepatocyte Growth Factor (HGF) is a TME factor known to promote cell migration and metastasis (103). HGF has also been shown to activate p38 MAPK (104). Given the requirement of p38 MAPK for TNBC motility, we tested the ability of HGF to induce regulated GR phosphorylation (105). Thus, MDA-MB-231 cells were treated with 50 ng/mL HGF for 0.5-48 hrs. Robust and persistent phosphorylation of GR S134 was observed after 1-2 hrs (Figure 3.3E and Figure 3.4F). These findings suggest that the TME induces ligand-independent GR S134 phosphorylation, nominating GR as an important sensor not only of host/life stress in the form of elevated corticosteroid levels, but for both cellular and local (i.e. TME-derived) cytokine-mediated stress signaling in TNBC cells.

To test the requirement for GR S134 in TGFβ1-regulated TNBC cell migration, we employed a CRISPR/Cas9 approach to create MDA-MB-231 cells expressing either wt-GR (control) or a point mutant GR in which S134 has been changed to Alanine (S134A-GR clone #1 and clone #2). We confirmed expression of either endogenous wt or S134A-GR via western blotting following treatment of cells with 10ng/mL of TGFβ1. Predictably, we observed equal levels of total GR in all cell lines, but no signal representing GR S134 phosphorylation in TNBC cells harboring S134A-GR (Figure 3.5A). Using MTT assays as a readout of cell viability and proliferation, we compared wt-GR and S134A-GR cell lines; cells harboring S134A GR remained viable and proliferated at similar rates relative to wt-GR+ controls (Day 1). However, CRISPR knock-in of S134A GR

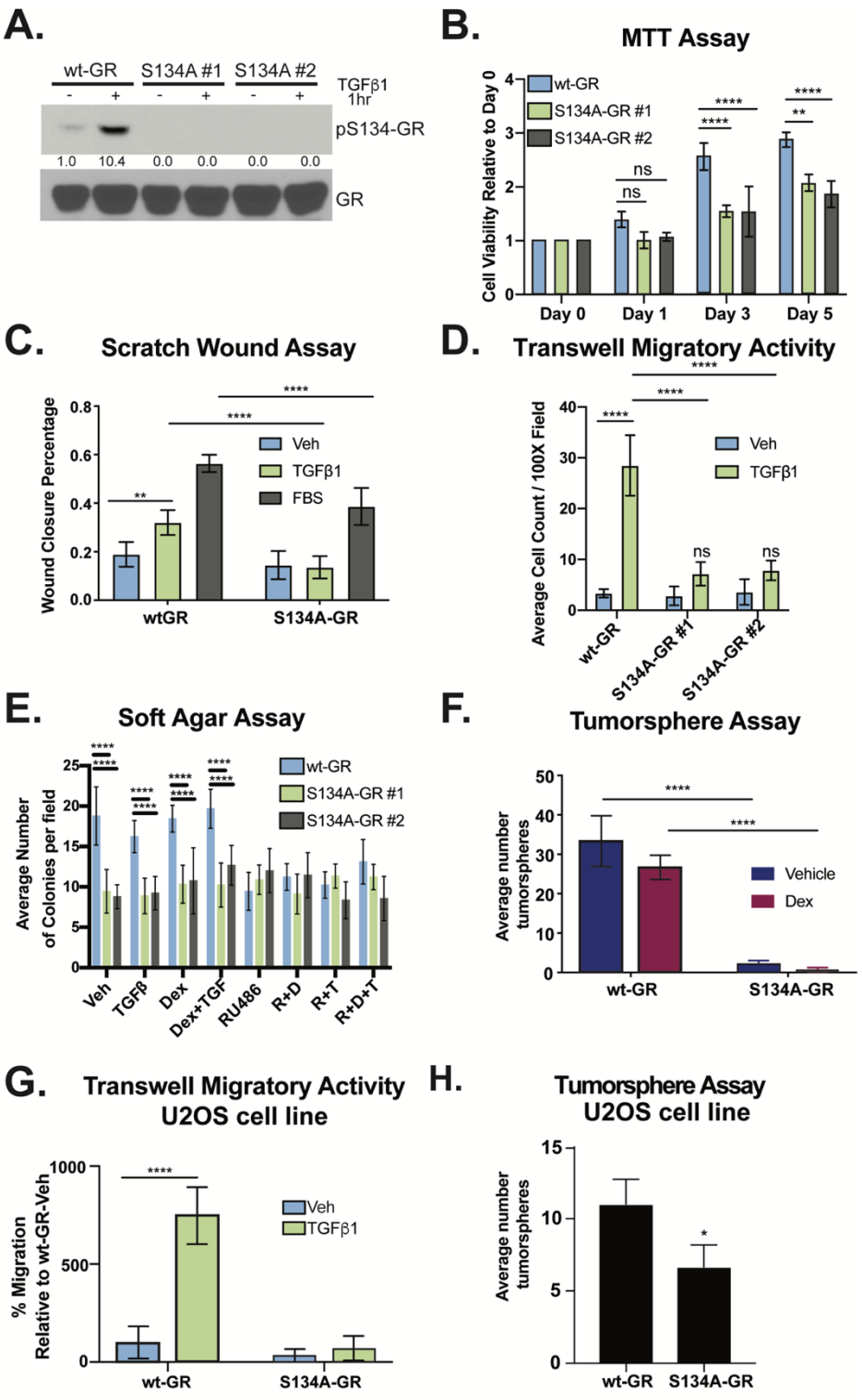

Figure 3.5 GR S134 is required for TGFβ1-mediated migration of TNBC cells.

(A) Phosphorylation of GR at S134 by 10ng/mL of TGFβ1 in wt-GR and S134A-GR MDA-MB-231 CRISPR models was examined by Western blot. Densitometry values of the pS134-GR levels are

indicated relative to vehicle-control. **(B)** Proliferation of MDA-MB-231 cells expressing either wt-GR or S134A-GR was examined using MTT growth assays. The mean of three biological replicates ± SD is shown. **(C)** MDA-MB-231 cells expressing either wt-GR or S134A-GR clone #1 were treated with veh, 10 ng/mL TGFβ1, or 10% FBS overnight and then analyzed by scratch wound assay. Cells were exposed to respective treatments during the course of the migration assay to stimulate migration. The fraction of wound area closure was determined by tracing images in ImageJ. The mean of three field images from each of the three biological replicates is shown ± SD. Significance was assessed by Two-way ANOVA and Tukey post-hoc for comparison within groups (**, $P < 0.01$ and ****, $P < 0.0001$). **(D)** Transwell migration assays were used to test the migratory activity of wt-GR and S134A-GR (clone #1 and clone #2) MDA-MB-231 cells with either vehicle or TGFβ1 (10 ng/mL) as the chemoattractant in the bottom chamber. Cells were allowed to migrate for 18 hrs. The mean of three biological replicates is shown ± SD. Significance was assessed by Two-way ANOVA and Tukey post-hoc for comparison within groups (****, $P < 0.0001$). **(E)** Soft-agar colony formation assays were used to test the effect of TGFβ1, Dex, RU486, and their respective combinatorial treatment on MDA-MB-231 cells expressing either wt-GR or S134A-GR (clone #1 and clone #2). The mean of four field images from each of the three biological replicates is shown ± SD. Significance was assessed by Two-way ANOVA and Tukey post-hoc for comparison within groups relative to veh wt-GR cells (****, $P < 0.0001$). **(F)** Secondary tumorsphere of wt-GR or S134A-GR MDA-MB-231 cells. Cells were treated with either Vehicle or 1μM Dex. Data are presented as the average ± SD of three biological replicates. Significance was assessed by Two-way ANOVA and Tukey post-hoc for comparison within groups (****, $P < 0.0001$). **(G)** Transwell migration assays were used to test the migratory activity of U2OS cells expressing either wt-GR or S134A-GR with either vehicle or 10 ng/mL TGFβ as the chemoattractant. The mean of the percentage of three biological replicates is shown ± SD. Significance was assessed by Two-way ANOVA and Tukey post-hoc for comparison within groups (****, $P < 0.0001$). **(H)** Secondary tumorsphere of wt-GR or S134A-GR U2OS cells. No treatment was added. Data are presented as the average ± SD of three biological replicates. Statistical significance was assessed by unpaired Student's t-test (*, $P < 0.05$).

resulted in reduced cell numbers evident at days 3-5 relative to wt-GR+ controls (Figure 3.5B). The migration of these models in response to 10 ng/mL TGFβ1 (18 hrs) was then measured using scratch wound assays. Fetal Bovine Serum (FBS) (10%) was included as a positive control that contains multiple soluble factors capable of stimulating cancer cell migration. Cells harboring either wt-GR or S134A-GR (clone #1) were pretreated with vehicle control, 10 ng/mL TGFβ1, or 10% FBS overnight; cells were then subjected to scratch wounds, re-treated with their respective treatments and allowed to migrate for 18 hrs. TGFβ1-mediated migration was significantly impaired in cells expressing S134A-GR (Figure 3.5C) relative to wt-GR. These findings were replicated in transwell migration assays (Figure 3.5D). Migration was stimulated with either vehicle or 10 ng/mL TGFβ1 as the chemoattractant (i.e. added to the bottom chamber). Again, robust TGFβ1-induced migratory activity occurred in wt-GR cells cultured in steroid hormone-free media lacking exogenously added GR ligands (i.e. Dex). However, cells harboring S134A-GR (i.e. two independent CRISPR clones) were significantly less migratory (18 hrs) relative to cells harboring wt-GR (Figure 3.5D). Similarly, we tested the invasive ability of wt-GR and S134A-GR clones. Cells were seeded and allowed to invade through Matrigel inserts towards either vehicle or 10 ng/mL TGFβ1 as the chemoattractant. Predictably, the invasive ability of both S134A GR clones was significantly impaired relative to cells expressing wt-GR (Figure 3.6).

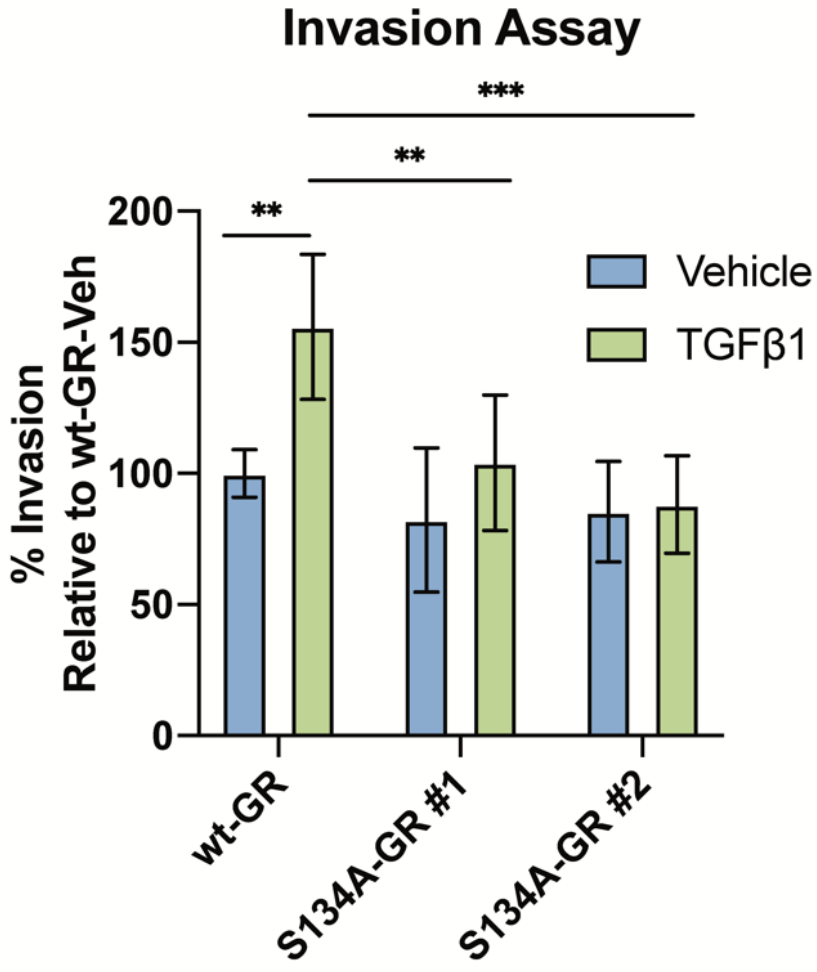

Figure 3.6 Invasive ability of MDA-MB-231 cells.

Cells were plated and allowed to invade through Matrigel transwell for approximately 18 hrs with either vehicle or 10 ng/mL of TGFβ1.

Anchorage independent growth in soft agar (i.e. an *in vitro* measure of cell transformation) is a hallmark of cancer cells that is indicative of the ability to grow and survive independently of basement membrane attachment. TNBC cells expressing S134A-GR exhibited impaired soft-agar colony formation relative to cells expressing wt-GR (Figure 3.5E). TNBC cells harboring wt-GR, but not S134A-GR (two clones), formed colonies in media containing steroid hormone-free fetal bovine serum (DCC) with either vehicle control or GR-agonists (e.g. Dex). However, while Dex or TGFβ1 did not appreciably increase basal soft-agar colony formation over that observed in DCC alone, the GR antagonist, RU486, blocked soft-agar colony formation, demonstrating the GR-dependence of this cancer cell biology in 3D conditions (Figure 3.5E). Similar results were observed in tumorsphere assays in which TNBC cells were plated at limiting dilution in ultra-low attachment dishes as an *in vitro* readout of cancer stem-like cell behavior (106); while addition of Dex to sphere media was without effect, MDA-MB-231 cells harboring S134A mutant GR failed to form tumorspheres relative to cells expressing endogenous wt-GR (Figure 3.5F). Impaired cell migration as measured by chemotaxis in transwell migration assays (Figure 3.5G) as well as attenuated tumorsphere formation (Figure 3.5H) were also observed using the previously described GR-null/low U2OS osteosarcoma cell line engineered to stably express S134A-GR relative to wt-GR (33). These data demonstrate that pS134-GR is critical for TGFβ-mediated cell migration and basal growth in suspension/3D (anchorage-independent growth and tumorsphere formation), even in the absence of exogenously added GR agonists.

The pS134-GR binding partner, 14-3-3ζ mediates TNBC cell migration

14-3-3 proteins are a conserved family of regulatory molecules that bind to diverse signaling proteins in eukaryotic cells. Galliher-Beckley et. al, first reported that 14-3-3ζ interacts with GR in a pS134-GR-dependent manner in U2OS osteosarcoma cells (33). To evaluate the role of 14-3-3ζ in GR+ TNBC, we probed 14-3-3ζ mRNA expression levels across breast cancer subtypes in the TCGA dataset and stratified patients based on the expression levels of ER, PR and HER2 receptors as determined by clinical immunohistochemistry analyses of primary tumors. Data from METABRIC were obtained from cBioPortal. The expression of 14-3-3ζ mRNA in patients with ER-/HER2- (TNBC) or Her2+ breast cancer was higher when compared to patients with ER+/HER2- breast cancer (Figure 3.7A). Similarly, high levels of 14-3-3ζ mRNA, as separated by the median cutoff of mRNA expression, correlate with poor overall survival in patients within the METABRIC cohort (Figure 3.7B). Accordingly, we observed abundant expression of 14-3-3ζ in several breast cancer cells lines, including MDA-MB-231, Hs578T and MDA-MB-468 (TNBC) cells as well as U2OS osteosarcoma cells (positive control). Weak 14-3-3ζ expression was observed in non-tumorigenic MCF10A cells (Figure 3.7C). To test the requirement for 14-3-3ζ in TGFβ1-mediated migration, we generated MDA-MB-231 cells stably expressing two distinct 14-3-3ζ-targeted shRNAs or a non-targeting vector control (shcontrol); 14-3-3ζ knockdown was confirmed in two separate pools by Western blotting (Figure 3.7D; upper panel). TGFβ1 induced robust cell migration in shcontrol but not sh14-3-3ζ TNBC models (Figure 3.7D). We confirmed that

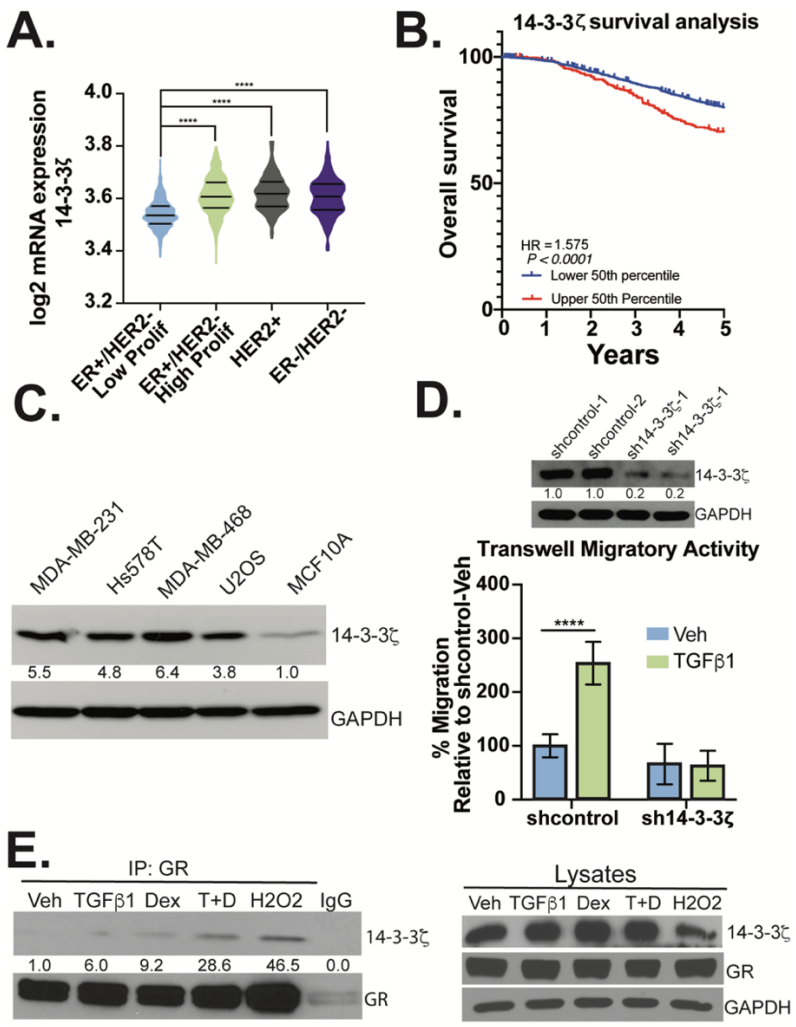

Figure 3.7 14-3-3ζ is required for TGFβ1-induced TNBC cell migration.

(A) Expression of 14-3-3ζ in breast cancer patients was analyzed using the METABRIC database (n=1700). Significance was assessed by One-way ANOVA and Tukey post-hoc for comparison between groups (****, $P < 0.0001$). **(B)** Survival Analysis for patients from the METABRIC cohort and with mRNA microarray profiling for 14-3-3ζ were stratified into two groups: expression higher than median mRNA expression of 14-3-3ζ (Upper 50th percentile) or lower than median (Bottom 50th percentile). The results were analyzed for significance with a logrank p-value of $P < 0.0001$ (n=1981). **(C)** Western blot analysis for 14-3-3ζ of different cell lines indicated. Densitometry values for the 14-3-3ζ levels are indicated relative to non-tumorigenic MCF10A cells. **(D)** Western blot analysis of 14-3-3ζ protein levels in MDA-MB-231 cells expressing either shcontrol or sh-14-3-3ζ; two pools of each respective shcontrol are shown. Densitometry values for the 14-3-3ζ levels are shown relative to shcontrol #1. Transwell migration assays were used to test the migratory activity of shcontrol and sh14-3-3ζ MDA-MB-231 cells. TGFβ1 (10 ng/mL) was used as the chemoattractant and cells were allowed to migrate for 18 hrs. The mean of three independent biological replicate experiments is shown ± SD. Statistical significance was assessed by Two-way ANOVA and Tukey post-hoc corrections (****, $P < 0.0001$). **(E)** Western blot analysis was performed on immunocomplexes and whole-cell lysates to evaluate the interaction of 14-3-3ζ with GR in response to vet, TGFβ1 (10 ng/mL), Dex (1μM), TGFβ1+Dex and H_2O_2 (100μM; positive control for GR phosphorylation). Densitometry values for the 14-3-3ζ levels in the GR IP groups are shown relative to vehicle-control. IgG was used as a negative control.

14-3-3ζ/GR interaction occurs in TNBC models (Figure 3.7E); MDA-MB-231 cells were subjected to treatment with either veh, TGFβ1, Dex, TGFβ1+Dex or H_2O_2 (a potent inducer of GR S134 phosphorylation). Similar to that observed in H2O2-treated U2OS osteosarcoma cells (33) co-immunoprecipitation assays revealed modest TGFβ or Dex-regulated interaction between GR and 14-3-3ζ that was further enhanced following combinatorial treatment of cells with both TGFβ1 and Dex. These data suggest that 14-3-3ζ and pS134-GR function in the same signaling pathway and/or cooperate to induce altered gene expression and subsequent migration of TGFβ1-responsive TNBC cells.

The GR transcriptome implicates MAPK-driven signaling in TNBC migration

Our data suggest that significant ligand-independent gene expression occurs via phosphorylation of GR S134. To further expand our understanding of the impact of pS134-GR on TNBC cell behavior, we performed RNA-seq studies in MDA-MB-231 cells expressing either wt-GR or S134A-GR (clone #1). Cells were treated with either vehicle, to capture basal homeostatic (i.e. ligand-independent) GR actions or with TGFβ1, as a regulated input to p38 MAPK activation and subsequent GR phosphorylation (6 hrs). Principal component analysis demonstrated intrinsic differences between both vehicle-treated and TGFβ1-treated models (Figure 3.8A). Remarkably, in the absence of a specific stimulus, the basal transcriptome of cells expressing S134A GR differs dramatically from that of cells expressing wt-GR. These data suggest that GR S134 acts as a homeostatic “sensor” of numerous cell-intrinsic and -extrinsic

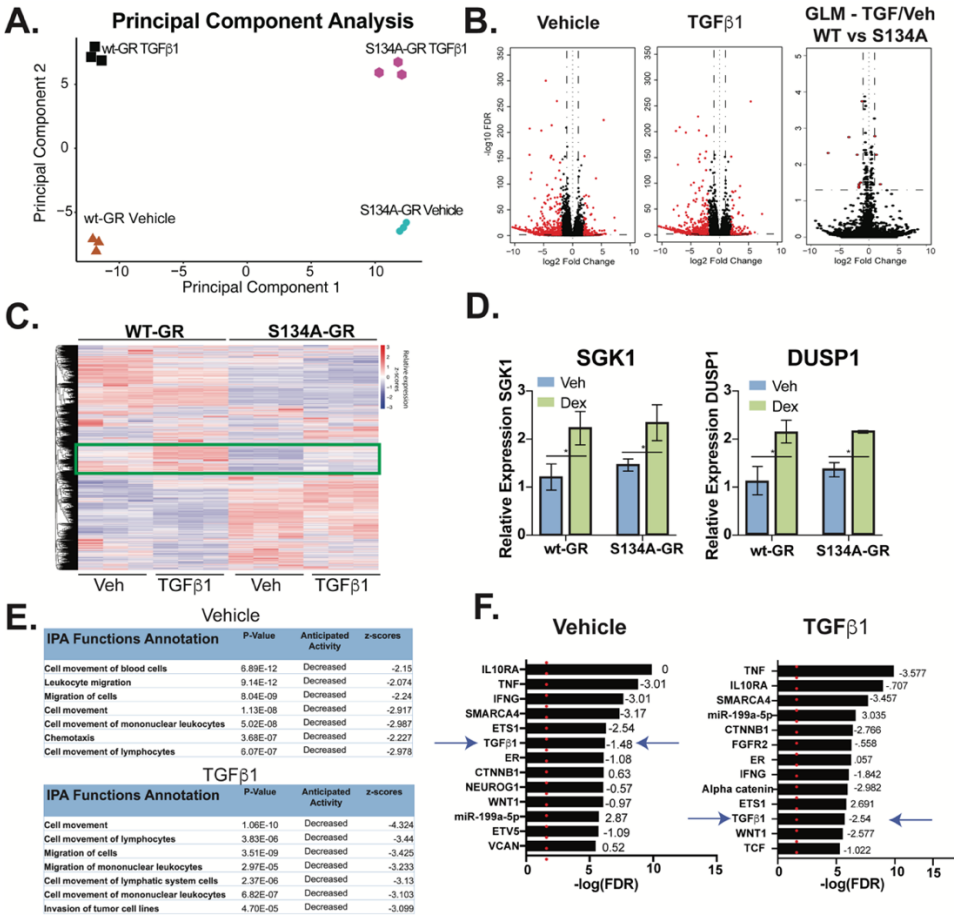

Figure 3.8 WT vs. pS134-GR transcriptomes in TGFβ1-treated MDA-MB-231 cells.

(A) Principal component analysis plot derived from RNA-seq shows the differences in transcriptomes between MDA-MB-231 cells expressing either WT or S134A-GR cells and treated with vehicle or 10 ng/mL TGFβ for 6 hrs. **(B)** Volcano plot showing differential expression of genes in wt-GR+ compared to S134A-GR+ TNBC cells treated for 6 hrs with either Vehicle (left) or 10 ng/mL of TGFβ1 (middle). Volcano plot using the generalized linear model approach in EdgeR (comparisons of wt-GR and S134A-GR in response to TGF) to illustrate the effects of TGFβ1 treatment of cells expressing wt-GR relative to cells expressing S134A-GR (right). Red dots indicate genes with an absolute log fold-change of 1.0 or more and a false discovery rate of less than .05. Genes for GLM are detailed in Table 3.1A **(C)** Supervised heatmap shows significant differences in gene expression as measured by RNA-seq in TGFβ1-treated MDA-MB-231 cells expressing either wt-GR or S134A-GR. Rectangle indicates a cluster of interest in which genes are upregulated in response to TGFβ1 in wt-GR cells but not in the S134A-GR cells. All genes that were used for differential expression analysis are represented in this heatmap (n=19,760). **(D)** *DUSP1* and SGK1 mRNA levels in were assessed using qRT-PCR following normalization to *18S* expression. Mean expression of three independent replicates ± SD is shown. **(E)** Cell function and mechanism analyses of pathways via IPA of differentially expressed genes with an absolute log fold-change of 1.5 or more and a p-adjusted value of less than .05 in wt-GR relative to S134A-GR TNBC cells treated for 6 hrs with either Vehicle or TGFβ1 (10 ng/mL). **(F)** Upstream regulator analyses via IPA of differentially expressed genes with an absolute log fold-change of 1.5 or more and a p-adjusted value of less than .05 in wt-GR relative to S134A-GR TNBC cells treated with wither Vehicle or 10 ng/mL of TGFβ1. Activation/inhibition z-scores are shown as well. Red dotted line indicates the significance value of 1.3 ($P < .05$).

signaling inputs to p38 MAPK, accounting for significant ligand-independent or "basal" differences between vehicle treated models. Volcano plots were used to further illustrate the effect of S134A-GR single point mutation in vehicle or TGFβ1-treated cells. Namely, vehicle-treated models clearly exhibited a broad array of transcription-wide differences, while fewer changes in mRNA expression were attributed to TGFβ1 treatment between wt and S134A GR+ models, as measured using the generalized linear model framework (GLM) in EdgeR (Figure 3.8B). GLM analysis identified a limited number of differentially expressed genes in response to TGFβ1 when comparing wt-GR+ and S134A-GR+ models. Notably, *LEFTY1*, *COL1A1*, and *OLFM2*, known mediators of TGFβ signaling, were identified as differentially expressed (red dots) using the GLM approach (Table 3.1A) (107, 108). Ingenuity Pathway Analysis (IPA) of this limited gene subset identified ERBB2 as well as TGFBR1/TGFβ1 (i.e. both receptor and cognate ligand) signaling as potential S134A GR-regulated pathways (Table 3.1B). Consistent with these results, comparison of the response to TGFβ1 between wt and S134A GR models also revealed a subset of ~80 TGFβ1-induced genes in cells harboring wt-GR that were not regulated by TGFβ1 in cells expressing S134A-GR (Figure 3.8C green rectangle and Figure 3.9A). Importantly, ligand-dependent GR activation (i.e. in Dex-treated cells) remained similar across these models as measured by qPCR analysis of two well-characterized GR-target gene (DUSP1 and SGK1) mRNAs, indicating that ligand-bound S134A-GR is not transcriptionally impaired (Figure 3.8D). Further studies are needed to evaluate the role of S134 in the global transcriptional

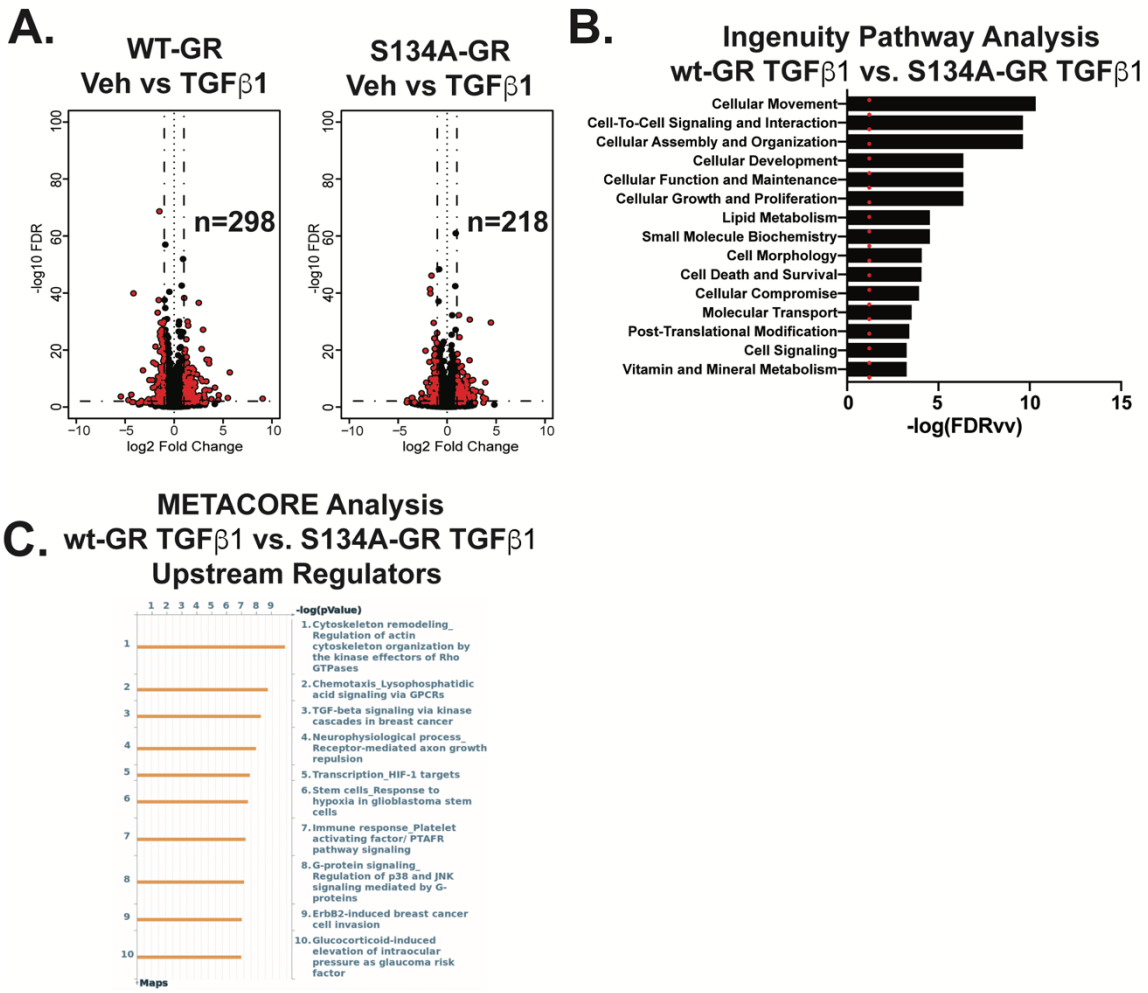

Figure 3.9 GR regulates the expression of cell movement related pathways.

(A) Volcano plot showing differential expression of genes in wt-GR+ and S134A-GR+ TNBC cells treated for 6 hrs with 10 ng/mL of TGFβ1. The number for differentially expressed upregulated genes is included (absolute log2 fold-change of 1 and a p-adj (Benjamini-Hochberg) <0.05). **(B)** IPA migration-related pathways in wt-GR vs S134A-GR cells treated with TGFβ (10 ng/mL); p-values and activation z-scores are indicated for each pathway. Genes included for this analysis are based on the following criteria: absolute log2 fold-change of 1.5 and a p-adj (Benjamini-Hochberg) <0.05. **(C)** Upstream regulators analysis via METACORE of genes that are compared between wt-GR and S134A-GR

A.

genes	logFC	FDR
COL1A1	-1.1680655	0.0001812
TNS4	1.03991074	0.00166555
LEFTY1	-3.4550619	0.00176006
STK19	-7.0604605	0.00479633
NEDD9	1.30523842	0.00536703
OLFM2	-2.0155828	0.00536703
ABAT	-1.4135953	0.03116907
KRT16	-1.6887167	0.03466654
EDN2	1.99562278	0.03466654
NLRC3	-1.7209648	0.03972399
RRAD	-1.7179054	0.04303584

B.

Upstream Regulator	p-value of overlap
ERBB2	0.0000199
LHX2	0.0000737
Brd4	0.000244
Tgf beta	0.000358
TBP	0.000496
miR-199a-5p	0.000604
TGFBR1	0.000853
Vegf Receptor	0.001
COLGALT1	0.001
TRAM2	0.001

Table 3.1 Ingenuity Pathway Analysis of GLM approach to compare responsiveness to TGFβ1 for wt-GR and S134A-GR cells.

(A) Differentially expressed genes with their respective false discovery rate and log2 fold change as retrieved from our EdgeR analysis for Figure 3.8B (right). Red rectangles indicate TGFβ1-regulated genes. **(B)** Genes included for IPA analysis are based on the following criteria: absolute log2 fold-change of 1.0 and a p-adj (Benjamini-Hochberg) <0.05. Because of the limited number of genes, no predictive z-score was reported by IPA.

response of liganded GR. Ingenuity Pathway Analysis and Gene Set Enrichment Analysis (GSEA) tools were then used to evaluate the impact of GR S134 modification on ligand-independent basal (vet) and TGFβ1-induced cellular pathways/behaviors. IPA analysis revealed that cellular migration is strongly represented in the genes that are primarily regulated in cells expressing wt-GR, but not in cells expressing S134A GR (i.e. gene sets associated with cell migration are decreased in S134A-GR TNBC cells regardless of treatment; Figure 3.8E and Figure 3.9B). This finding further strengthens our hypothesis that phosphorylation of GR on S134 is critical for migration of TNBC cells. Interestingly, the TGFβ1 pathway itself is significantly downregulated in S134A-GR cells, and consistent with these results, this is also readily apparent in TGFβ1-treated cells, as was independently identified via both the upstream regulator analysis in the IPA platform and METACORE (Figure 3.8F and Figure 3.9C). In sum, the transcriptomes of cells harboring either wt-GR or S134A-GR are remarkably different basally, perhaps because GR S134 acts as an important ligand-independent sensor of multiple homeostatic intrinsic (basal) and extrinsic (TME-derived factors) cellular stress inputs to the p38 MAPK pathway (33, 86).

Using GSEA analysis for the Kyoto Encyclopedia of Genes and Genomes (KEGG) pathways study, we identified the MAPK pathway as significantly downregulated in cells harboring S134A-GR (Figure 3.10A and Table 3.2). Interestingly, we found that there are also basal differences in the MAPK KEGG module (Figure 3.10A). This indicates that one or more key components of the

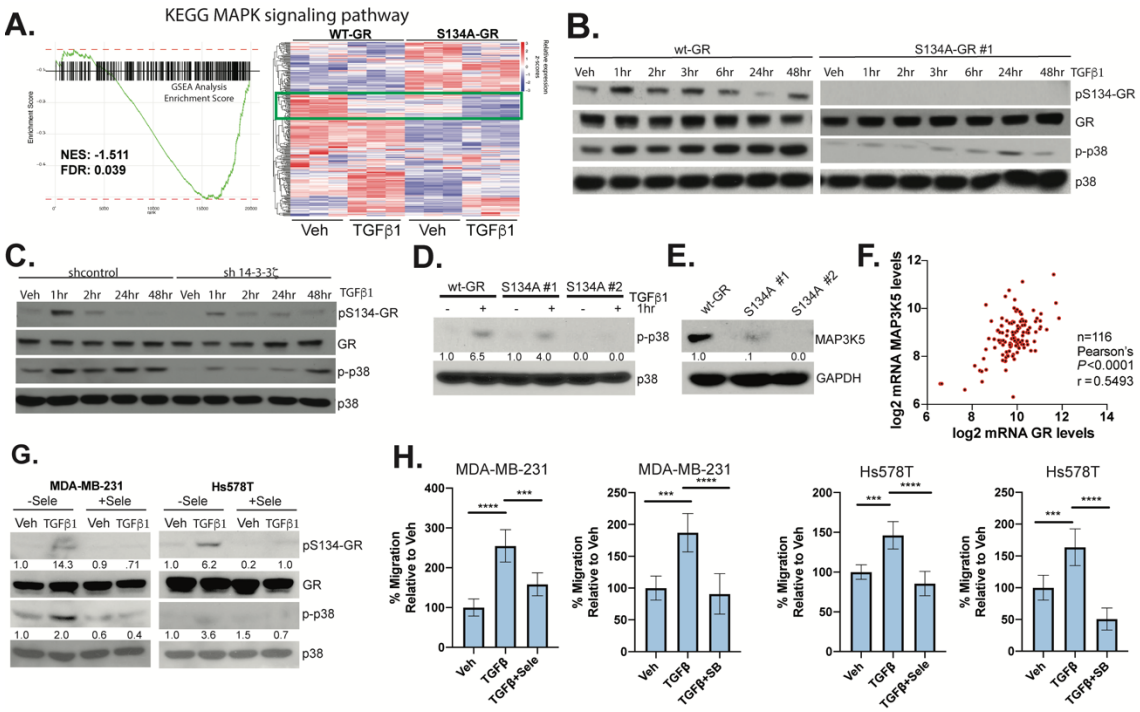

Figure 3.10 Phosphorylation of GR S134 is critical for MAPK signaling.

(A) Gene Set Enrichment Analysis and associated MAPK gene heat map reveal a dramatic loss of expression of genes important for MAPK signaling in TNBC cells expressing S134A-GR compared to wt-GR. **(B)** Representative Western blot analysis of pS134-GR, total GR, p-p38 and total p38 protein levels (loading control) in MDA-MB-231 cells expressing either wt-GR or S134A GR clone #1 (upper panel), and **(C)** either shcontrol or sh-14-3-3ζ . Cells were treated with 10 ng/mL TGFβ1 at the indicated timepoints. Representative experiments of at least three independent repeats are shown. **(D)** WT-GR or S134A GR clone #1 and clone #2 were treated with 10ng/mL TGFβ1 to confirm previous findings with regards to p38 MAPK phosphorylation. Densitometry values for the p-p38 levels are shown relative to vehicle-control in wt-GR. **(E)** MAP3K5 protein expression is shown for wt-GR, S134A clone #1 and S134A clone #2. Densitometry values for the MAP3K5 levels are shown relative to wt-GR. **(F)** TCGA normalized data was log2 transformed for TNBC patients. Correlation between MAP3K5 and GR was calculated by Pearson's correlation. **(G)** Western blot analysis of pS134-GR, total GR, p-p38, and total p38 in MDA-MB-231 cells pre-treated with either 10μM Selonsertib (MAP3K5) or DMSO control for 30 mins followed by either vehicle control or 10 ng/mL of TGF for 1hr. Total p38 serves as a loading control. Densitometry values for pS134-GR and p-p38 levels are indicated relative to vehicle-control of each cell line. **(H)** Transwell migration assays were used to test the migratory activity of MDA-MB-231 cells in response using either vehicle or TGFβ1 (10 ng/mL) as the chemoattractant in the bottom chamber. Additionally, cells were treated with either 10μM SB203580 (SB) or 10μM Selonsertib (Sele) in both the upper and lower chamber. Cells were allowed to migrate for 18 hrs. The mean of the percentage of three biological replicates is shown ± SD. Significance was assessed by Two-way ANOVA and Tukey post-hoc for comparison within groups (***, $P < 0.001$,****, $P < 0.0001$).

Pathway	pvalue	padj	NES
KEGG_REGULATION_OF_ACTIN_CYTOSKELETON	0.001217	0.024128	-1.60409
KEGG_LONG_TERM_POTENTIATION	0.001453	0.024128	-1.67508
KEGG_FATTY_ACID_METABOLISM	0.001585	0.024128	-1.74649
KEGG_RENAL_CELL_CARCINOMA	0.001441	0.024128	-1.80565
KEGG_CITRATE_CYCLE_TCA_CYCLE	0.00161	0.024128	-1.80927
KEGG_PROPANOATE_METABOLISM	0.001587	0.024128	-1.81435
KEGG_ACUTE_MYELOID_LEUKEMIA	0.001481	0.024128	-1.82204
KEGG_PPAR_SIGNALING_PATHWAY	0.001479	0.024128	-1.84088
KEGG_ASCORBATE_AND_ALDARATE_METABOLISM	0.001686	0.024128	-1.86282
KEGG_PATHOGENIC_ESCHERICHIA_COLI_INFECTION	0.001481	0.024128	-1.86462
KEGG_PYRUVATE_METABOLISM	0.001595	0.024128	-1.88159
KEGG_GLYCOLYSIS_GLUCONEOGENESIS	0.001477	0.024128	-1.89576
KEGG_RIBOSOME	0.001393	0.024128	-1.91921
KEGG_PATHWAYS_IN_CANCER	0.002257	0.029245	-1.47133
KEGG_MAPK_SIGNALING_PATHWAY	0.002358	0.029245	-1.51255
KEGG_TRYPTOPHAN_METABOLISM	0.003221	0.035237	-1.64188
KEGG_BIOSYNTHESIS_OF_UNSATURATED_FATTY_ACIDS	0.003221	0.035237	-1.87253
KEGG_PANCREATIC_CANCER	0.004354	0.040493	-1.60844
KEGG_LEUKOCYTE_TRANSENDOTHELIAL_MIGRATION	0.004011	0.040493	-1.6705
KEGG_ADHERENS_JUNCTION	0.004202	0.040493	-1.68157

Table 3.2 pS134-GR regulates pathways related to cell migration and other advanced cancer behaviors.

The top 15 pathways identified in the GSEA analyses for the KEGG molecular signatures are shown with p-values and respective FDR, determined by the R fgsea package.

MAPK pathway are likely to be regulated by GR S134 phosphorylation. Indeed, TGFβ1-induced activation of p38 MAPK, as measured by via active-site phosphorylation, appears to be arrested in cells expressing S134A GR relative to cells expressing wt-GR (Figure 3.10B and see densitometric analyses of aggregated data from multiple repeats in Figure 3.11A). Similarly, 14-3-3ζ knock-down resulted in greatly decreased TGFβ1-induced p38 activation with no change in total p38 expression levels (Figure 3.10C and see densitometric analyses of aggregated data from multiple repeats in Figure 3.11B). Consequently, sh14-3-3ζ cells also exhibited less pS134-GR. To confirm these findings, we tested for phosphorylation of p38 MAPK in response to TGFβ1 and found that it is greatly attenuated in both S134A GR+ clones (Figure 3.10D). These data suggest that pS134-GR is an important regulator of one or more kinases upstream of p38 MAPK (i.e. that are required for p38 activation). We thus probed our RNA-seq data within the MAPK pathway KEGG signature, thereby nominating the mitogen-activated protein kinase kinase kinase 5 (MAP3K5, also called MEKK5 or ASK1) as a possible factor that integrates these pathways. MAP3K5 interacts with 14-3-3ζ to facilitate activation of downstream kinases MEK3/6 and p38 MAPK (109). Indeed, MAPK3K5 protein levels were significantly downregulated in two clones harboring S134A-GR relative to wt-GR (Figure 3.10E). Moreover, in an independent experiment using S134A-GR clone #1, we observed downregulation of MAP3K5 at both the mRNA and protein levels (Figure 3.11C). Although known to be associated with other cancer types, to our knowledge, MAP3K5 has not been implicated in breast cancer. Similar to

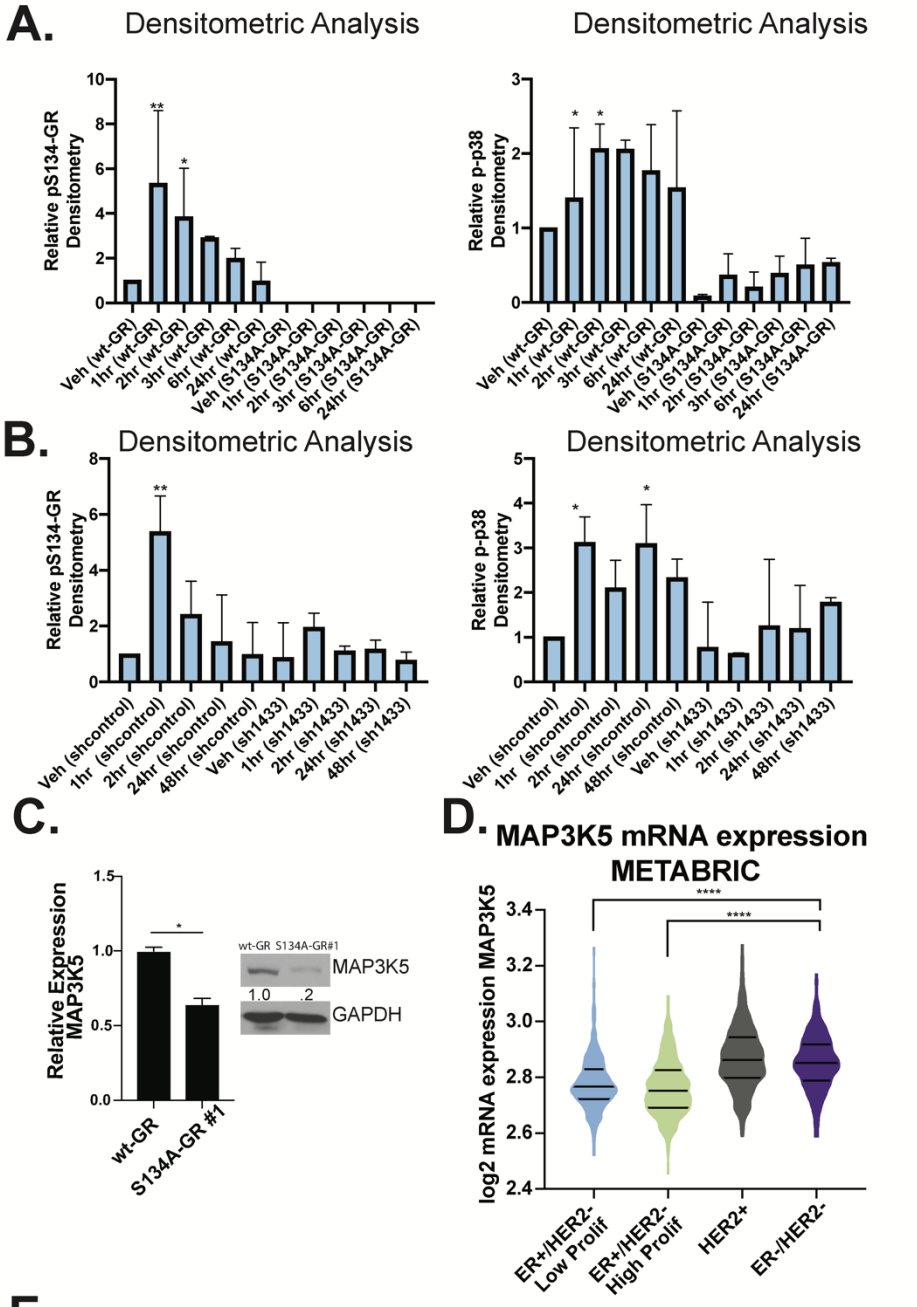
A.
Densitometric Analysis
Relative pS134-GR Densitometry
Veh (wt-GR)
1hr (wt-GR)
2hr (wt-GR)
3hr (wt-GR)
6hr (wt-GR)
24hr (wt-GR)
Veh (S134A-GR)
1hr (S134A-GR)
2hr (S134A-GR)
3hr (S134A-GR)
6hr (S134A-GR)
24hr (S134A-GR)
Densitometric Analysis
Relative p-p38 Densitometry
B.
Densitometric Analysis
Relative pS134-GR Densitometry
Veh (shcontrol)
1hr (shcontrol)
2hr (shcontrol)
24hr (shcontrol)
48hr (shcontrol)
Veh (sh1433)
1hr (sh1433)
2hr (sh1433)
24hr (sh1433)
48hr (sh1433)
Densitometric Analysis
Relative p-p38 Densitometry
C.
Relative Expression MAP3K5
wt-GR
S134A-GR #1
wt-GR S134A-GR#1
MAP3K5
1.0 .2
GAPDH
D.
MAP3K5 mRNA expression
METABRIC
log2 mRNA expression MAP3K5
ER+/HER2- Low Prolif
ER+/HER2- High Prolif
HER2+
ER-/HER2-
E.
wt-GR
S134A-GR
Veh .5 1 2 Veh .5 1 2 TGFβ1
pERK 1/2
1.0 0.8 0.8 0.7 1.0 0.9 0.9 1.3
ERK 1/2
wt-GR
S134A-GR
Veh .5 1 2 Veh .5 1 2 TGFβ1
pJNK
1.0 1.2 2.7 1.6 3.7 3.4 5.9 4.0
JNK
F.
wtGR
S134A-GR #1
S134A-GR #2
Veh 1hr 2hr 3hr 6hr 24hr Veh 1hr 2hr 3hr 6hr 24hr Veh 1hr 2hr 3hr 6hr 24hr TGFβ1
pSMAD2
1.0 333.6 261.1 93.0 96.5 152.2 9.7 205.8 127.6 72.5 30.0 40.5 6.4 289 111.7 118.1 88.0 56.9
SMAD2

Figure 3.11 MAP3K5 expression is elevated in TNBC relative to other breast cancer subtypes.

(A) Densitometric analysis for pS134-GR levels and p-p38 levels of two independents experiments representative of Figure 3.10B. Values are relative to the vehicle-control of the wt-GR group and are presented as the mean ± SEM. One-way ANOVA and Fisher's LSD test posthoc were used to evaluate statistical significance (*, $P < 0.05$, **, $P < 0.01$). **(B)** Densitometric analysis for pS134-GR levels and p-p38 levels of two independents experiments representative of Figure 3.10C. Values are relative to the vehicle-control of the shcontrol vehicle group and are presented as the mean ± SEM. One-way ANOVA and Fisher's LSD test posthoc were used to evaluate statistical significance (*, $P < 0.05$, **, $P < 0.01$). **(C)** *MAP3K5* mRNA levels were assessed using qRT-PCR following normalization to *TBP* expression; inset shows MAP3K5 protein expression (densitometric levels relative to wt-GR). Mean expression of three independent replicates ± SD is shown. **(D)** Relative mRNA expression of MAP3K5 in different breast cancer subtypes from the METABRIC cohort (n=1700). One-way ANOVA and Tukey post-hoc corrections were used to evaluate statistical significance (****, $P < 0.0001$). **(E)** pERK1/2 and pJNK levels were assessed as well as total ERK1/2 and JNK levels. Timepoints are shown for 10ng/mL of TGFβ1 treatment. Densitometric levels for pS134-GR are shown relative to vehicle-control. **(F)** Western blot analysis of pSMAD2 and SMAD2 levels in MDA-MB-231 cells treated with 10ng/mL of TGFβ1. Densitometric values for phospho-SMAD2 are indicated relative to vehicle-control in wt-GR+ cells.

expression of pS134-GR and 14-3-3ζ (above), MAP3K5 mRNA levels are elevated in TNBC relative to other breast cancer subtypes represented in the METABRIC (Figure 3.11D) and MAP3K5 and GR mRNA expression levels are strongly correlated in TNBC patients (Figure 3.10F) (86). Notably, inhibition of MAP3K5 with the selective inhibitor, Selonsertib, blocked phosphorylation of GR (Figure 3.10G) and inhibited TGFβ1-induced migration (Figure 3.10H) in both MDA-MB-231 and Hs578T cells. Similarly, inhibition of p38 MAPK using SB203580, halted TGFβ1-mediated migration in both TNBC models (Figure 3.10H). Taken together these results indicate that phosphorylation of GR on S134 is critical for the expression of key MAPK pathway intermediates. Specificity controls indicated that serum-induced activation of JNK and p42/p44 MAPKs (ERK1/2) were unaffected in TNBC cells harboring S134A GR (Figure 3.11E), suggesting that pS134-GR is a highly selective regulator of the p38 MAPK "module" characterized by the three kinase cascade initiated by MAP3K5 in TNBC cells. While the TGFβ1-induced activation of SMADs is thought to occur independently of p38 MAPK, we observed a slight attenuation of TGFβ1-induced SMAD2 phosphorylation (i.e. primarily apparent after 2 hrs) in cells harboring S134A-GR (Figure 3.11F). These data suggest that pS134-GR may potentiate sustained SMAD2 phosphorylation and activation, perhaps in part via regulation of the signaling components required for intact p38 MAPK signaling (Figure 3.10). Further studies are needed to address weather GR crosstalk with the TGFβ1 signaling occurs at the level of SMAD regulation.

Liganded global transcription is altered in S134 GR mutant cells

To interrogate transcriptional consequences of liganded GR S134 mutation, cells containing either WT or S134A GR were treated with vet or Dex (1 μM) for 6 hours and processed for RNA-seq. As seen previously, hierarchical clustering revealed differences in basal (irrespective of ligand) gene expression between the models (Figure 3.12A). Principal component analysis determined 47% of the variance between samples was due to GR status (Figure 3.12B). In contrast, 38% of variance was because of differences in the Dex-stimulated transcriptome of these two models (Figure 3.12A, B) as visualized by cluster 3. Differential expression analysis revealed a large number of genes that were lost in S134A + Dex samples compared to wild-type + Dex (Figure 3.12C). A total of 80 genes, were differentially expressed when treating wt-GR models with Dex. Notably, these genes were exclusively upregulated in the context of wt-GR but not S134A GR.

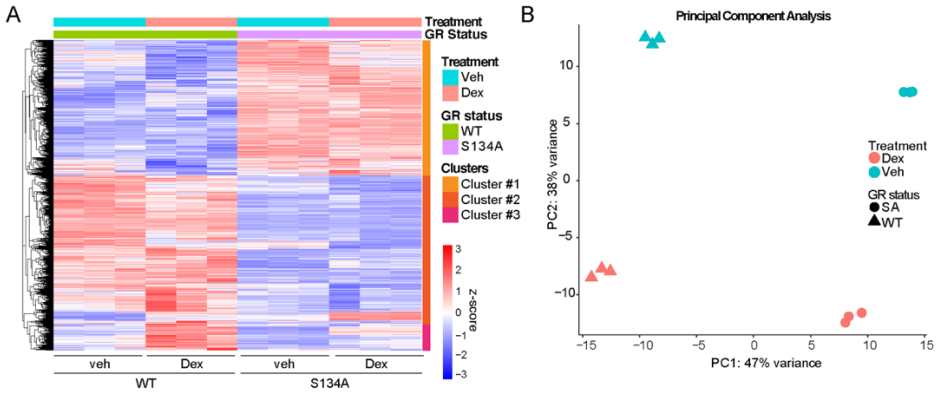

E

Molecular and Cellular Functions	p-value range	# Molecules
Cellular Movement	1.02E-03 – 1.62E-11	203
Cell-to-Cell Signaling and Interaction	1.03E-03 – 2.73E-08	183
Cellular Assembly and Organization	7.11E-04 – 2.73E-08	77
Cellular Function and Maintenance	9.10E-04 – 2.03E-06	151
Molecular Transport	1.02E-03 – 2.03E-06	177

F

Pathway Analysis	FDR	NES
Ribosome	0.02671838	-2.3456524
Glycolysis Gluconeogenesis	0.02671838	-2.2429239
Pentose Phosphate Pathway	0.02671838	-1.9724393
Pyruvate Metabolism	0.02671838	-1.9212976
PPAR Signaling Pathway	0.02671838	-1.9148257
Ascorbate And Aldarate Metabolism	0.02671838	-1.8983408
Propanoate Metabolism	0.02671838	-1.8675412
Biosynthesis Of Unsaturated Fatty Acids	0.02701133	-1.8405801
Citrate Cycle TCA Cycle	0.02671838	-1.83366
Histidine Metabolism	0.03468531	-1.786889

* False discovery rate (p-adj)
* NES → Normalized Enrichment Score

Figure 3.12 Liganded glucocorticoid receptor transcriptome in wt-GR and S134A-GR cells.

(A) Heatmap showing differences in gene expression of wt-GR and S134A-GR. All genes are shown (n=). **(B)** Principal component analysis plot derived from RNA-seq shows the differences in transcriptomes between MDA-MB-231 cells expressing either WT or S134A-GR cells and treated with vehicle or 1μM Dex for 6 hrs. **(C)** Volcano plot showing differential expression of genes in wt-GR+ compared to S134A-GR+ TNBC cells treated for 6 hrs with Dex. **(D)** Venn Diagram showing the upregulated genes (log FC > 1.5 and BH <.05) in both wt-GR and S134A-GR. **(E)** Table with results from IPA analysis of genes that are differentially express. **(F)** Table with results from Gene Set Enrichment Analysis for differentially expressed genes between wt-GR and S134A-GR.

S134A GR mutation alters TNBC cell metabolomics

We next performed metabolic experiments using the Seahorse platform to examine the functional consequences of GR S134A mutation. Mitochondrial respiration was measured using oxygen consumption rate (OCR); TNBC cells expressing S134A-GR displayed significant defects in both basal and maximal mitochondrial respiration suggesting mitochondrial dysfunction (Figure 3.13A-B). These findings are in agreement with our previous findings with regards to the wt-GR and S134A-GR transcriptome. Furthermore, ATP production and mitochondrial coupling efficiency were significantly decreased in S134A GR+ cells (Figure 3.13B-C), irrespective of ligand treatment. Additionally, comparative analysis of the 'KEGG Oxidative Phosphorylation' pathway gene list revealed global differences between cells expressing either WT or mutant GR (Figure 3.13D). We next expanded bioenergetic analyses to include extracellular acidification rate (ECAR) as a readout of glycolysis using the energy phenotype test. Profiling demonstrated that Dex-treated MDA-MB-231 cells expressing wt-GR displayed a more glycolytic/energetic phenotype compared to veh-treated cells (Figure 3.13E, F). This metabolic response was not maintained in cells expressing S134A GR (Figure 3.13E). Together, these studies suggest that GR phosphorylation is critical for both normal mitochondrial respiration, and Dex-induced bioenergetics phenotypes.

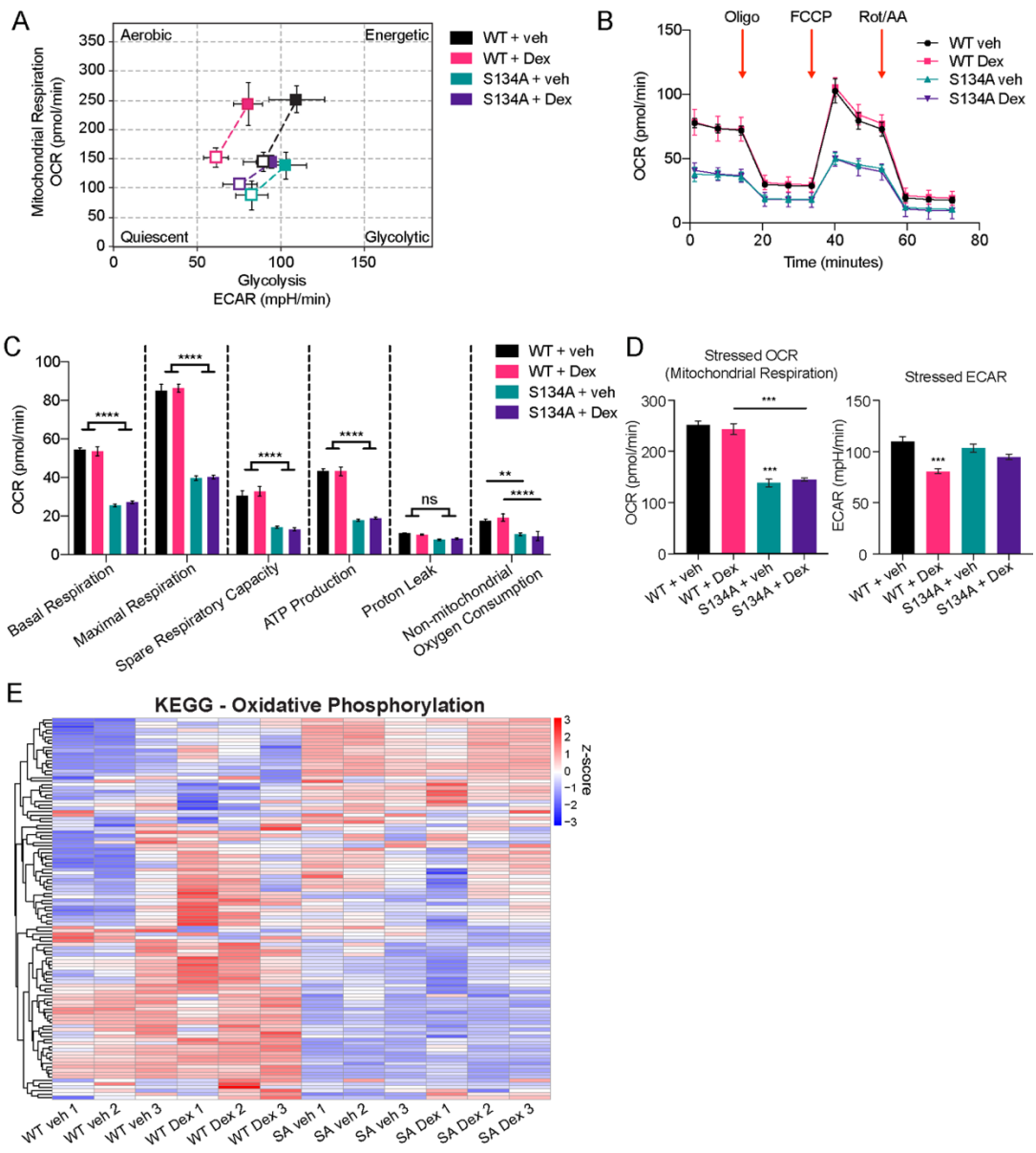

Figure 3.13 Metabolomics associated to wt-GR and S134A-GR cells.

(A) OCR and ECAR rates as measured by Seahorse Cell Energy Phenotype test in wt-GR and S134A-GR cells treated with either vet or Dex. **(B and C)** OCR rates as measured by the Seahorse Mito Stress Test. **(D)** OCR and ECAR in stress as measured by the Seahorse Mito Stress Test. **(E)** Heatmap showing analysis of KEGG-Oxidative Phosphorylation genes and its expression in wt-GR and S134A-GR cells treated with either veh or Dex in triplicates.

To further explore Dex-mediated changes to the pS134 GR transcriptome, we compiled a list of differentially expressed genes (815 genes) for further analysis. Quantitative PCR validation confirmed that Dex-induced expression of key metabolic genes (*PDK4, PGK1, PFKFB4*) is lost in S134A GR-expressing cells (Figure 3.14A). GR activation by Dex was recently shown to encourage tumor cell migration and metastasis *in vitro* and *in vivo* (25) and our RNA-seq data implicate S134 phosphorylation in this readout of advanced cancer biology. Some key motility genes lose Dex responsiveness in S134A GR mutant cells (*NEDD9, RUNX3*), while others (*CSF1*) are not responsive to Dex treatment but are similarly decreased in S134A mutant cells (Figure 3.15A).

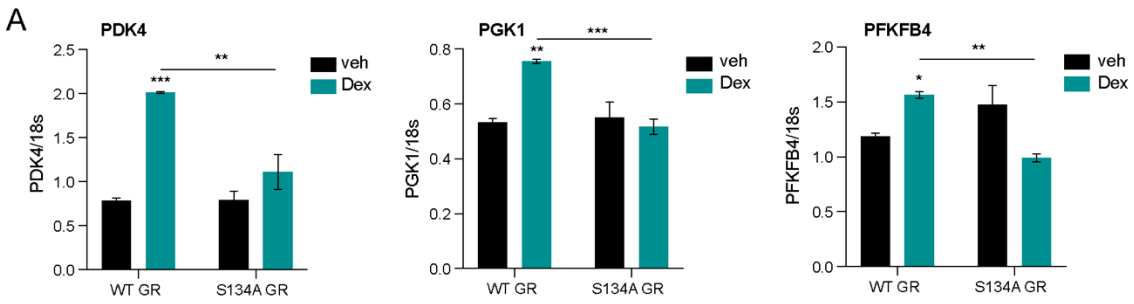

Figure 3.14 PDK4 is regulated by phosphorylation of GR on Ser134. (A) qPCR analysis of the following genes: PDK4, PGK1 and PFKB4.

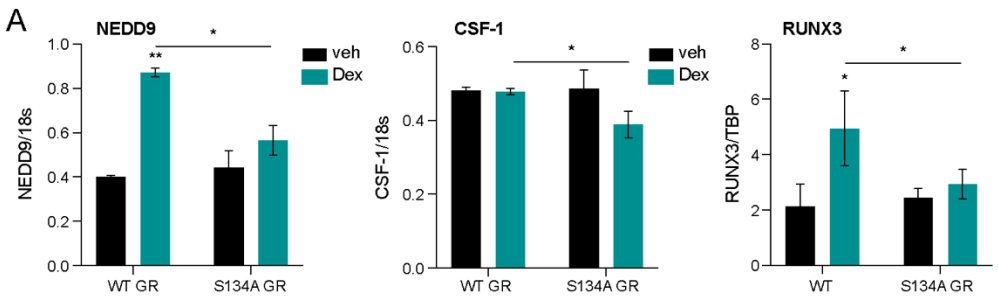

Figure 3.15 Other motility genes are responsive to phosphorylation of GR on Ser134. (A) qPCR analysis of the following genes: NEDD9, CSF-1 and RUNX3.

A pS134-GR gene signature predicts poor survival in breast cancer patients

After evaluating the actions of liganded-GR, we then focus on exploring ways to measure unliganded pS134-GR activities in TNBC. We speculated that pS134-GR-regulated gene sets important for TGFβ1 signaling may predict prognosis and disease progression in patients with breast cancer. Using our transcriptome (RNA-seq) data, we further evaluated all genes that were uniquely upregulated in cells expressing wt-GR but not S134A GR (i.e. those genes whose TGFβ1-induced regulation requires an intact GR S134). Thus, we compared the expression of genes between the vehicle and TGFβ1-treated groups for each TNBC cell line. Using a cutoff of log2 fold-change of +1.5 and a Benjamini-Hochberg p-value of 0.05, we identified all TGFβ1-upregulated genes relative to vehicle controls. A total of 90 genes were upregulated by TGFβ1 in MDA-MB-231 cells expressing either wt-GR or S134A GR. Of these TGFβ1-induced genes, 38 were upregulated only in cells harboring wt-GR, and 8 were significantly upregulated only in cells expressing S134A-GR, while 44 genes were upregulated in both cell lines (Figure 3.16A). A heatmap approach was used to plot the log2 normalized expression values of the 38 genes upregulated by TGFβ1 in cells expressing wt-GR but not S134A-GR (Figure 3.16B,Table 3.3 and 3.4). We further identified a 24-gene cluster of TGFβ1-regulated genes that require GR S134 using the same threshold of log2 fold-change of >1.5 and a Benjamini-Hochberg p-value of 0.05 (Table 3.3 and 3.4). Representative genes (*LEFTY2*, *PIK3IP1*) were further validated by qPCR in TGFβ1-treated (10 ng/mL; 6 hrs) cells. As predicted by our RNAseq data, we observed TGFβ1-induced

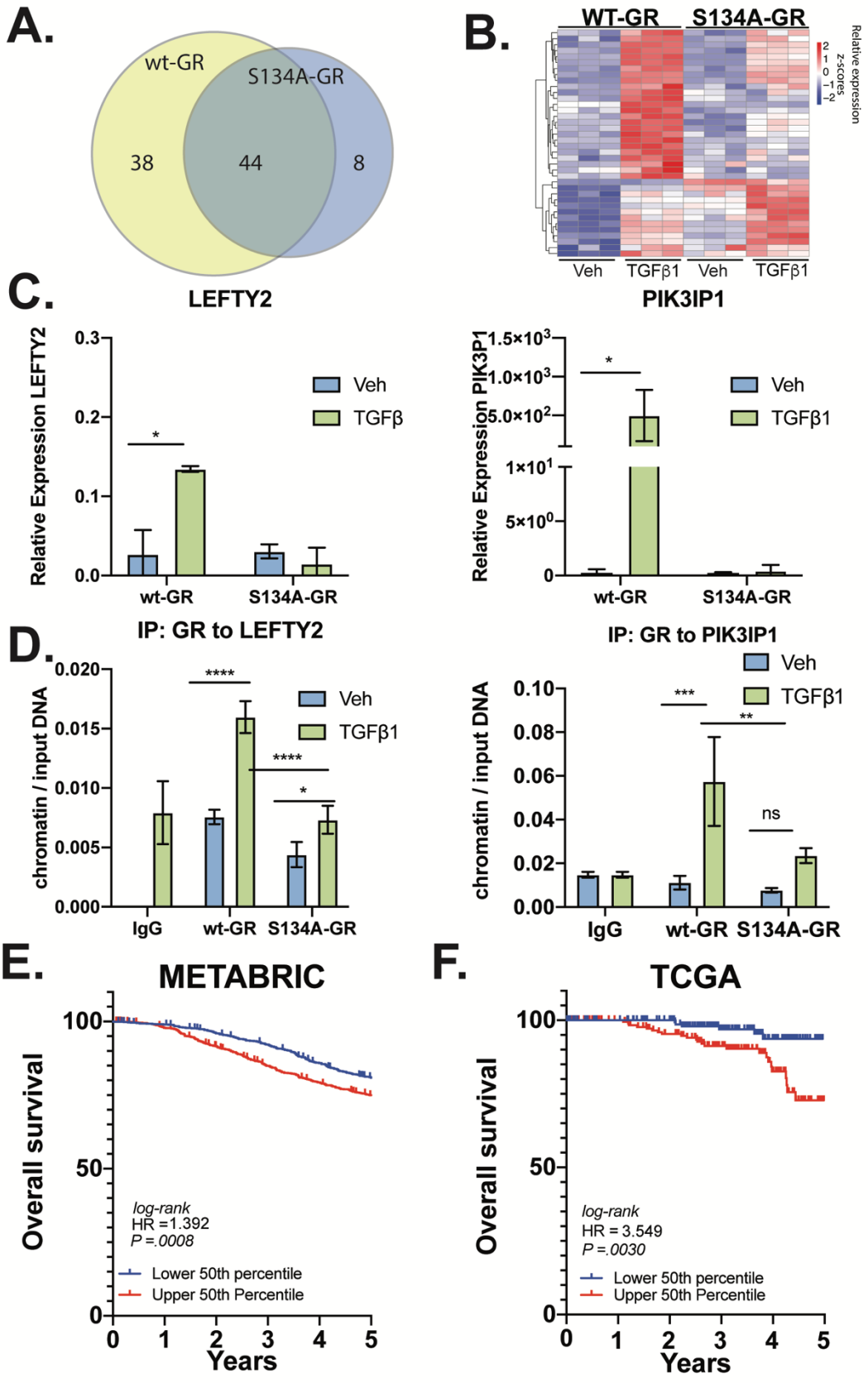
A.
wt-GR
S134A-GR
38
44
8
B.
WT-GR
S134A-GR
Relative expression
z-scores
Veh
TGFβ1
Veh
TGFβ1
C.
LEFTY2
PIK3IP1
Relative Expression LEFTY2
Veh
TGFβ
wt-GR
S134A-GR
Relative Expression PIK3P1
Veh
TGFβ1
wt-GR
S134A-GR
IP: GR to LEFTY2
IP: GR to PIK3IP1
D.
chromatin / input DNA
Veh
TGFβ1
IgG
wt-GR
S134A-GR
ns
E.
METABRIC
Overall survival
log-rank
HR =1.392
P =.0008
Lower 50th percentile
Upper 50th Percentile
Years
F.
TCGA
Overall survival
log-rank
HR = 3.549
P =.0030
Lower 50th percentile
Upper 50th Percentile
Years

Figure 3.16 P-S134-GR promotes the expression of a 24-gene signature that correlated with poor prognosis in BC.

(A) Venn diagram showing genes that are upregulated by TGFβ1 in MDA-MB-231 cells expressing either wt-GR or S134A-GR. The cutoffs used to define upregulation were a Benjamini-Hochberg value of less than .05 and a log2 fold-change of at least 1.5. **(B)** Supervised clustering of the 39 genes significantly upregulated in wt-GR cells by TGFβ1. **(C)** *LEFTY2* and *PIK3IP1* mRNA levels were assessed by qRT-PCR following normalization to *Actin.* Wt-GR and S134A-GR MDA-MB-231 cells were treated with either vehicle or TGFβ1 (10 ng/mL) for 6 hrs. Mean expression of three independent replicates ± SD is shown. Statistical significance was assessed by Two-way ANOVA and Tukey post-hoc for comparison within groups (*, $P < 0.05$) **(D)** Either wt-GR or S134A-GR MDA-MB-231 cells were treated with either vehicle or TGFβ1 (10 ng/mL) for 1 hrs. ChIP assays for the LEFTY2 and PIK3IP1 promoters to evaluate recruitment of GR were performed. The mean of three independent biological replicates are shown ± SD. Statistical significance was assessed by Two-way ANOVA and Tukey post-hoc for comparison within groups (*, $P < 0.05$; ****, $P < 0.0001$). **(E)** Kaplan-Meier curves are shown for the METABRIC dataset (n=1904). Patients were separated by calculating the median expression of the previously identified GR S134-dependent 24-gene signature. This analysis was limited to five years of survival data. The results are significant with a logrank p-value of $P = .0008$. **(F)** SurvExpress (78) was used to stratify TCGA breast cancer cohort based on their median prognostic index as determined by SurvExpress with the TGFβ1 pS134-GR 24-gene signature. The results were analyzed for significance with a logrank p-value of $P = .0030$.

Gene Symbol	log2FoldChange	pvalue	padj
DLEU7	1.54340251	0.00801964	0.04562588
JUNB	2.0048481	6.36E-16	7.08E-14
LBH	1.6299323	0.00011293	0.00141348
SNAI1	1.8391123	1.36E-16	1.65E-14
C1orf106	1.63049473	1.22E-10	5.87E-09
CCL20	1.58700941	4.17E-08	1.27E-06
NRP2	1.69574113	7.04E-12	4.09E-10
PIK3IP1	1.67743145	2.94E-06	5.83E-05
SYT8	2.09359236	0.00108456	0.00939907
KRT16	1.72951275	1.29E-07	3.52E-06
NLRC3	1.52288619	1.17E-07	3.22E-06
LEFTY1	2.84570735	0.00419959	0.02733495
NKD1	1.92830218	0.00045685	0.00455362
KPNA7	1.58566944	0.00288501	0.02047414
LTBP3	1.72120177	2.02E-11	1.09E-09
MDFI	1.65242689	1.17E-10	5.68E-09
SYN1	2.33053191	1.40E-05	0.00023104
LEFTY2	9.043364	9.14E-05	0.00117715
MYOZ1	4.51522433	0.00030435	0.00324087
GPR183	2.40678208	0.00181688	0.01435271
MATK	2.09381788	0.00025102	0.00278165
STK19	5.4868137	4.61E-05	0.0006562
HRAS	3.01936596	0.00605211	0.03638413
COL8A2	1.5583494	0.0002988	0.00319517

Table 3.3 Twenty-four genes are upregulated by TGFβ1-induced pS134-GR.

The log2 fold change and p-values and p-adj (Benjamini-Hochberg) associated with the pS134-GR gene-signature are shown in the wt-GR cells.

Gene Symbol	log2 Fold Change	p-value	p-adjusted
HRAS	3.019365961	0.00605211	0.036384127
MAFIP	3.268853595	0.00367505	0.024613145
SLITRK6	1.72116739	3.81E-05	0.000552521
KPNA7	1.58566944	0.00288501	0.020474138
LOC91450	2.076380103	0.00608628	0.036546396
ZNHIT3	3.176767351	0.00867929	0.048195619
KRT16	1.729512748	1.29E-07	3.52E-06
LTBP3	1.721201771	2.02E-11	1.09E-09
GPR183	2.406782077	0.00181688	0.014352711
KCNA7	3.13822709	4.18E-05	0.000601421
SNAI1	1.839112301	1.36E-16	1.65E-14
SYT8	2.093592362	0.00108456	0.009399066
STK19	5.486813698	4.61E-05	0.0006562
LINC01583	1.916215426	3.75E-08	1.15E-06
CCL20	1.587009408	4.17E-08	1.27E-06
LEFTY2	9.043364002	9.14E-05	0.00117715
JUNB	2.0048481	6.36E-16	7.08E-14
LBH	1.629932302	0.00011293	0.001413482
NLRC3	1.522886186	1.17E-07	3.22E-06
SYN1	2.330531914	1.40E-05	0.000231038
LINC00862	1.685695952	5.12E-05	0.000714687
LOC100130417	1.646304037	0.002849	0.020338567
TMEM100	1.995398253	0.00111809	0.009607882
PCDH1	1.845377218	2.12E-05	0.000333444
CLTCL1	1.576389055	3.50E-08	1.09E-06
ADTRP	1.522940629	9.04E-13	6.11E-11
NRP2	1.695741134	7.04E-12	4.09E-10
LEFTY1	2.845707345	0.00419959	0.027334949
MYOZ1	4.515224331	0.00030435	0.003240868
DLEU7	1.543402513	0.00801964	0.04562588
ACKR3	2.520424805	5.39E-05	0.000746588
C1orf106	1.630494726	1.22E-10	5.87E-09
NKD1	1.928302177	0.00045685	0.004553617
MDFI	1.652426893	1.17E-10	5.68E-09
COL8A2	1.558349404	0.0002988	0.003195173
MATK	2.093817881	0.00025102	0.002781646
ABAT	1.732787484	4.93E-10	2.14E-08
PIK3IP1	1.677431453	2.94E-06	5.83E-05

Table 3.4 Log2 Fold Change and p-adjusted values for genes illustrated in the heatmap for the wt-GR cells.

upregulation of both *LEFTY2* (~4.3 fold increase) and *PIK3IP1* (~200 fold increase) in cells expressing wt-GR, but not in cells expressing S134A-GR (Figure 3.16C).

Additionally, using ChIP assays, we demonstrated robust recruitment of wt-GR species to Glucocorticoid Response Elements (GRE)-containing promoter regions of both *LEFTY2* and *PIK3IP1* in response to TGFβ1 alone. However, consistent with our qPCR results, recruitment of S134A GR to these regions was significantly diminished (*LEFTY2*) or failed to occur (*PIK3IP1*) in CRISPR models expressing phospho-mutant GR (Figure 3.16D). These data indicate that in the absence of ligand, pS134-GR is recruited to both *LEFTY2* and *PIK3IP1* in response to TGFβ1. Further studies are needed to evaluate the impact of pS134-GR on the global cistrome in the context of TNBC.

To further evaluate the importance of the pS134-GR gene signature in breast cancer patients, we used the METABRIC dataset to calculate the average expression of the above defined 24 pS134-GR-induced genes for each patient tumor and stratified patient populations based on a median-cutoff for the average expression of the gene signature. Using Kaplan-Meier curves for analyses of overall survival, we observed that patients whose breast tumors exhibited an average expression of the gene signature within the upper 50^{th} expression percentile experienced poor survival relative to patients whose tumors fell within the lower 50^{th} percentile (Figure 3.16E). This difference was significant with a log

rank p-value of 0.0008 (Figure 3.16E). To confirm our findings in the METABRIC dataset, we employed the SurvExpress tool with the TCGA breast cancer dataset (78) and observed similar results with significant separation based on overall survival (Figure 3.16F). These results suggest that the presence of pS134-GR, as measured using a 24-gene signature, confers poor prognosis in breast cancer patients, regardless of subtype. More studies are needed to further explore the utility of tracking either pS143-GR or pS134-GR gene-signatures as potential biomarkers of advanced cancer behaviors (i.e. p38 MAPK-mediated tumor cell dissemination) in breast cancer patient subpopulations.

Discussion

Herein, we report that TGFβ1 promotes p38 MAPK-dependent phosphorylation of GR S134 in TNBC models. Our studies demonstrate that ligand-independent but p38-driven activation of pS134-GR represents a convergence of stress-activated signaling pathways with cellular homeostatic responses, including to local pro-inflammatory cytokines and growth factors (Figure 3.3 and 3.4). We conclude that pS134-GR is a critical effector of migratory and invasive TNBC cell behaviors linked to TGFβ1 signaling in TNBC models, in part explaining why high GR expression predicts poor outcome in women diagnosed with TNBC (22). Our results suggest that pS134-GR promotes basal TNBC cell survival and TGFβ1-induced migration/invasion even in the absence of exogenously added GR ligands, but rather in response to intrinsic or TME stressors; a pS134-GR gene signature distinct from that induced by Dex

(24) predicts poor outcome across all breast cancer subtypes. Additionally, we explore the effects of phosphorylation on S134 in liganded GR. We found that pS134-GR is essential for metabolic reprogramming of MDA-MB-231 cells. Taken together, our data suggest that targeting pS134-GR and associated p38 MAPK signaling pathway effectors (MAP3K5) downstream of TGFβ1 or related factors in TNBC patients could be highly beneficial.

Breast cancer patients are frequently treated with Dex (i.e. a potent GR agonist) to alleviate common side effects of chemotherapy. However, in the context of cancer, Dex can promote migration and importantly, pS134-GR (activated-GR) dramatically alters basal and cytokine-induced gene expression in the absence of abundant GR ligands (Figure 3.8). Namely, pS134-GR (but not Dex) is required for TNBC cell migration (Figure 3.5C and Figure 3.5D), invasion (Figure 3.6), anchorage-independent growth (Figure 3.5E) and tumorsphere formation (Figure 3.5F), *in vitro* readouts of advanced cancer behaviors that track with metastatic potential (90). Our findings are clinically relevant since GR appears to have an active role in the progression of TNBC (24). Our data suggest that TNBC patients may have high expression of functionally active pS134-GR even when GR agonists are limiting. The presence of elevated pS134-GR levels in TNBC relative to luminal BC cases (86) may explain why GR expression correlates with poor prognosis in TNBC but tracks with good prognosis in luminal BC (22). Interestingly, GR S134 contributes to basal anchorage-independent cell growth (Figure 3.5E), a measure of both survival and

proliferation. We were surprised that in the presence of TGFβ1 (or other cell intrinsic or extrinsic agents that activate p38), exogenously added Dex was not required/dispensable for pS134-GR-driven gene expression and TNBC cell migration/invasion *in vitro*. Further studies are needed to test if TNBC cells (*in vitro*) or tumor/stromal tissues (*in vivo*) produce measurable GR ligands and if so, at what intracellular or intratumoral concentrations. Additionally, although our data showed that both wt-GR and S134A-GR respond similarly to Dex at well-characterized GR-target genes (*SGK1* and *DUSP1*), additional Dex-regulated genes are likely to be highly sensitive to modification of GR S134 (33). Accordingly, we found that the PDK4 is responsive to Dex-liganded activation of pS134-GR. Importantly, we identified that the regulation of PDK4 is essential for the promotion of metabolic reprogramming of MDA-MB-231 cells using Seahorse assays. Further studies are needed to explore if there are other phenotypes that are regulated by liganded pS134-GR.

Post-translational modifications of SRs expressed in breast cancer cells are predicted to have tremendous impact on the clinical course and tumor characteristics (110). For example, S294-phosphorylated PRs regulate gene expression that modulates luminal breast cancer stem/stem-like cell properties and promotes tumor cell plasticity and therapeutic resistance (85). GR is closely related to PR within the HR superfamily. GR and PR recognize the same DNA binding sites in chromatin, regulate many of the same genes, and even bind many of the same ligands such as RU486 (mifepristone) with similar affinities

(111). Interestingly, pS134 GR-driven anchorage-independent growth was insensitive to Dex but was blocked by RU486 (Figure 3.5E). Similarly, we previously described ligand-independent but MAP kinase-dependent actions of pS294-PR in luminal BC models and tumor tissues (112). Our RNA-seq studies revealed that intact GR S134 is required for the expression of genes that promote MAPK activity in TNBC (Figure 3.10). A growing body of literature implicates MAPK signaling in cellular processes required for dangerous breast cancer progression, including EMT, stemness and resistance to chemotherapy (113). Importantly, inhibition of p38 MAPK activity has led to decreased migration in breast cancer cell lines (105) including MDA-MB-231 and Hs578T herein (Figure 3.10H) . Our studies revealed that MAP3K5 expression is regulated by pS134-GR. MAP3K5 is essential for the activation of downstream MEK3/6 (MKK3/6) which in turn activates p38 MAPK in the 3-kinase cascade or module required for phosphorylation of GR S134 (109, 114). Notably, because MAP kinase kinase kinase (MKKK) expression is typically limited (i.e. protein expression is low relative to that of MKKs or MAPKs) (115), a relatively modest change in MKKK (i.e. the top of the 3-kinase cascade; MAP3K5) abundance may confer large changes in activation of MAP kinase (i.e. the bottom of the 3-kinase cascade; p38) (Figure 3.17). Overall, our data support the existence of a potent feedforward loop in response to TGFβ1 and other TME-derived agents that activate p38 MAPK; p38 MAPK-dependent GR S134 phosphorylation promotes increased expression of MAP3K5, thereby reinforcing robust MEK3/6 and p38 MAPK pathway activation (95, 116, 117). Thus, when tumor cells experience

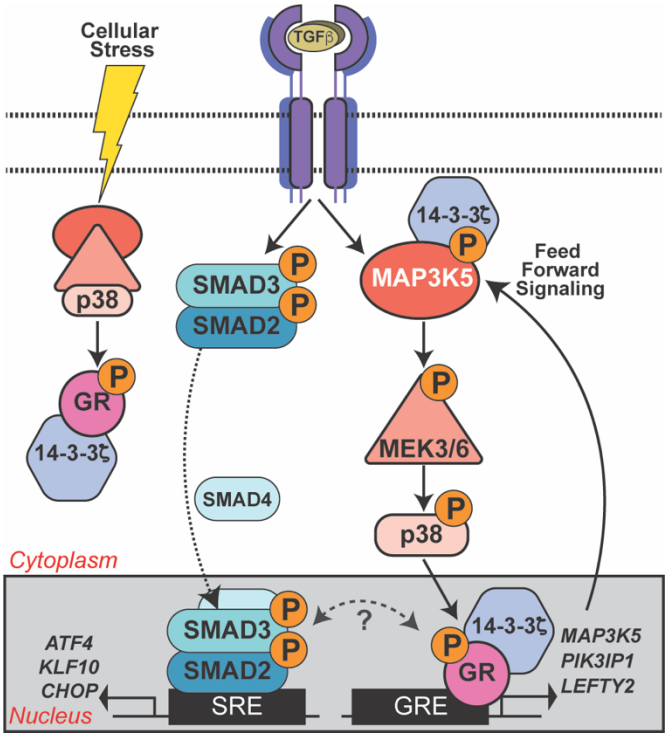

Figure 3.17 GR S134 phosphorylation creates a feed-forward signaling loop that potentiates further activation of the p38 MAPK pathway downstream of TGFβ1 in TNBC models.

Schematic of the conserved three kinase cascade that represents the p38 MAPK module (i.e. MAP3K5, MEK3/6, and p38 MAPK) and known cooperation between 14-3-3ζ and MAP3K5 (109). Cellular stress as well as TME-derived factors (TGFβ1) input to activation of SMADs and p38 MAPK signaling, resulting in phosphorylation of GR on S134. Ligand-independent pS134-GR target genes include key components of the p38 MAPK pathway (MAP3K5) needed for intact p38 signaling. Potential cooperation of 14-3-3ζ and pS134-GR with the SMAD-dependent arm of the TGFβ1 signaling pathway is shown (dotted two-way arch under question mark).

Cellular stress and/or when TGFβ1 is abundant in the TME, pS134-GR self-perpetuates its own phosphorylation by inducing the expression of MAP3K5 which in turns activates p38 MAPK in cooperation with 14-3-3ζ. Finally, this signaling axis enables sustained biological responses such as anchorage-independent growth or persistent cell migration of TNBC cells (Figure 3.17).

S134 phosphorylation is known to promote GR interaction with 14-3-3ζ (33). A growing body of evidence has implicated 14-3-3ζ in breast cancer progression (35). The 14-3-3 family of proteins function as important scaffolds for MAPK modules and numerous other signaling molecules. Relevant to our studies on TNBC cell migration herein, 14-3-3ζ mediates increased invasion of ER- breast cancer cells (118). We find that like pS134-GR, 14-3-3ζ is required for TGFβ-mediated migration of TNBC models. Interestingly, TNBC cells expressing phospho-mutant S134A GR phenocopy wt-GR cells expressing sh14-3-3ζ models; cell migration is profoundly impaired upon loss of this MAP3K5-dependent arm of the p38 signaling pathway. Accordingly, 14-3-3ζ has been shown to be important for the activity of MAP3K5 and p38 in other models (119). Taken together, we conclude that 14-3-3ζ orchestrates p38-dependent phosphorylation of GR S134 and interacts with pS134-GR; co-IP assays confirmed regulated GR/14-3-3ζ interaction in TNBC cells (Figure 3.7E). The precise role(s) of 14-3-3ζ interaction with pS134-GR is unknown. All HRs rapidly and dynamically shuttle between the cytoplasmic and nuclear compartments. Similar to other HR family members (ER, PR, AR), pS134-GR may interface with

rapidly activated cytoplasmic signaling pathways at or near the cell membrane. Via cytoplasmic interaction with 14-3-3ζ, pS134-GR may help nucleate or stabilize functional p38 MAPK modules thereby enabling ultrasensitive signal transduction. Additionally, nuclear 14-3-3ζ proteins may contribute to pS134-GR transcriptional activity or gene promoter selection, perhaps via sustained recruitment of required kinases or other signaling molecules into pS134-GR-containing transcription complexes. These are topics for future study.

The role of post-translational modifications of GR and their impact on breast cancer prognosis have not yet been elucidated. Herein, we identified genes that are dependent on pS134-GR for their expression; this gene signature may be exploited to more accurately predict which breast cancer patients are more likely to succumb to metastatic disease. For our analysis, we included data for all breast cancer patients from both METABRIC and TCGA. We determined that our 24-gene signature is able to stratify BC patients according to their overall survival. Because we used all breast cancer patients for our analysis, it is possible that pS134-GR has detrimental effects for prognosis in breast cancer patients overall (i.e. this observation is not limited to TNBC). ChIP assays (Figure 3.16D) show recruitment of GR to TGFβ-induced genes via pS134-GR, *PIK3IP1* and *LEFTY2,* in the absence of exogenously added Dex. Future studies aim to confirm genome-wide occupancy of unliganded pS134-GR at novel target genes defined by our signature. Finally, TNBC patients are routinely treated with corticosteroids to alleviate the side effects of chemotherapy. Notably, taxane

chemotherapies (e.g. Paclitaxel) activate a cellular stress response that induces robust p38 MAPK activation and sustained GR S134 phosphorylation (86). In future, in addition to standard-of-care approaches, co-targeting pS134-GR and p38 MAPK could provide a better way to limit disease progression in TNBC and other BC subtypes that express pS134-GR.

Chapter 4 Breast tumor kinase (Brk/PTK6) mediates advanced breast cancer phenotypes via SH2-domain dependent activation of RhoA and aryl hydrocarbon receptor (AhR) signaling

Introduction

Endogenous ligands (cortisol) or exogenous ligands (Dex) can activate GR transcriptional activity. When activated, the GR promotes the expression of gene programs that are essential for cancer phenotypes such as migration, invasion and anchorage-independent growth (120). We previously identified that GR interacts with the AhR, a bHLH/PAS domain transcription factor related to the hypoxia inducible factors (HIFs) (121). We also reported cross-talk between stress hormone-driven GR signaling and HIF-regulated stress response pathways in TNBC (122). The interaction of GR and AhR promotes cancer pro-survival phenotypes in response to cellular stressors, including hypoxia and chemotherapy treatment (e.g., paclitaxel) in TNBC cell lines (121). Notably, the interaction of GR and AhR/HIF1α is essential for the inducible expression of PTK6 (121).

PTK6 is an intracellular tyrosine kinase overexpressed in approximately 86% of invasive ductal breast cancer cases, whereas it is weakly expressed or undetectable in normal breast tissues (123). Furthermore, PTK6 expression is correlated with tumor grade in invasive ductal carcinoma *in situ* patients (123). PTK6 is essential for EGF- and HGF-mediated tumor cell migration in breast cancer models (124). PTK6 mediates its oncogenic actions in part by modulating the actions of Rac1, Ras and Rho GTPases in luminal breast cancer models (123, 125). Additionally, PTK6 is essential for the phosphorylation and subsequent activation of p38 MAPK and ERK5, serine/threonine kinases that

have been implicated in migratory phenotypes and cancer stem cell (CSC) generation (124, 126, 127). Similarly, PTK6 expression has been associated with induction of anchorage-independent growth in prostate and breast cancers (48, 128, 129). Therefore, targeting PTK6 is attractive as a treatment strategy in breast and other cancers.

PTK6 protein structure is closely related to that of c-Src tyrosine kinase, although it lacks a myristoylation site responsible for plasma membrane anchoring (130). In addition to a kinase domain, it contains the Src-homology domains SH2 and SH3 (62). Unlike other kinases that are overexpressed in cancer, it is not clear whether the kinase domain is the principal domain mediating PTK6's tumorigenic activity. Recent reports indicate that inhibition of kinase activity is not sufficient to block the oncogenic actions of PTK6 in breast cancer. For example, in luminal breast cancer, HGF- or EGF-mediated migration requires PTK6 expression but not the kinase domain (124). More importantly, inhibiting the kinase domain with various small molecules that only inhibit the unphosphorylated form of PTK6 (Type II inhibitors), does not appreciably decrease tumor growth or proliferation in either luminal or triple-negative breast cancer models (62). These observations suggest that PTK6 structural domains other than the kinase domain, are critical for cancer cell biology. Both the SH3 and SH2 domains play an important role in protein-protein interactions (131-133) via proline-rich or 105hosphor-tyrosine motifs, respectively. Specifically, the sequence pY-(D/E)-(D/E)-Y was identified as a binding site for the SH2 domain

of PTK6 (134). There is evidence of *PTK6* somatic mutations in renal cell carcinoma and gastric cancers that not only span the kinase domain, but also involve the SH2 and SH3 domains (45). These mutations have profound effects on PTK6 kinase activity and substrate binding by modulating autophosphorylation or substrate activation (62). Therefore, before considering PTK6 as a viable pharmacological target for TNBC, it is essential to dissect the domain-specific functions of PTK6.

Herein, *in vivo* studies demonstrated that PTK6 has little effect on primary tumor growth, but significantly contributes to TNBC metastasis to lungs. To test the requirement of PTK6 kinase, SH2, and SH3 domains for TNBC phenotypes, we stably expressed wild-type (wt), kinase-dead (KM), or different domain mutant constructs of PTK6 in a previously characterized MDA-MB-231 PTK6 knockout (KO) cell line (121). A screen for domain-dependent signaling revealed that the PTK6 SH2-domain mediates activation of RhoA and AhR transcriptional activity; chemical inhibitors to either pathway repressed cell motility or migration. Moreover, pairing RhoA with paclitaxel enhanced growth inhibitory effects in TNBC models. Together, our data reveal that the PTK6 SH2 domain serves as a hub to coordinate two key downstream signaling pathways, RhoA and AhR, that mediate stemness, cell migration and/or chemotherapy sensitivity in TNBC.

Results

Enriched PTK6 expression is associated with tumor progression *in vivo*

We previously demonstrated that PTK6 is highly expressed in human breast carcinomas as compared to normal breast tissue and that *PTK6* expression in the normal mouse mammary gland is HIF-dependent and induced following a single dose of GR agonist (dexamethasone; Dex). Similarly, PTK6 mRNA and protein is robustly induced following Dex treatment of primary human TNBC explants cultured *ex vivo* (39). Building on these observations, analysis of The Cancer Genome Atlas (TCGA) invasive breast cancer database (SurvExpress – (135)) indicated that higher PTK6 expression is correlated with decreased survival in high-risk breast cancer patients (ER+ and ER- cases) (Figure 4.1A). SurvExpress risk groups are defined by estimating a prognostic index using the Cox model algorithm (27). We then analyzed *PTK6* mRNA expression in ER-negative patients using KM Plotter tool restricted to the TCGA database and found that high PTK6 expression is also correlated with decreased overall survival in this patient cohort (Figure 4.1B).

Patients with TNBC have the highest rate of recurrence and succumb to metastatic disease sooner post-diagnosis than ER+ patients (80, 136). Metastasis occurs according to a series of sequential steps including local invasion, intravasation, survival in circulation, extravasation, and finally colonization, believed to be the rate-limiting step (137). We have shown PTK6 is required for survival in non-adherent conditions in TNBC cells (121) and that GR/HIF regulates cellular stress-dependent up-regulation of PTK6, such that loss

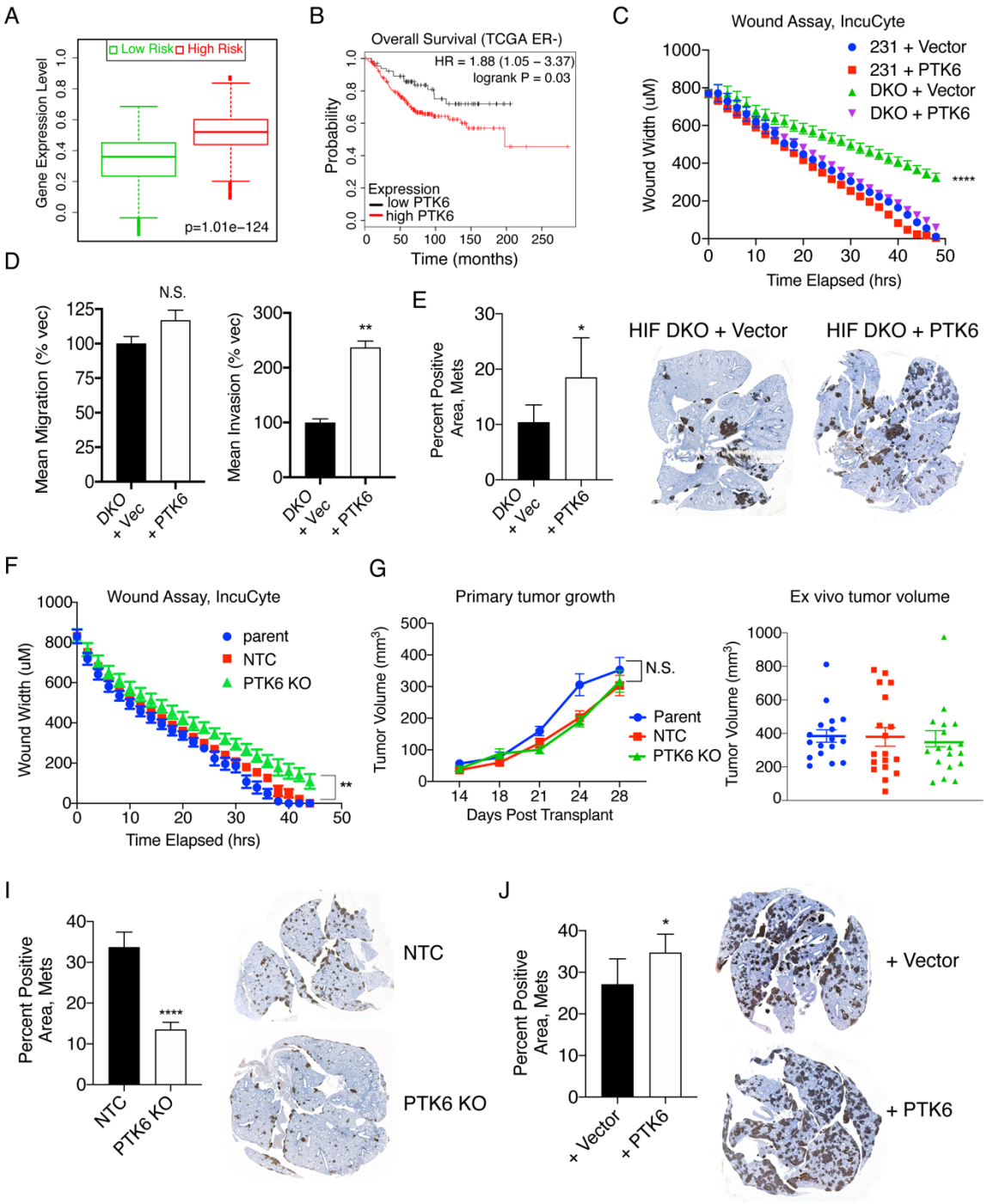

Figure 4.1 Elevated PTK6 expression is correlated with lower overall survival of breast cancer patients and promotes cell motility, invasion and lung metastasis.

(**A**) SurvExpress was used to examine the prognostic index of patients in the TCGA Invasive Breast Cancer cohort based on PTK6 expression. (**B**) Overall survival of ER-negative patients stratified on PTK6 mRNA expression using KM plotter (TCGA database). (**C**) A high-throughput scratch wound assay was used to measure wound width over time (n=4 wells/genotype; data representative of three replicate experiments). (**D**) Transwell assays were used to chemoattract serum-starved HIF-1/HIF-2 double knockout (DKO) MDA-MB-231 cells to 10% FBS that were

stably transfected with vector only (+Vector) or re-expressed PTK6 (+PTK6) to compare migration or cell invasion; bar graphs represent the grand mean ± SEM of three biological experiments; NS = not significant. I MDA-MB-231 HIF DKO + vector or HIF DKO + PTK6 cells were injected into the tail vein of 8-10-week old female NSG mice and metastatic burden measured by densitometry analysis following immunostaining for an anti-human mitochondrial marker (brown staining). Whole immunostained lung sections representative of the mean percent positive area of metastasis are included. (**F**) A high-throughput scratch wound assay was used to compare the time elapsed to wound filling when a mixture of Cas9-deleted PTK6 KO cells are compared to parent or non-targeting control (NTC) gRNA transfected cells (n=4 wells/genotype; data representative of three replicate experiments). (**G**) Parent, NTC or PTK6 KO cells were injected in the mammary fat pad and tumor volume ± SEM compared over time. At experiment endpoint, tumors were excised and the tumor volumes ± SEM compared *ex vivo*. (**I-J**) MDA-MB-231 NTC or PTK6 KO (**I**) or parent + Vector or +PTK6 (**J**) cells were injected into the tail vein of 8-10-week old female NSG mice and the extent of metastatic colonization measured by densitometry analysis as described in I. All metastasis data are expressed as ± SD; at least 5 animals/genotype were compared.

of HIF-1 and HIF-2 significantly decreases PTK6 expression (122). To test the functional relevance of PTK6 expression in promoting invasion and colonization, MDA-MB-231 cells lacking HIF-1 and HIF-2 (HIF double knockout, DKO) and parent MDA-MB-231 cells were modified to over-express *PTK6* (Figure 4.2A and 4.2B). Forced expression of *PTK6* in HIF DKO cells rescued wound healing defects observed for HIF DKO + Vector cells, however forced expression of *PTK6* had no effect on HIF-intact parental cells (231 +Vector, Figure 4.1C). Add-back of *PTK6* to HIF DKO cells did not impact basal migratory capacity stimulated by complete media in transwell assays. However, invasion through Matrigel was enhanced 2.7-fold (Figure 4.1D). When tested in an experimental metastasis tail vein assay, PTK6 expression enhanced colonization compared to HIF DKO + Vector cells (Figure 4.1E). To test the effects of loss of PTK6, we also generated an admixture of CRISPR-Cas9 deleted PTK6 knockout (KO) clones, to minimize clonal heterogeneity effects *in vivo*. By western blotting, we confirmed that this mixture of Cas9-deleted PTK6 KO clonal lines lacked detectable PTK6 protein, as we previously reported for PTK6 KO clone 27 (Figure 4.2C) (121). Cells lacking PTK6 had minor, albeit statistically significant defects, in wound healing relative to either parent (non-transfected) MDA-MB-231 cells or cells transduced with a non-targeting control gRNA (NTC) (Figure 4.1F). Of note, neither forced expression of PTK6 nor deletion of PTK6 affected cell proliferation *in vitro* (Figure 4.2D-F). Next, parent, NTC or PTK6 KO cells were injected into the cleared, inguinal mammary gland to generate tumors. Interestingly, there were no significant differences in mean tumor volume among all genotypes at the

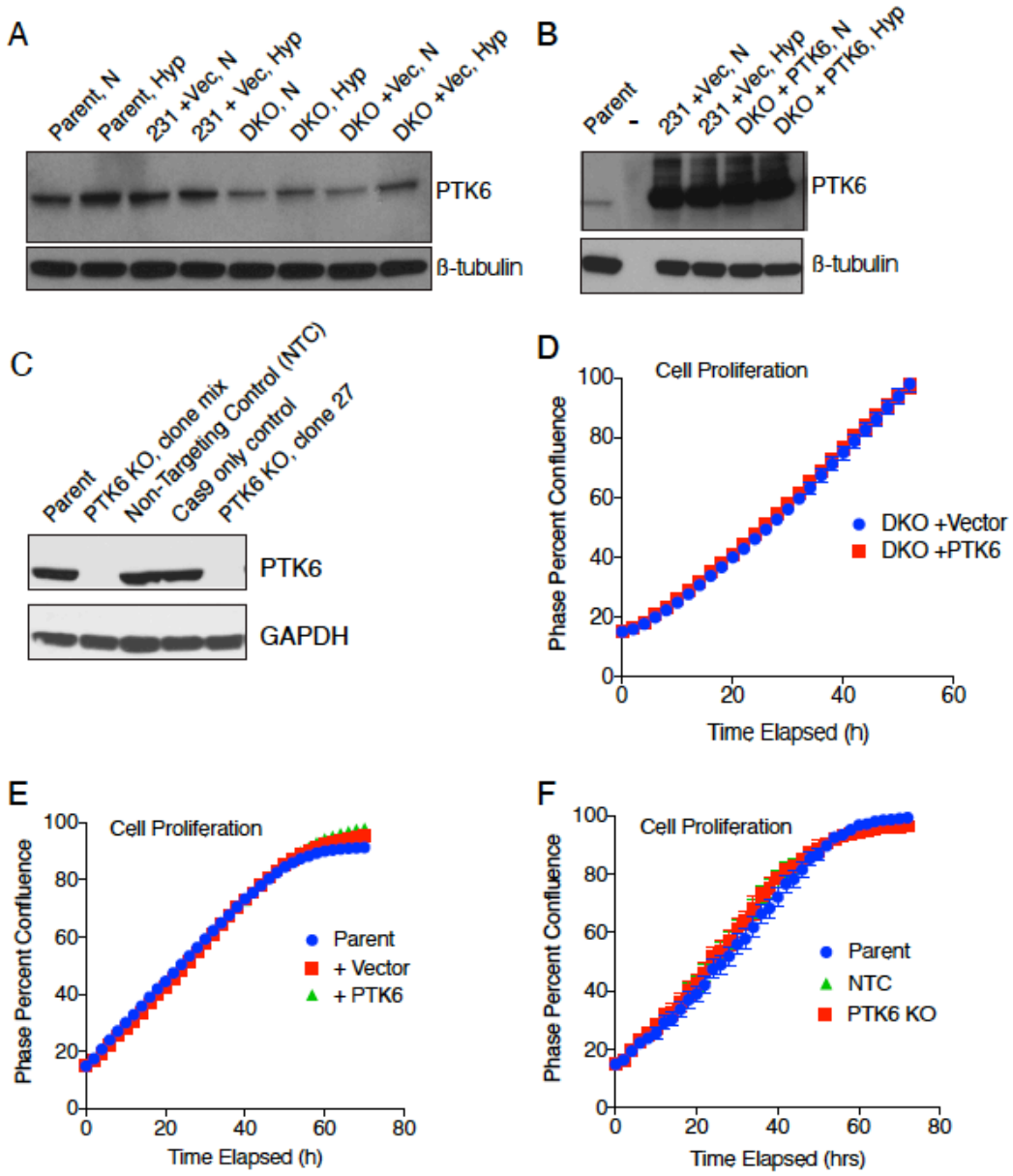

Figure 4.2 Characterization of PTK6 genetically modified MDA-MB-231 TNBC cell lines.

(**A**) PTK6 expression levels in parental (non-transfected; parent), Vector (Vec)-transduced 231 cells or HIF DKO 231 cells transduced with Vector or wild type PTK6 were compared using cells grown to 80% confluence and then exposed to normoxia (N) or hypoxia (Hyp, 0.5% O2) for 24h prior to harvest and protein extraction. ß-tubulin serves as a loading control. **(B)** PTK6 expression levels in parental, parental + Vec or HIF DKO 231 cells transduced with either Vec or wild type PTK6 using cells grown to 80% confluence and then exposed to normoxia (N) or hypoxia (Hyp, 0.5% O2) for 24h prior to harvest and protein extraction. ß-tubulin serves as a loading control. **(C)** PTK6 expression following CRISPR-Cas9-mediated deletion. PTK6 levels were compared among parent, non-targeting gRNA and Cas9-only control transfected MDA-MB-231 cells, and either a PTK6 clonal KO line (clone 27) or an admixture of PTK KO clones created using the Dharmacon Edit system as described in the materials and methods. PTK6 was not detectable in either KO model. GAPDH serves as the loading control. **(D-F)** Cell proliferation in genetically modified cells shown in panels A-C was measured over time using the phase percent confluence algorithm of the IncuCyte S3 live cell imager. MDA-MB-231 and HIF DKO cells were plated in 96 well plate

(Corning) at 1 x 104 cells/well in 200 µL growth media. Cells were allowed to grow from 20% confluency one day post-plating to 100% confluency (~80 h of imaging). Images were obtained every 2 h. The mean ± SEM is shown; the error bars were frequently too small to be plotted using Prism software. Data are representative of at least three independent replicate experiments.

study endpoint (Figure 4.1G). In contrast, in experimental metastasis assays, deletion of PTK6 reduced the area of lungs occupied by metastasis by ~2.3-fold (Figure 4.1I) whereas the over-expression of PTK6 more subtly enhanced lung metastatic burden (Figure 4.1J). Together, these results confirm the biological relevance of our PTK6 data mining observations since poor survival is typically driven by metastatic growth following onset of chemotherapeutic resistance. These data implicate a direct role for PTK6-mediated oncogenic signaling in TNBC cell invasion and lung colonization, properties of cancer cells that confer poor prognosis.

The PTK6 SH2 domain is critical for motility of TNBC cells

PTK6 is an important mediator of TNBC cell migration (121); however, the kinase domain is not required for migration (124), suggesting that other PTK6 domains related to its scaffolding actions are important. To elucidate the contribution of specific PTK6 domains, we stably re-expressed FLAG-tagged wild type (WT), kinase inactive (KM), constitutively active (C-terminal Y447 point-mutation to F447; YF), SH2 deleted (SH2-del), or SH3 deleted (SH3-del) PTK6 in previously characterized MDA-MB-231 PTK6 knock-out (KO) cells (121) (Figure 4.3A, B). We first performed soft agar assays using cells treated with EGF to stimulate anchorage-independent proliferation. Either PTK6 KO cells or cells expressing KM-PTK6 formed decreased numbers of colonies compared to cells expressing WT PTK6, indicating that PTK6 kinase activity contributes to anchorage-independent cell proliferation in this assay (Figure 4.3C). In contrast,

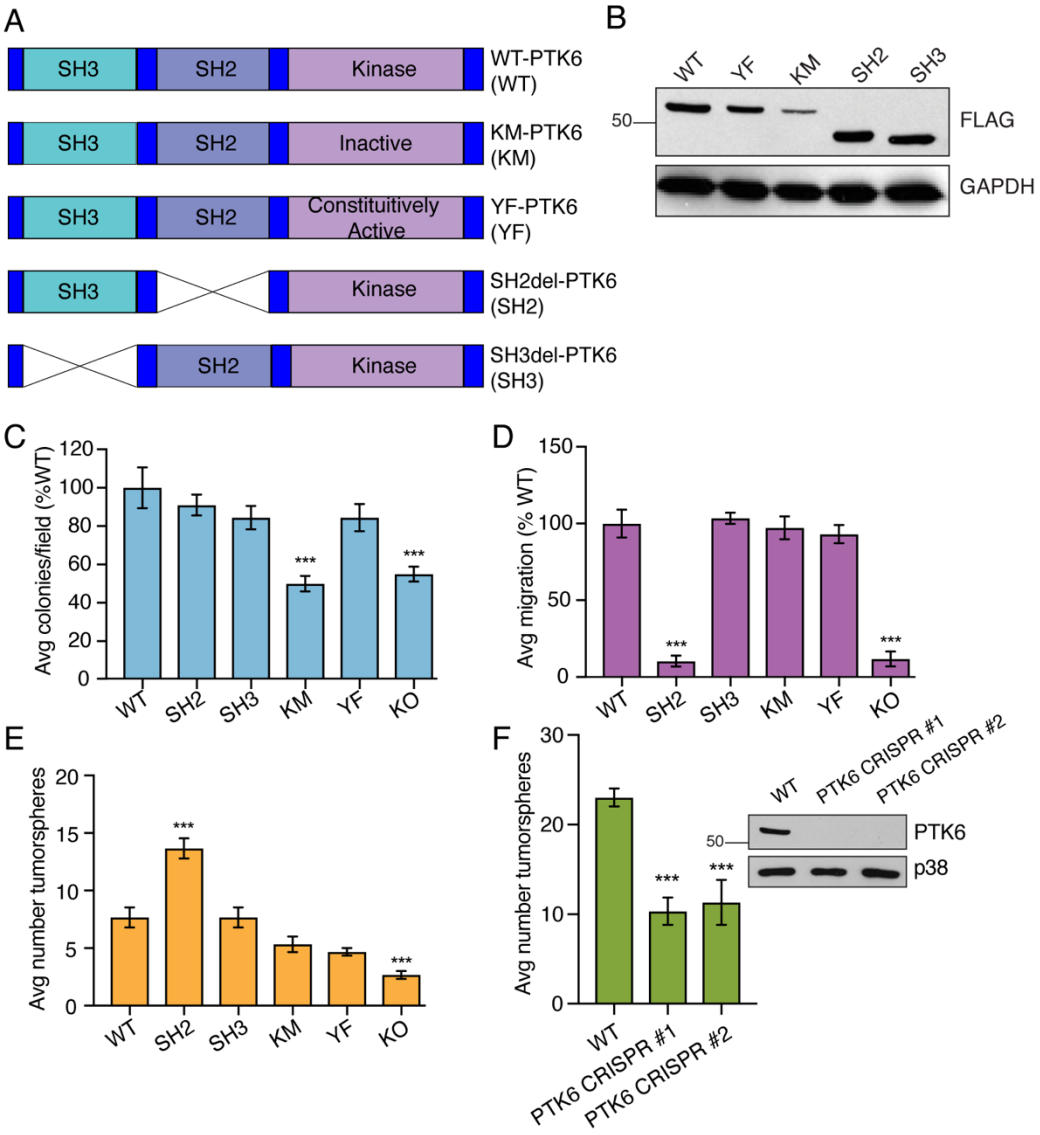

Figure 4.3 PTK6 SH2 domain is critical for TNBC motility.

(**A**) PTK6 domain structure schematic. (**B**) Western blot of MDA-MB-231 PTK6 KO cells re-expressing FLAG-tagged PTK6 domain mutant constructs. (**C**) Anchorage-independent growth was assessed in soft agar supplemented with EGF. (**D**) Transwell migration of MDA-MB-231 PTK6 domain mutants was examined in response to an HGF gradient (50 ng/mL). Data is shown as grand mean ± SD of n = 3 experiments with 3 replicate transwells each. I PTK6 knockout models. Inset confirms knockout of PTK6 using CRISPR/Cas9n (**F**) Tumorsphere-forming assays were performed in domain mutant and (**G**) PTK6 knockout models. Inset confirms knockout of PTK6 using CRISPR/Cas9n. Graphed data were analyzed by one-way ANOVA with multiple comparisons tests and are representative of n = 4 independent experimental repeats; *** $p <$ 0.001.

deletion/inactivation of the other PTK6 domains had no effect on soft agar colony formation.

We next examined TNBC motility by transwell migration using HGF. HGF, a chemokine produced by immune cells in the tumor microenvironment, stimulates cancer cell migration via activation of the Met receptor (138). MDA-MB-231 cells expressing SH2-del PTK6 failed to migrate, while KM-PTK6 cell motility was equal to that of cells expressing WT PTK6 (Figure 4.3D). Since PTK6 is required for TNBC survival in non-adherent conditions (121), we next examined growth of PTK6 domain mutant models in tumorsphere self-renewal assays. This assay measures the ability of single cells to form multicellular spheres in non-adherent conditions in defined medium containing bFGF and EGF. Sphere formation is a property of tumor cells with cancer stem cell (CSC)-like potential. Notably, clonal PTK6 KO cells formed fewer spheroids relative to cells expressing WT PTK6. Surprisingly however, SH2-del PTK6-expressing cells formed increased numbers of spheroids relative to cells expressing either WT, SH3-del, KM, or YF PTK6 (Figure 4.3E). These observations were confirmed in pooled CRISPR/Cas9 *PTK6* silenced (KO) MDA-MB-231 models (Figure 4.3F) and a Dharmacon PTK6 KO model generated by admix of 3 clones (Figure 4.2). Together, these data suggest that the PTK6 SH2 domain, rather than the kinase domain, is most critical to TNBC motility, but that this domain also negatively regulates tumorsphere formation.

PTK6 SH2-dependent signaling pathways in TNBC

To identify relevant signaling pathways in TNBC cells expressing WT, KM, or SH2-del PTK6, we performed a reverse phase protein array (RPPA) screen. A panel of 296 antibodies was used to profile and compare global changes in total protein content as well as specific posttranslational modifications. Supervised hierarchical clustering revealed a distinct cluster of proteins that are differentially expressed in WT compared to SH2-del PTK6 expressing cells (Figure 4.4A; bottom box, solid line), while some proteins remain unchanged (Figure 4.4A; top box, broken line). Unsupervised clustering of protein expression data revealed that SH2-del PTK6 expressing cells segregated independently from both WT and KM PTK6 cells, suggesting that kinase inactive PTK6 does not differ from WT PTK6 with regard to activation of the well-characterized signaling proteins represented on the array (Figure 4.4B). To identify changes in signaling pathways, we performed Ingenuity Pathway Analysis (IPA) using only probed proteins that were determined to be PTK6-dependent by their absence in PTK6 KO samples. These proteins were profiled for changes between the SH2-del and WT PTK6 samples (Table 4.1). The top down-regulated (i.e. decreased/absent in SH2-del models) pathway was AhR signaling (Table 4.1). This finding is interesting in light of our previously reported interaction between AhR and GR (121). Notably, RhoGDI signaling was increased in SH2-del PTK6 expressing cells (Table 4.1). The GDP dissociation inhibitors of Rho proteins (RhoGDI) are a family of proteins that sequester motility effector Rho GTPases in the cytoplasm, thus preventing their activation at the membrane (139).

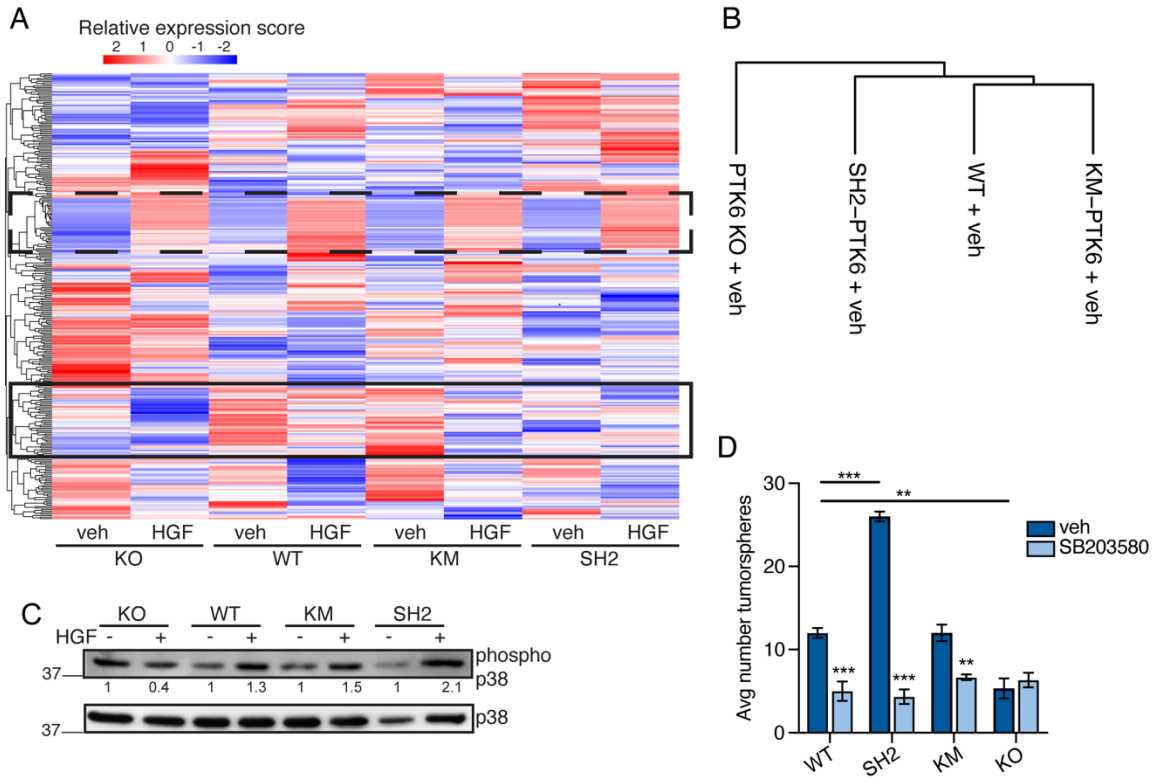

Figure 4.4 SH2-dependent pathways in MDA-MB-231 cells.

(**A**)Heatmap by unsupervised consensus clustering of protein lysates analyzed for protein expression by RPPA. Broken line box indicates protein staining intensities unchanged between samples. Solid line box highlights RPPA intensities that appear different in SH2-del PTK6 expressing cells. (**B**) Supervised clustering dendrogram of samples. (**C**) Immunoblot analysis of p38 MAPK activation by HGF (50 ng/mL). Phospho-p38 densitometry (indicated underneath) was calculated by first normalizing to total p38 MAPK, then calculating fold change over vehicle for each cell line. Data is representative of n = 3 independent repeats. (**D**) Primary tumorsphere assays in MDA-MB-231 PTK6 domain mutant models. Cells were treated with DMSO (vehicle) or SB203580 (10 mM) for 7 days. Data were analyzed by one-way ANOVA with posthoc corrections (n = 3); *** $p < 0.001$, ** $p < 0.01$.

Vehicle

Pathway	z-score	log p-value
AhR Signalling	-2.4	17.4
p38 MAPK Signalling	1.134	5.18
ERK/MAPK Signalling	1.219	32.8

HGF

Pathway	z-score	log p-value
RhoGDI Signalling	2.7	5.41
Wnt/b-catenin Signalling	1	8.21
p38 MAPK Signalling	1.134	5.18

Table 4.1 PTK6 dependent pathways (i.e. lost in PTK6 KO cells) were examined in PTK SH2-del expressing MDA-MB-231 cells.

IPA was performed for these pathways in WT vs SH2-del models. Top significant canonical pathways are listed.

As such, RhoGDI proteins are negative regulators of Rho GTPases. IPA also revealed a modest increase in p38 MAPK signaling in SH2-del PTK6 expressing cells (Table 4.1). Together, these data suggest that the PTK6 SH2 domain could regulate oncogenic signaling in TNBC via AhR, Rho GTPases, and/or p38 MAPK. We therefore performed subsequent studies to explore the functional effect of these signaling pathways in PTK6 SH2-del TNBC cells.

PTK6 SH2 domain mediates p38 MAPK signaling in TNBC cells

To confirm IPA results that p38 MAPK signaling is upregulated in SH2-del PTK6 breast cancer cells, we used immunoblotting to examine p38 phosphorylation induced by exposure to HGF. Densitometry analysis showed that 119hosphor-p38 was increased in SH2-del PTK6 TNBC cells (Figure 4.4C). The p38 MAPK pathway is a canonical stress pathway, and because growth in suspension mimics a stressful condition for epithelial cells, we again grew PTK6 domain mutant cells in forced suspension using spheroid conditions. Inhibition of p38 MAPK with SB203580 dramatically reversed the growth advantage in SH2-del PTK6 MDA-MB-231 cells cultured in suspension (Figure 4.4D). These findings suggest that while PTK6 clearly contributes to spheroid growth (Figure 4.3E), the SH2 domain of intact PTK6 limits the cellular stress-induced activation of p38 MAPK signaling associated with stemness properties in TNBC cells.

PTK6 SH2 domain mediates Rho activation in TNBC cells

Given that IPA analysis suggested decreased Rho activation in PTK6 KO and SH2-del PTK6 expressing cells, we performed pull-down assays in HGF-stimulated MDA-MB-231 cells expressing either WT or SH2-del PTK6 in order to observe changes in Rho activation. RhoA was strongly activated by HGF in WT PTK6 TNBC cells (Figure 4.5A). In contrast, RhoA was not activated in SH2-del PTK6 cells after HGF stimulation (Figure 4.5A). This result is supported by decreased migration of SH2-del PTK6 expressing cells and suggests that the PTK6 SH2 domain is required for activation of RhoA. We then confirmed that RhoA was expressed in two conventional TNBC cell lines (MDA-MB-231 and Hs578T) and in a TNBC taxane-refractory cell line isolated from patient-derived xenograft (PDX) model, cHCI-10 (Figure 4.5B) (79). We next used a Rho-specific inhibitor to assay migration potential in a panel of TNBC cells. Consistent with Rho pull-down results, transwell migration to HGF was significantly decreased in all Rho-inhibited cells (Figure 4.5C). In contrast, RhoA inhibition had no effect on soft agar colony formation of MDA-MB-231 cells expressing either WT PTK6 or SH2-del PTK6 (Figure 4.5D). Together, these data suggest that PTK6 is an important upstream regulator of RhoA via its SH2 domain; however, negative co-immunoprecipitation data suggest that this may occur via an indirect mechanism.

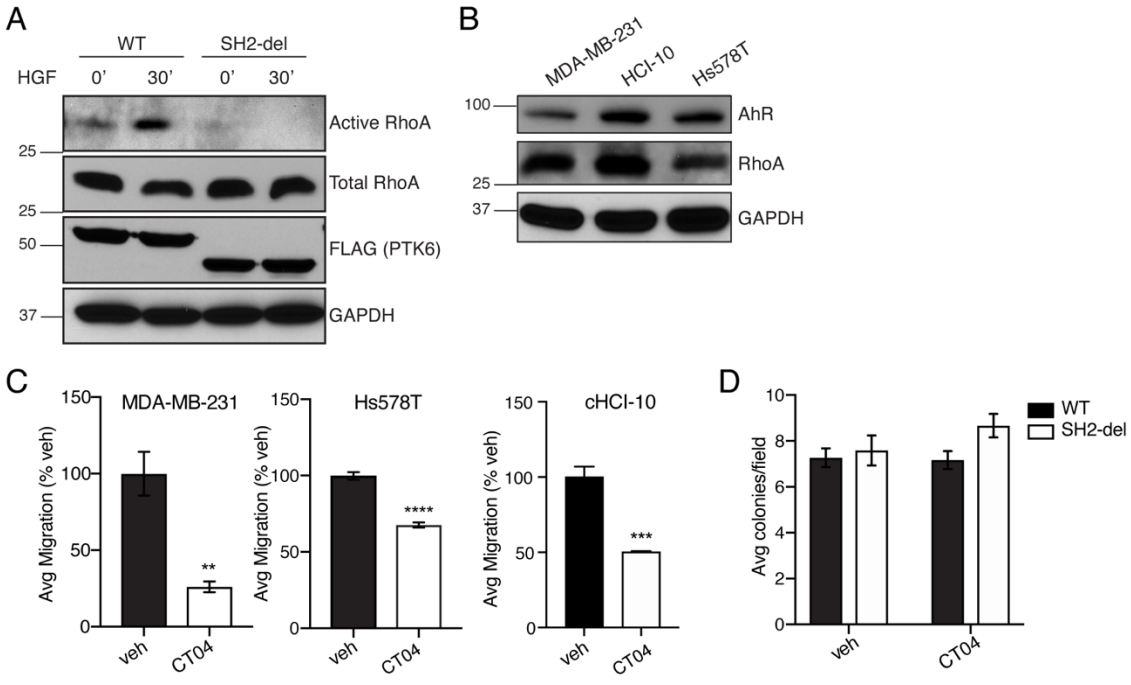

Figure 4.5 PTK6 SH2 domain is required for RhoA activation.

(**A**) RhoA activation assay using GST-Rhotekin-RBD pull down in MDA-MB-231 cells expressing WT or SH2-del PTK6. (**B**) Expression of Rho and AhR was examined in a panel of TNBC models by immunoblotting. (**C**) Rho inhibition by CT04 (1 µg/mL) in a panel of TNBC cell lines. Transwell migration (MDA-MB-231 and Hs578T) was stimulated by HGF (50 ng/mL). Significance was determined by one-way ANOVA with multiple comparisons testing; ** $p < 0.01$, *** $p < 0.001$. (**D**) Soft agar colony formation of WT and SH2-del PTK6 expressing cells in the presence of Rho inhibitor CT04 (1 µg/mL). Graphed data are representative of at least n = 3 independent replicates.

Rho inhibition sensitize TNBC cells to paclitaxel

Since PTK6 mediates paclitaxel chemoresistance (121), we next determined if Rho or AhR inhibitors (CT04 and CH223191, respectively) also mediate cell growth inhibition in combination with paclitaxel (Paclitaxel) in MDA-MB-231 or cHCI-10 PDX cells, which are refractory to paclitaxel (79). Cells were seeded into 96- well dishes, allowed to adhere overnight and then treated with increasing doses of each inhibitor alone, or in combination with paclitaxel. Each well was imaged over time in the IncuCyte S3 live cell imager. The IC_{30} and IC_{50} doses ± SEM for each drug are summarized in Table 4.2. IC values for the Rho inhibitor, CT04, could not be determined for MDA-MB-231 cells since only the 1 μg/mL dose of CT04 exposure significantly inhibited cell growth by the assay endpoint of 96 h (Figure 4.6A); the same dose (1μg/mL) was used in migration assays. Example dose-dependent effects of each drug on growth inhibition are shown in Figure 4.6A-D.

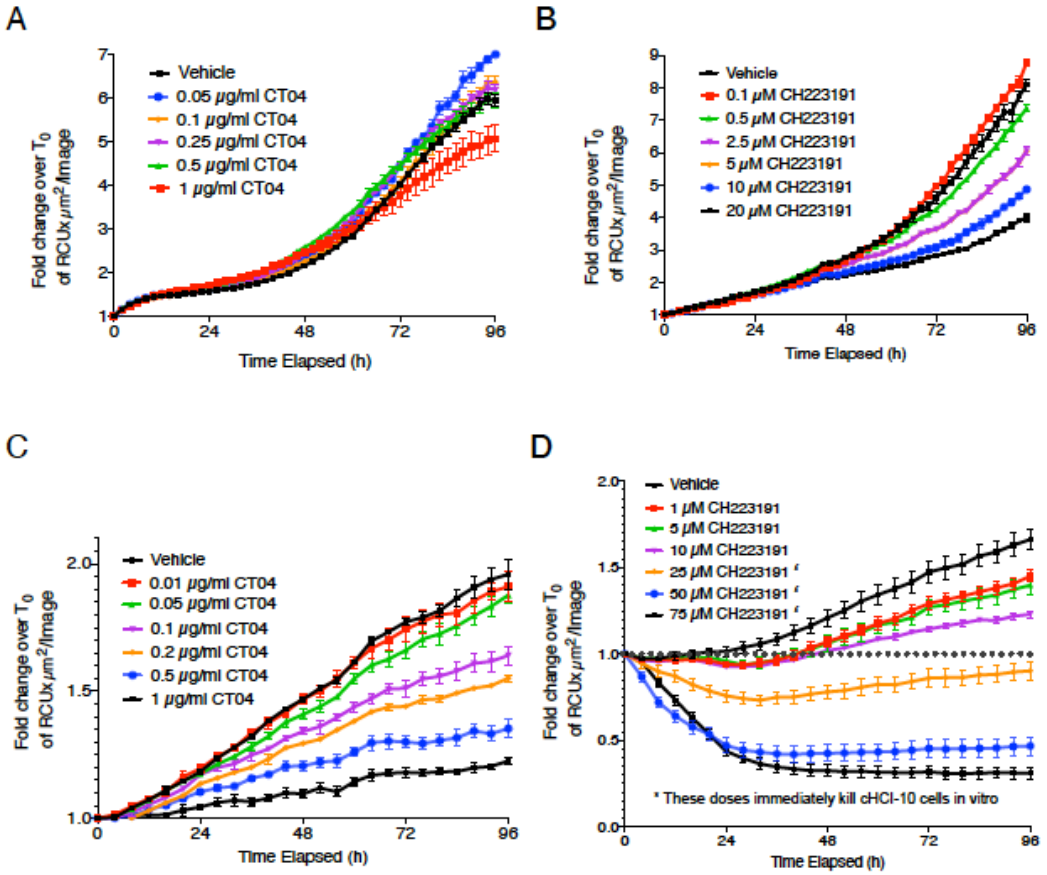

Figure 4.6 Dose-dependent effects of CT04 or CH223191 on growth inhibition in MDA-MB-231 and cHCI-10 TNBC cells.

One day after plating, cells were incubated in the presence of MiamiGreen and exposed to increasing doses of each drug and then imaged over time using the IncuCyte S3 live cell imager. Growth inhibition was measured by comparing green object counts normalized to t = 0 values and expressed as a fold change (fold change over T0 of RCU x µm2/Image). **(A)** 231 + CT04, **(B)** 231 + CH223191, **(C)** cHCI-10 + CT04, **(D)** cHCI-10 + CH223191.

DRUG	cHCI-10 IC_{30}	cHCI-10 IC_{50}	MDA-MB-231 IC_{30}	MDA-MB-231 IC_{50}
PACLITAXEL	80.49 ± 15.86 nM	188.00 ± 37.90 nM	4.22 ± 1.80 nM	9.87 ± 4.19 nM
CH223191	11.51 ± 3.22 µM	26.17 ± 6.76 µM	6.85 ± 1.16 µM	12.05 ±- 1.62 µM
CT04	3.76 ± 0.81 nM (0.009 ± 0.02 µg/ml)	8.81 ± 1.84 nM (0.22 ± 0.05 µg/ml)	N.D.	N.D.

Table 4.2 Calculated IC30 and IC50 doses of Paclitaxel, CT04 or CH223191 in taxane-sensitive MDA-MB-231 and taxane-refractory cHCI-10 TNBC cells

Calculated IC_{30} and IC_{50} doses of Paclitaxel, CT04 or CH223191 in taxane-sensitive MDA-MB-231 and taxane-refractory cHCI-10 TNBC cells as determined in Prism 8.0 using a best-fit algorithm (the log of inhibitor versus normalized response model). Data are shown as the grand mean IC value ± SEM calculated from at least three independent biological replicate experiments. The IC values were not determined (N.D.) in MDA-MB-231 cells for CT04 since there was minimal effect of CT04 on growth inhibition up to a 1 µg/mL dose (refer to Figure 4.6).

We next performed isobole testing using the Loewe additivity formula to determine a combination index (CI) for growth inhibition. In MDA-MB-231 cells, CT04 (1 μg/mL) was paired with increasing doses of paclitaxel, which induced a synergistic repression of cell growth, producing a combination index (CI) of 0.51; data are shown in the presence of 5 nM Paclitaxel (Figure 4.7A) (140). In contrast, there was no additive benefit in MDA-MB-231 cells of enhancing inhibition of cell growth when CH223191 (2.5 μM) was added to increasing doses of Paclitaxel. The growth curve of combination therapy overlapped with the curve of Paclitaxel alone; data shown are in the presence of 5 nM paclitaxel (Figure 4.7B).

In taxane-refractory cHCI-10 cells, when cells were exposed to 0.1 μg/mL CT04 and to increasing concentrations of paclitaxel, CT04 strongly synergized with paclitaxel. A combination index of 0.59 was calculated; data shown are in the presence of 75 nM paclitaxel (Figure 4.7C). In contrast, the AhR inhibitor, CH223191, was more effective as a single agent (5 or 10 μM) in cHCI-10 cells as compared to either paclitaxel alone or when paired with paclitaxel (Figure 4.7D). When CH223191 was held constant (8 μM), treatment with paclitaxel produced either neutral (CI close to 1.0) or antagonistic effects (CI>1.0) in a dose-dependent manner. For example, when paclitaxel levels were lowered from 190 nM to 80 nM, the CI value increased from 1.33 to 2.15, whereas the CI was calculated to be 0.91 at a dose of 440 nM paclitaxel. Near the IC_{50} value of paclitaxel (75 nM) for cHCI-10 cells, there was no benefit of adding CH223191;

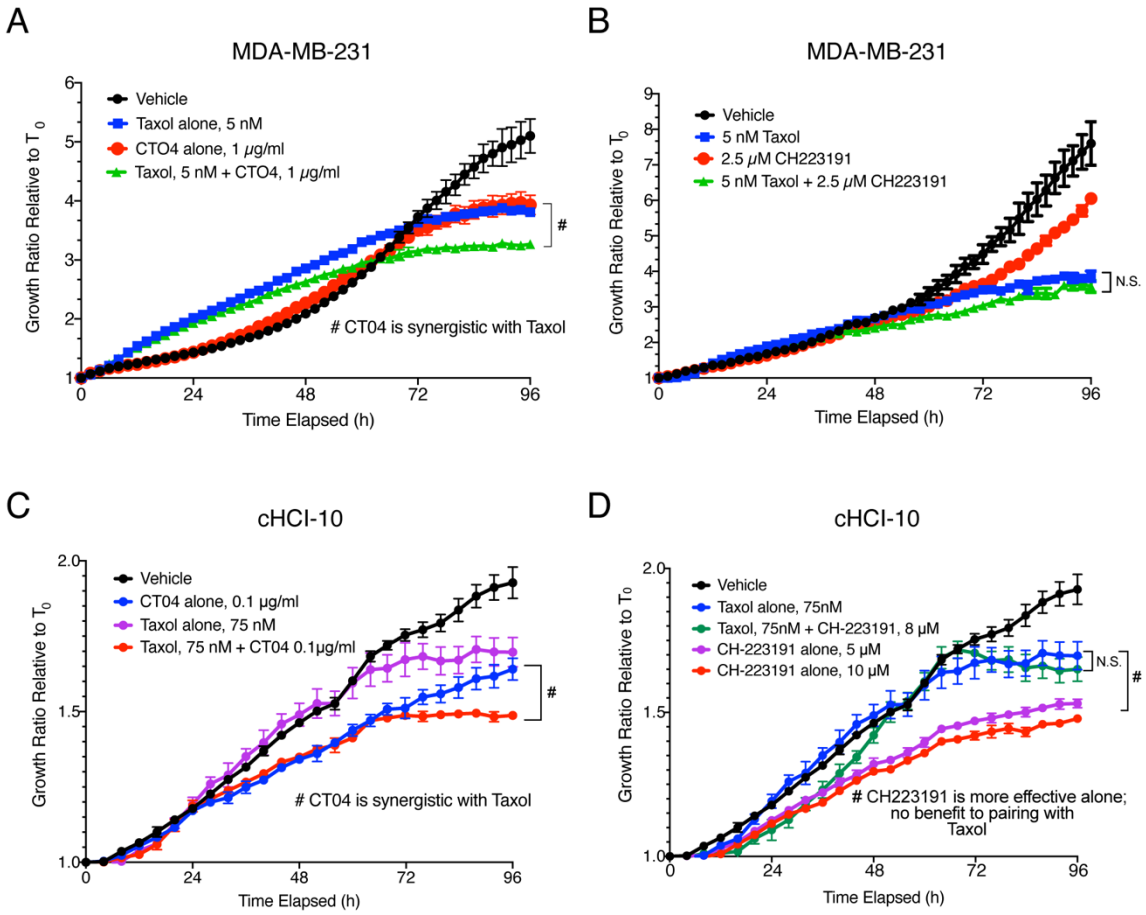

Figure 4.7 Pairing CT04 of CH223191 with paclitaxel is synergistic in TNBC models.

(A-D). Tumor cell growth was measured over time using the IncuCyte S3 live-cell imager as described in the materials and methods. Holding either CT04 or CH223191 constant near each cell-line's specific IC_{50} value, increasing concentrations of paclitaxel were added to the cells and the change in the growth ratio relative to time after drug was added (t = 0) was plotted over time (hours). All data are shown as the mean ± SEM for technical replicates at each time point; each line graph shown is representative of at least 3 independent experiments. # indicate significant differences in the growth ratio among treatments. **I** A representative cartoon model of the oncogenic activities of PTK6 in TNBC. PTK6 expression is regulated by the AhR/GR/HIFs transcriptional complex (39, 121, 122). In turn, PKT6 is a key signaling node of HGF-mediated oncogenic signaling in TNBC. Specifically, the SH2 domain of PTK6 is integral in the regulation of both RhoA and p38 MAPK. As shown, deletion of the SH2 domain, promotes tumorsphere formation via activation of the p38 MAPK. However, deletion of the SH2 domain decreased RhoA and AhR oncogenic activity in our TNBC models (i.e. cellular migration, cellular growth and chemoresistance).

data shown are in the presence of 75 nM paclitaxel (Figure 4.7D). Therefore, treatment of cHCI-10 cells with the Rho inhibitor (CT04) appeared to restore sensitivity to taxanes, but there was no benefit to adding CH223191 to a paclitaxel regimen in this TNBC model. However, these data suggest that TNBC patients who progress on taxanes may remain sensitive to AhR inhibition as a monotherapy.

AhR/PTK6 association via the PTK6 SH2 domain is required for TNBC motility

We next sought to delineate the mechanism underpinning the observed loss of AhR signaling in SH2-del PTK6 cells. Further analysis of AhR-regulated signaling molecules from our RPPA dataset revealed a number of differentially regulated proteins (Figure 4.8A, purple box) including cyclin D1, cyclin E1, and 127hosphor-p65 NF-KB. These proteins have been implicated in cell motility and adhesion (141-143), as well as cell cycle regulation (144, 145). AhR has traditionally been studied as a regulator of environmental toxins and carcinogens (146, 147). AhR is well-known to partner with the aryl hydrocarbon receptor nuclear translocator (ARNT), which is also the obligated heterodimeric partner of HIF1α and HIF2α to form the HIF1 or HIF2 transcription factors. More recently, AhR has been implicated in epithelial cell survival, promotion of EMT, and motility (148-150). Additionally, AhR has been reported to contain phosphotyrosine motifs (151). We showed previously that HGF (i.e. MET receptor signaling) stimulates PTK6 auto-phosphorylation on tyrosine and kinase activation.

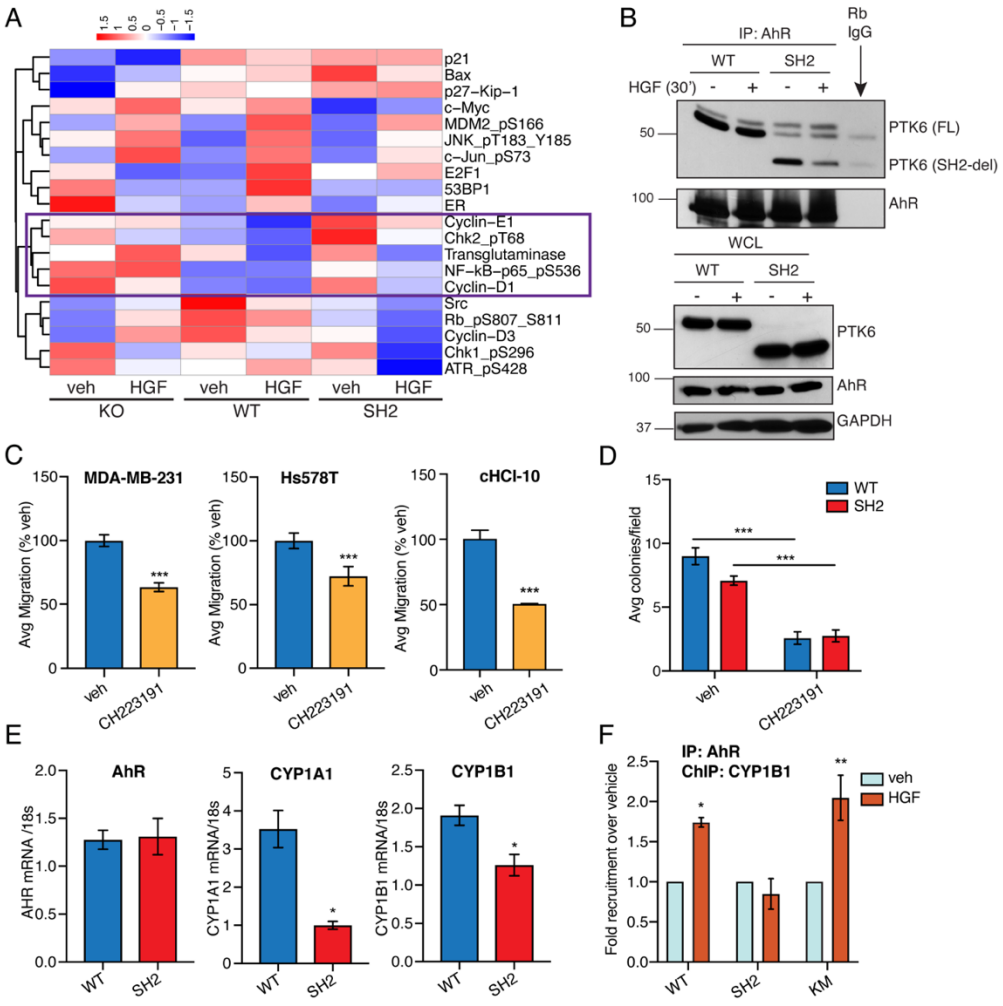

Figure 4.8 AhR activity requires PTK6 SH2 domain.

(**A**) Unsupervised heatmap of RPPA dataset identified by IPA "AhR Signaling". (**B**) MDA-MB-231 cells expressing WT or SH2-del PTK6 were starved and treated with veh or HGF (50 ng/mL; 30 min). AhR-containing complexes were isolated using AhR-specific antibodies and protein G-agarose beads. Western blots were performed on immunocomplexes and whole-cell lysates (FL; full length). Representative blot of n = 3 experimental repeats are shown. (**C**) TNBC migration was examined with AhR inhibitor CH223191 (10 μM). Data were analyzed by Student's *t*-test for significance; ** $p < 0.01$, *** $p < 0.001$ (n = 4). (**D**) Colony formation with AhR inhibitor CH223191 (10 μM). Data was analyzed by two-way ANOVA with post-hoc corrections; *** $p < 0.001$ (n = 3). I mRNA levels of *AhR* and canonical target genes *CYP1A1* and *CYP1B1* in MDA-MB-231 cells stably expressing WT or SH2-del PTK6. Data was analyzed by Student's *t*-test; * $p < 0.05$ (n = 3). (**F**) Recruitment of AhR to the *CYP1B1* promoter region was examined by ChIP-PCR. Data are shown as fold recruitment over vehicle control of combined n = 3 experiments and two-way ANOVA with post-hoc corrections was used to test significance; * $p < 0.05$, ** $p < 0.01$.

Therefore, the presence of co-immunoprecipitated PTK6 and AhR was examined in HGF-treated WT and SH2-del PTK6 expressing MDA-MB-231 cells by immunoblotting. Strikingly, whereas AhR strongly associated with WT PTK6 independent of HGF stimulation, its association with SH2-del PTK6 was diminished to background levels upon HGF stimulation (Figure 4.8B). These data suggest that the PTK6 SH2-domain is needed to support sustained PTK6/AhR interaction when PTK6 is autophosphorylated/activated.

We next turned to AhR antagonism (CH223191) in a panel of TNBC models that expressed AhR (Figure 4.5B) and discovered that AhR inhibition reduced HGF-directed TNBC cell migration in transwell assays (Figure 4.8C). AhR inhibition also decreased anchorage independent colony formation (Figure 4.8D). However, as shown in Figure 4.3C, there was no difference in proliferation/survival as measured by soft agar colony formation between WT and SH2-del PTK6 expressing cells. Given that migration assays were performed over the course of 24 h, it is unlikely that the effect on TNBC migration is due to inhibition of the cell cycle. These data indicate that a sustained AhR/PTK6 interaction predominantly dependent upon the intact PTK6 SH2 domain is required for TNBC motility signaling. In contrast, AhR appears to regulate soft agar growth independently of the PTK6 SH2 domain.

Phosphorylation of AhR tyrosine 9 residue is required for DNA binding (151). To investigate whether AhR target gene expression is impacted in SH2-del

PTK6 cells, we performed qRT-PCR for two AhR target genes *CYP1A1* and *CYP1B1*, two extrahepatic enzymes responsible for metabolism of drugs, carcinogens, and endogenous compounds (148, 150). Interestingly, although AhR mRNA itself was unchanged, *CYP1A1* and *CYP1B1* expression was significantly reduced in SH2-del PTK6 MDA-MB-231 cells (Figure 4.8E). To examine AhR recruitment to *CYP1B1* promoter regions, we conducted ChIP assays in WT and SH2-del PTK6 MDA-MB-231 cells. Robust recruitment of AhR to the *CYP1B1* promoter site was observed with HGF stimulation in both WT and KM PTK6 cells (Figure 4.8F). However, AhR recruitment was strikingly reduced in SH2-del PTK6 cells (Figure 4.8F) indicating that the PTK6 SH2 domain, and not its kinase activity, is required for AhR localization to *CYP1B1* DNA. These data hint at a novel role for PTK6 in the transcription of AhR target genes.

AhR and PTK6 co-expression are associated with poor prognosis

On the basis of our findings that AhR plays an important role in both TNBC motility and colony formation, we next examined whether this is recapitulated in patient specimens following isolation of primary organoids from human breast tumor samples. Three-dimensional epithelial organoid cultures are representative of central breast cancer features and facilitate high-throughput drug screening (152). We first performed qRT-PCR on organoids derived from both normal and malignant tissues to determine whether AhR expression was altered. Indeed, we found that *AHR* mRNA levels were increased in invasive DCIS tumor-derived organoids compared to organoids from normal breast tissue (Figure 4.9A). Consistent with previous reports, *PTK6* transcript levels were also

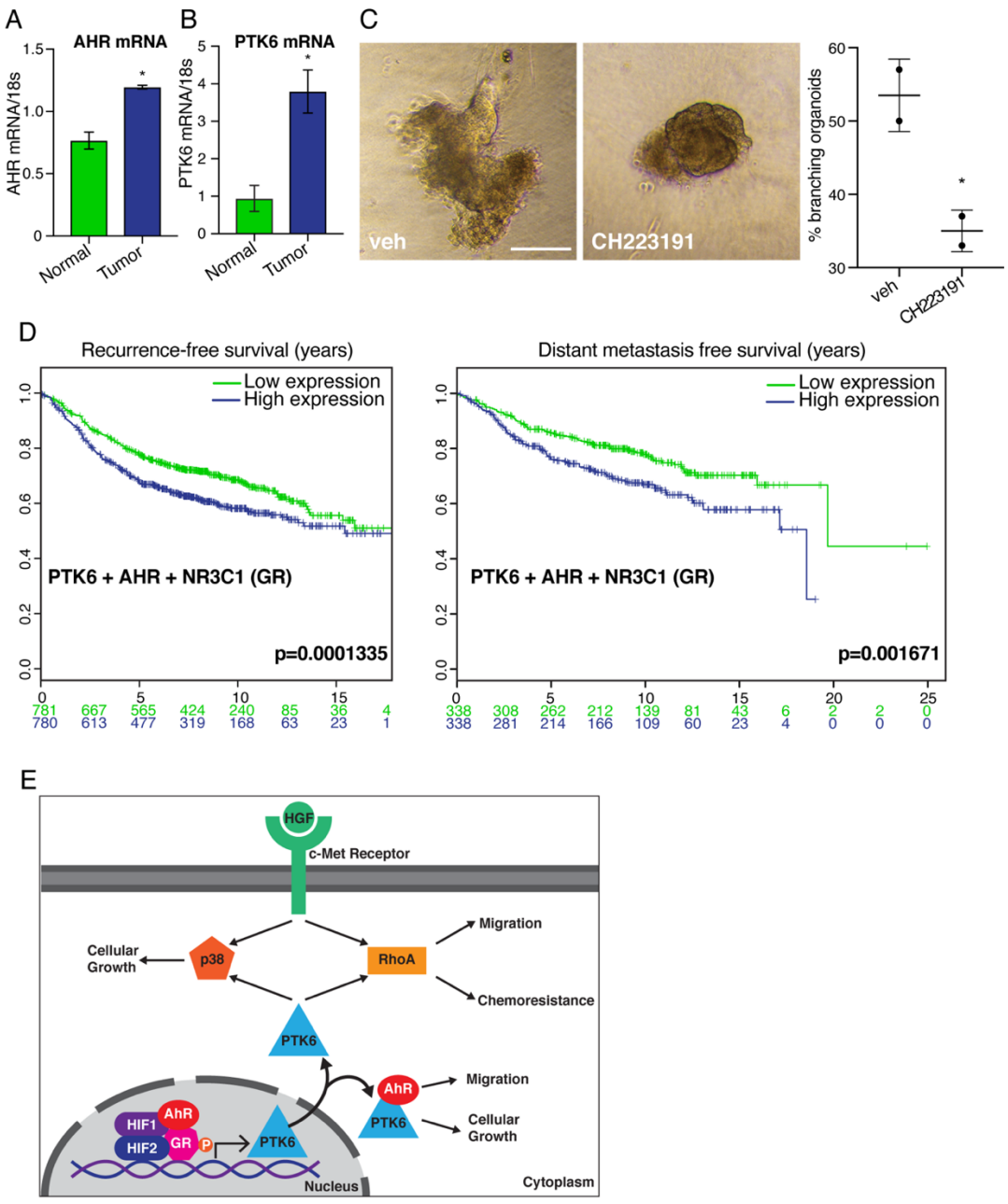

Figure 4.9 AhR and PTK6 expression promote aggressive breast cancer phenotypes.

(**A**) AhR and (**B**) PTK6 mRNA expression was analyzed in organoids isolated from human breast tumor samples or normal adjacent tissue. Data were analyzed by Student's *t*-test; * $p < 0.05$. Data represents the mean ± SD (n = 2). (**C**) Organoids were grown from human malignant tissue and treated with vehicle or CH223191 (10 μM). Representative images of two separate experiments are shown. Branching organoids were quantified by manual counting in ImageJ (n = 5 fields/sample) and expressed as a percentage of total organoid number. Significance was determined by Student's *t*-test; * $p < 0.05$. (**D**) SurvExpress was used to stratify recurrence-free survival (left) and distant metastasis free survival (right) based on median expression of PTK6, AhR, and GR (NR3C1) across all breast cancer subtypes.

higher in tumor samples than normal tissue (Figure 4.9B) (123). We next examined tumor-derived organoid invasion into a Matrigel/Collagen I matrix and found that CH223919 reduced organoid branching (Figure 4.9C). To investigate the relationship between AhR, PTK6, and GR (known to induce PTK6 transcription) in the context of patient outcomes, we employed the SurvExpress tool to analyze survival data using publicly available datasets. Interestingly, co-expression of PTK6, AhR, and GR correlated with a decrease in relapse-free and distant metastasis-free survival (Figure 4.9D). These data demonstrate that the relationship between AhR and PTK6 and metastatic burden is not limited to our cell line models, but also extends to human tumor samples, suggesting that targeting AhR in PTK6+, and likely GR+, TNBC may be useful in the treatment of stage IV metastatic disease. In summary, our data indicate that in TNBC GR/HIF-induction of PTK6 results in a feed-forward signaling cascade dependent on PTK6 SH2 domain-mediated activation of AhR and Rho pathways, leading to increased cell migration, whereas synergy with paclitaxel chemotherapy was observed upon inhibition of Rho (CT04), but not AhR (CH223191) in the TNBC models tested herein (Figure 4.9E).

Discussion

Herein, we have generated PTK6 KO, kinase-dead, and domain-specific cell lines in order to dissect the roles of the different functional domains of PTK6 and their actions in breast cancer. We previously showed that PTK6 is directly regulated by the HIF transcription factors. Our studies clearly show that PTK6 expression negatively correlates with overall survival and that re-expression of

PTK6 in the context of HIF DKO cells rescues cell motility, invasion and lung metastasis (Figure 4.1). Likewise, whereas deletion of PTK6 does not impair primary tumor growth, deletion of PTK6 represses lung metastasis in a tail vein assay, whereas the forced expression of *PTK6* slightly enhances lung metastasis. Using a variety of PTK6 domain mutants, we now show that the kinase domain of PTK6 is dispensable for TNBC migration and tumorsphere formation and that these activities are instead regulated by the SH2-domain of PTK6 (Figure 4.3). Additionally, we report that the SH2-domain of PTK6 is essential for the HGF-induced activation of RhoA (Figure 4.5 and Table 4.1) and is strongly associated with AhR binding to phosphorylated/activated PTK6 (Figure 4.8). The SH2 domain is known to bind substrate phosphotyrosine motifs; these scaffolding actions appear to be central to execution of PTK6-mediated CSC phenotypes and to cell migration in TNBC cells. Together, our results indicate PTK6 acts as a key hub/integrator of oncogenic signaling pathways for these biological activities. This conclusion is supported by our RPPA studies, which confirmed the regulation of distinct cellular signaling pathways by either the PTK6 kinase domain, which impacted proliferation/survival, relative to the PTK6 SH2 domain, which mediates migration potential and stemness properties.

Specifically, we observed that deletion of the SH2 domain promoted tumorsphere formation but decreased chemotactic migration of TNBC cells. This dichotomy reflects the complexity of PTK6 signaling in cancer. The PTK6 SH2 domain mediates substrate interactions that are weaker than those of c-Src, and,

therefore, were thought to be primarily responsible for regulating catalytic activity (45). It is therefore possible that removal of the SH2 domain also alters PTK6 kinase activity. However, mutation of the C-terminal Y447 residue, which results in a constitutively active PTK6 protein, did not mimic SH2-del biology (Figure 4.3). Furthermore, p38 phosphorylation was increased in SH2-del PTK6 expressing TNBC cells. Along with results showing that WT and kinase-dead (KM) PTK6+ cancer cell behaviors are indistinct in the context of migration and tumorsphere formation, we can conclude that the SH2 domain is primarily responsible for mediating PTK6 oncogenic signaling. This novel observation is highly relevant to PTK6 drug design as previous efforts have focused on targeting PTK6 kinase activity (62).

Therapeutic strategies targeting PTK6 to date have largely focused on targeting the kinase domain with small molecule inhibitors that recognize the ATP-binding pocket of the kinase domain (153). While PTK6 kinase inhibition appears useful in colon cancer models, this strategy failed to decrease tumorigenesis *in vitro* in either luminal and TNBC models of breast cancer (46, 62), stalling their progress to successful clinical trials. To our knowledge PTK6 SH2 domain-specific inhibitors do not yet exist. Lack of chemical inhibitors to this domain is likely due to the challenging nature of designing such inhibitors to large non-enzyme domains (154). However, our data clearly demonstrate that inhibition of two downstream effectors of PTK6 that are mediated by the SH2 domain (RhoA, AhR) are effective in decreasing PTK6 oncogenic activity in

TNBC. However, since CT04 (RhoA inhibitor) is a ~24 kDa protein, targeting AhR via the small molecular inhibitor CH223191 may be more amenable for future pre-clinical studies in rodents as an anti-metastatic agent. In taxane-sensitive MDA-MB-231 cells and in taxane-refractory cHCI-10 PDX cells, CT04 was synergistic with paclitaxel, suggesting that adding a Rho inhibitor to a paclitaxel regimen may benefit patients who are progressing on taxanes alone. These data also demonstrate that PTK6-mediated chemoresistance to paclitaxel can be reversed by co-treatment with paclitaxel and a Rho inhibitor. In contrast, CH223191 did not enhance paclitaxel-induced growth inhibition in MDA-MB-231 cells and it was neutral or antagonistic to paclitaxel in the cHCI-10 model. Interestingly, CH223191 alone inhibited cHCI-10 cell growth, suggesting its use as a monotherapy in taxane-resistant patients may be beneficial. Even if CH223191 is not additive to paclitaxel to enhance tumor cell growth inhibition, it clearly represses cell motility and invasion, at least *in vitro*. Additional studies are required to validate PTK6 and GR as valuable biomarkers that may predict Rho or AhR inhibition response in combination with taxanes, or other cytotoxic agents, in TNBC. PTK6 has been shown to directly bind to and activate Rac1 GTPase in luminal breast cancer models (123, 125, 155). Our RPPA data identified increased RhoGDI signaling in SH2-del expressing TNBC cells (Table 4.1). Here, we demonstrate that the PTK6 SH2 domain is required for the activation of RhoA in TNBC cell lines (Figure 4.8). These data suggest that the PTK6 SH2-domain is critical for RhoA-signaling mediation of motility in TNBC. However, no direct protein interactions were found between RhoA and PTK6 in

TNBC cells. It is possible that PTK6 interacts with RhoGDIs instead of directly interacting with RhoA through the SH2-domain since proteomic analyses have identified RhoGDI as tyrosine-phosphorylated proteins in cancer cells (156). In addition, the mechanism by which RhoGDIs negatively regulate Rho GTPases remains largely undefined. Taken in the context of our current data, we propose that PTK6 sequesters RhoGDIs via the SH2 domain, allowing for increased RhoA activation. Alternatively, PTK6 activation of RhoA may occur via paxillin phosphorylation as was reported previously for Rac1 (75). Further studies are needed to dissect the role of PTK6 in the activation of the Rho pathway.

Similarly, another candidate pathway that is regulated downstream of engagement with PTK6, in part via the SH2 domain, is the stress kinase p38 MAPK, which has been implicated in EMT, a process resembling stemness in cancer cells (157, 158). MAPK activation occurs after dual phosphorylation of their Thr-Gly-Tyrosine motifs by upstream MEK (MAP kinase kinase) family members (159). Notably, PTK6 expression was previously shown to amplify EGF-stimulated p38-driven pro-survival phenotypes, and mammary gland-specific expression of PTK6 in *WAP-PTK6* transgenic mice resulted in greatly elevated p38 MAPK activity in mammary tissues, delayed involution, and latent mammary tumor formation (126). These findings support our data showing that inhibition of p38 MAPK decreased PTK6-induced TNBC cell growth in suspension. Conversely however, our data show that loss of the PTK6 SH2 domain increases p38 phosphorylation. Taken together, these results suggest

that PTK6 activates p38 MAPK via other PTK6 domains and that this activity is further elevated upon deletion of the SH2 domain. Consistent with this hypothesis, the PTK6 SH2 domain may regulate p38 MAPK signaling by modulating protein-tyrosine phosphatase (PTP) activity. PTP enzymes are themselves phosphorylated on tyrosine residues, providing binding sites for SH2-containing proteins (155). Alternatively, access to downstream effector pathways may be altered upon loss of the PTK6 SH2 domain (i.e. via altered competition for PTK6 binding), thereby favoring activation of the p38 pathway via the PTK6 kinase or SH3 domains. Further studies are required to elucidate the complex mechanisms of PTK6-mediated activation/inactivation of p38 MAPK and regulation of cancer cell stem-like properties.

Pathway analysis of RPPA antibody intensity data also nominated AhR signaling as a critical signaling pathway downstream of the PTK6 SH2 domain. We find that AhR inhibition reduces both TNBC cell motility and chemotaxis-mediated migration (Figure 4.8C, 4.8D). We were surprised to note that when PTK6 and AhR were unable to interact in SH2-del PTK6 expressing cells, AhR target gene expression was also disrupted (Figure 4.8B, 4.8E), implicating PTK6 in AhR-dependent regulation of transcription. In support of this, the AhR 137hosphor-tyrosine 9 motif was shown to be critical for AhR transcriptional activity (151). AhR target genes CYP1A1 and CYP1B1 are members of the CYP450 enzyme family and are responsible for the metabolism of polycyclic aromatic hydrocarbons found in both endogenous and exogenous compounds

(160). Furthermore, these enzymes are known to be involved in carcinogenesis via production of carcinogenic metabolites (148). Increased levels of these enzymes are found in colon, bladder, and breast cancer (161, 162). Interestingly, PTK6 and AhR are both overexpressed in colon and bladder cancers (163-165), indicating that this phenomenon is not exclusive to breast neoplasia. GR has also been implicated in bladder and colon cancer (75); recent literature linking AhR signaling with GR in hypoxic conditions suggests that GR-regulated HIF-1α dimerizes with ARNT (166, 167) leading to cross-talk between the AhR/ARNT and GR/HIF pathways. Furthermore, activation of GR with glucocorticoids was shown to promote breast cancer metastasis (25). Taken in the context of our previous data reporting hypoxia-induced PTK6 expression (122) and the results described herein, we suggest that PTK6 simultaneously orchestrates GR and AhR signaling pathways to promote disease progression and overall poor prognosis in these patients (Figure 4.9) (75, 122). The interdependence of these molecules may mediate a sustained signaling response, resulting in tumor cell dissemination and survival in circulation.

In conclusion, we propose that inhibition of PTK6 should not be limited to targeting the PTK6 kinase domain but should also target the PTK6 SH2-domain. Our data show that Rho or AhR inhibition reduces both TNBC motility and soft agar growth *in vitro.* Targeting PTK6 via these SH2 domain interactors could increase overall survival and decrease metastatic spread in TNBC patients, which warrants further investigation. Despite our results that implicate Rho and

p38 MAPK as important effector proteins of PTK6, targeting these ubiquitous proteins clinically will be challenging and will require targeting their effector proteins for clinical efficacy (152, 168, 169). Conversely, AhR is an attractive targetable mediator of carcinogenesis/transformation of epithelial cells (170). As a ligand-activated transcription factor and nuclear receptor, useful small molecule receptor antagonists would need to be optimized for future use in pre-clinical studies aimed at treating breast and other PTK6+ cancers.

Chapter 5 Conclusions

Summary and Conclusions

We conclude that GR is a key mediator of TNBC progression. We identified that ligand-independent but p38 MAPK-induced phosphorylation of GR on S134 is essential for its deleterious actions as a driver of TNBC migration, invasion, anchorage-independent cell growth, and tumorsphere formation. At the molecular level, pS134-GR is required for basal expression of MAP3K5, a required MAP kinase-kinase-kinase component of the intact p38 MAPK module. These are key discoveries for identifying how cellular stress-mediated events may increase progression of breast cancer. Our work demonstrates how GR is the integrator of cellular stress, local cytokines (TGFβ1) and growth factors (HGF). Cellular stress in the context of cytokines and growth factors can induce phosphorylation of GR on S134 and this acts as an input signaling process to activate GR. Glucocorticoid receptor then acts in a “more malignant” manner by direct regulation of genes that mediate advanced cancer phenotypes. Although more research is required, it is thought provoking to believe that GR acts differently in non-TNBC and TNBC, because of post-translational modifications such as phosphorylation that predominate in TNBC. These phosphorylation events alter GR actions in cellular signaling profoundly. In a similar manner, these GR modifications are mediated by different forms of cellular stress (i.e. hypoxia, ROS, inflammation). Notably, as demonstrated in our work, TGFβ1 increases phosphorylation of GR in multiple TNBC models. These phosphorylation events on GR are mediated by the p38 cellular stress-induced MAPK. P38 MAPK is regulated by a diverse array of stress processes including

chronic inflammation (reviewed in (66)). For example, when chronic inflammation ensues in esophageal tissue, this increases the TGFβ1 levels which in turn leads to fibrosis (i.e. “wound that never heals”) (171). In a similar manner, these events and the analogous cellular signaling axis (i.e. signaling inputs to 142hosphor-GR) are highly relevant to breast cancer progression (Figure 3.13).

Additionally, we also identified that phosphorylation of GR on S134 is required for the ligand-mediated expression of PDK4, an important gene required for metabolic homeostasis in TNBC. Metabolic reprogramming is required for many processes that are essential for EMT such as migration and stem-cell like behavior (172). PDK4 has been previously identified to be essential in the regulation of EMT, metabolic programming, apoptosis, and stemness. In a recent report, it was shown that miR-211 decreases the expression of PDK4 in breast cancer cell lines (TNBC and non-TNBC). Moreover, high expression of PDK4 correlated with lower overall survival in both ER-positive and ER-negative breast cancer. Similar to our results, miR-211 was shown to suppress the glycolytic pathway, thus high levels of PDK4 promote glycolysis (173). By increasing aerobic glycolysis, breast cancer cells sustain the Warburg effect and in turn can induce EMT (reviewed in (172)).

MAP3K5/ASK1 is another cellular stress-related protein that is understudied in the context of cancer. Notably, MAP3K5/ASK1 actions in TNBC are not yet fully understood in breast cancer, specifically in TNBC. We identified

that its expression is increased in TNBC. Additionally, we identified that it is an important mediator of TGFβ1-induced GR phosphorylation and cancer cell migration. However, due to its importance in apoptosis in non-cancer cellular signaling, it is possible that MAP3K5 is involved in inducing oncogenesis of TNBC in various ways. For example, it is well known that 14-3-3ζ is important for the activity of MAP3K5/ASK1 in various models. Because 14-3-3ζ has been implicated in many processes of breast cancer, it is possible that ASK1/MAP3K5 is also an important factor for pathogenesis of breast cancer (34, 35, 174) .

Glucocorticoid receptors are a tremendously complex steroid hormone receptor that responds differently depending on the cellular context as seen in Chapter 3. Thus, in future studies, we plan to better define how post-translational modifications such as phosphorylation on S134 alter GR occupancy of DNA. Recent studies have shown that using single cell RNA-Seq dissects several population subtypes even in the presence of the same conditions (175). These findings highlight the highly specific context-dependent mechanisms of GR in cell signaling and cancer biology.

GR is essential for the expression of PTK6 and yet the specific role of PTK6 in TNBC remains unknown; we decided to explore PTK6-dependent actions in TNBC. Using MDA-MB-231 cells, we expressed different mutant versions of PTK6. We identified that the SH2 domain is important for various phenotypes in TNBC. Specifically, using an *in vivo* approach we identified PTK6

as a major player in promoting TNBC metastasis to the lungs. Domain-dependent functions were identified by screening different important phenotypes for TNBC such as growth, migration, and tumorsphere formation. We identified that the SH2-domain is essential for promoting migration in TNBC, yet its loss induces cells to form more tumorspheres. In the context of metastasis and possible TNBC dissemination, this has many implications. First, it is possible that PTK6 is relevant for the integration of both stemness and metastasis signaling pathways. Thus, when SH2-specific functions are activated, TNBC cells are able to migrate. However, upon losing SH2-specific activity, TNBC cell functions will skew towards forming more tumorspheres (stem-cell like behavior). When PTK6 is not promoting migration, it is promoting stem-cell like behavior via engagement with separate signaling pathways. Both migration and stemness are essential processes for EMT.

Significance

We identified a pS134-GR 24-gene signature induced by TGFβ1 that may serve as a valuable paired diagnostic with which to identify patients who have GR-driven breast tumors and are thus at high risk of succumbing to metastatic disease. As GR is a ubiquitous steroid hormone receptor, pS134-GR may function similarly in other endocrine-related and/or highly metastatic forms of neoplasia (i.e. prostate cancer, ovarian cancer, melanoma). More work is needed to explore these avenues for clinical translation.

Further studies are needed to better understand how to inhibit cellular-stress and glucocorticoid-mediated processes in the context of breast cancer. Many of these processes are required for cellular homeostasis and more importantly for immunological response to pathogens. Accordingly, immunotherapy has become a possible way to treat TNBC. Recent reports have shed light about the use of these agents, such as pembrolizumab, in TNBC patients (11). Inhibition of GR signaling will potentially further promote the actions of immunotherapy in solid tumors. It has been well established that GR and its ligands are immunosuppressive (13). Thus, inhibition of GR could induce immune activation and further potentiate the action of the adaptive and innate immune system against TNBC. On the other hand, few research projects have investigated the role of GR in the mesenchymal/hematopoietic-derived cells of the tumor microenvironment such as macrophages, T-cells, B-cells, fibroblasts and others. It is becoming increasingly important to understand what the role of GR in these types of cells is and what is the state of post-translational modifications of GR. Single-cell sequencing could be used to better understand GR in these contexts.

Additionally, in terms of potential treatments for TNBC, our data show that RhoA inhibition with paclitaxel may enhance growth inhibition. Further studies are needed to evaluate the interface between RhoA pathways and GR. We speculate that there is some interaction between these key players of migration. Potentially, co-inhibition may potentiate inhibition of oncogenesis in GR+ tumors. Further

studies will aim to better define this potential interaction in TNBC and its possible role in therapeutic approaches.

References

1. Siegel RL, Miller KD, Jemal A. Cancer statistics, 2020. CA Cancer J Clin. 2020;70(1):7-30. Epub 2020/01/09. doi: 10.3322/caac.21590. PubMed PMID: 31912902.

2. SEER. Cancer Stat Facts: Female Breast Cancer 2020 [May 22, 2020]. Available from: https://seer.cancer.gov/statfacts/html/breast.html.

3. Hammond ME, Hayes DF, Dowsett M, Allred DC, Hagerty KL, Badve S, et al. American Society of Clinical Oncology/College of American Pathologists guideline recommendations for immunohistochemical testing of estrogen and progesterone receptors in breast cancer (unabridged version). Arch Pathol Lab Med. 2010;134(7):e48-72. Epub 2010/07/01. doi: 10.1043/1543-2165-134.7.e48. PubMed PMID: 20586616.

4. Hammond ME, Hayes DF, Dowsett M, Allred DC, Hagerty KL, Badve S, et al. American Society of Clinical Oncology/College Of American Pathologists guideline recommendations for immunohistochemical testing of estrogen and progesterone receptors in breast cancer. J Clin Oncol. 2010;28(16):2784-95. Epub 2010/04/21. doi: 10.1200/JCO.2009.25.6529. PubMed PMID: 20404251; PubMed Central PMCID: PMCPMC2881855.

5. Network NCC. Breast Cancer (Version 4.2020) 2020 [cited 2020 May 17, 2020].

6. Martin M, Rodriguez-Lescure A, Ruiz A, Alba E, Calvo L, Ruiz-Borrego M, et al. Molecular predictors of efficacy of adjuvant weekly paclitaxel in early breast cancer. Breast Cancer Res Treat. 2010;123(1):149-57. Epub 2009/12/29. doi: 10.1007/s10549-009-0663-z. PubMed PMID: 20037779.

7. Hugh J, Hanson J, Cheang MC, Nielsen TO, Perou CM, Dumontet C, et al. Breast cancer subtypes and response to docetaxel in node-positive breast cancer: use of an immunohistochemical definition in the BCIRG 001 trial. J Clin Oncol. 2009;27(8):1168-76. Epub 2009/02/11. doi: 10.1200/JCO.2008.18.1024. PubMed PMID: 19204205; PubMed Central PMCID: PMCPMC2667821.

8. Hayes DF, Thor AD, Dressler LG, Weaver D, Edgerton S, Cowan D, et al. HER2 and response to paclitaxel in node-positive breast cancer. N Engl J Med. 2007;357(15):1496-506. Epub 2007/10/12. doi: 10.1056/NEJMoa071167. PubMed PMID: 17928597.

9. Bardia A, Mayer IA, Vahdat LT, Tolaney SM, Isakoff SJ, Diamond JR, et al. Sacituzumab Govitecan-hziy in Refractory Metastatic Triple-Negative Breast

Cancer. N Engl J Med. 2019;380(8):741-51. Epub 2019/02/21. doi: 10.1056/NEJMoa1814213. PubMed PMID: 30786188.

10. Robson M, Im SA, Senkus E, Xu B, Domchek SM, Masuda N, et al. Olaparib for Metastatic Breast Cancer in Patients with a Germline BRCA Mutation. N Engl J Med. 2017;377(6):523-33. Epub 2017/06/06. doi: 10.1056/NEJMoa1706450. PubMed PMID: 28578601.

11. Schmid P, Cortes J, Pusztai L, McArthur H, Kummel S, Bergh J, et al. Pembrolizumab for Early Triple-Negative Breast Cancer. N Engl J Med. 2020;382(9):810-21. Epub 2020/02/27. doi: 10.1056/NEJMoa1910549. PubMed PMID: 32101663.

12. Giovannelli P, Di Donato M, Galasso G, Di Zazzo E, Bilancio A, Migliaccio A. The Androgen Receptor in Breast Cancer. Front Endocrinol (Lausanne). 2018;9:492. Epub 2018/09/14. doi: 10.3389/fendo.2018.00492. PubMed PMID: 30210453; PubMed Central PMCID: PMCPMC6122126.

13. Oakley RH, Cidlowski JA. The biology of the glucocorticoid receptor: new signaling mechanisms in health and disease. J Allergy Clin Immunol. 2013;132(5):1033-44. Epub 2013/10/03. doi: 10.1016/j.jaci.2013.09.007. PubMed PMID: 24084075; PubMed Central PMCID: PMCPMC4084612.

14. Evans RM. The steroid and thyroid hormone receptor superfamily. Science. 1988;240(4854):889-95. Epub 1988/05/13. doi: 10.1126/science.3283939. PubMed PMID: 3283939; PubMed Central PMCID: PMCPMC6159881.

15. Weikum ER, Knuesel MT, Ortlund EA, Yamamoto KR. Glucocorticoid receptor control of transcription: precision and plasticity via allostery. Nat Rev Mol Cell Biol. 2017;18(3):159-74. Epub 2017/01/06. doi: 10.1038/nrm.2016.152. PubMed PMID: 28053348; PubMed Central PMCID: PMCPMC6257982.

16. Hapgood JP, Avenant C, Moliki JM. Glucocorticoid-independent modulation of GR activity: Implications for immunotherapy. Pharmacol Ther. 2016;165:93-113. Epub 2016/06/12. doi: 10.1016/j.pharmthera.2016.06.002. PubMed PMID: 27288728; PubMed Central PMCID: PMCPMC5195849.

17. Luisi BF, Xu WX, Otwinowski Z, Freedman LP, Yamamoto KR, Sigler PB. Crystallographic analysis of the interaction of the glucocorticoid receptor with DNA. Nature. 1991;352(6335):497-505. Epub 1991/08/08. doi: 10.1038/352497a0. PubMed PMID: 1865905.

18. Hoffman JA, Trotter KW, Ward JM, Archer TK. BRG1 governs glucocorticoid receptor interactions with chromatin and pioneer factors across the genome. Elife. 2018;7. Epub 2018/05/25. doi: 10.7554/eLife.35073. PubMed PMID: 29792595; PubMed Central PMCID: PMCPMC5967868.

19. Ritter HD, Antonova L, Mueller CR. The unliganded glucocorticoid receptor positively regulates the tumor suppressor gene BRCA1 through GABP beta. Mol Cancer Res. 2012;10(4):558-69. Epub 2012/02/14. doi: 10.1158/1541-7786.MCR-11-0423-T. PubMed PMID: 22328717.

20. Samarasinghe RA, Di Maio R, Volonte D, Galbiati F, Lewis M, Romero G, et al. Nongenomic glucocorticoid receptor action regulates gap junction intercellular communication and neural progenitor cell proliferation. Proc Natl Acad Sci U S A. 2011;108(40):16657-62. Epub 2011/09/21. doi: 10.1073/pnas.1102821108. PubMed PMID: 21930911; PubMed Central PMCID: PMCPMC3189065.

21. Block TS, Murphy TI, Munster PN, Nguyen DP, Lynch FJ. Glucocorticoid receptor expression in 20 solid tumor types using immunohistochemistry assay. Cancer Manag Res. 2017;9:65-72. Epub 2017/03/16. doi: 10.2147/CMAR.S124475. PubMed PMID: 28293120; PubMed Central PMCID: PMCPMC5345989.

22. Pan D, Kocherginsky M, Conzen SD. Activation of the glucocorticoid receptor is associated with poor prognosis in estrogen receptor-negative breast cancer. Cancer Res. 2011;71(20):6360-70. Epub 2011/08/27. doi: 10.1158/0008-5472.CAN-11-0362. PubMed PMID: 21868756; PubMed Central PMCID: PMCPMC3514452.

23. Regan Anderson TM, Ma S, Perez Kerkvliet C, Peng Y, Helle TM, Krutilina RI, et al. Taxol Induces Brk-dependent Prosurvival Phenotypes in TNBC Cells through an AhR/GR/HIF-driven Signaling Axis. Mol Cancer Res. 2018;16(11):1761-72. Epub 2018/07/12. doi: 10.1158/1541-7786.MCR-18-0410. PubMed PMID: 29991529; PubMed Central PMCID: PMCPMC6214723.

24. West DC, Kocherginsky M, Tonsing-Carter EY, Dolcen DN, Hosfield DJ, Lastra RR, et al. Discovery of a Glucocorticoid Receptor (GR) Activity Signature Using Selective GR Antagonism in ER-Negative Breast Cancer. Clin Cancer Res. 2018;24(14):3433-46. Epub 2018/04/11. doi: 10.1158/1078-0432.CCR-17-2793. PubMed PMID: 29636357; PubMed Central PMCID: PMCPMC6530562.

25. Obradovic MMS, Hamelin B, Manevski N, Couto JP, Sethi A, Coissieux MM, et al. Glucocorticoids promote breast cancer metastasis. Nature. 2019;567(7749):540-4. Epub 2019/03/15. doi: 10.1038/s41586-019-1019-4. PubMed PMID: 30867597.

26. Shi W, Wang D, Yuan X, Liu Y, Guo X, Li J, et al. Glucocorticoid receptor-IRS-1 axis controls EMT and the metastasis of breast cancers. J Mol Cell Biol. 2019;11(12):1042-55. Epub 2019/02/07. doi: 10.1093/jmcb/mjz001. PubMed PMID: 30726932; PubMed Central PMCID: PMCPMC6934157.

27. Kanai A, McNamara KM, Iwabuchi E, Miki Y, Onodera Y, Guestini F, et al. Significance of glucocorticoid signaling in triple-negative breast cancer patients: a

newly revealed interaction with androgen signaling. Breast Cancer Res Treat. 2020;180(1):97-110. Epub 2020/01/29. doi: 10.1007/s10549-020-05523-7. PubMed PMID: 31989378.

28. Dwyer AR, Truong TH, Ostrander JH, Lange CA. Steroid Receptors as MAPK Signaling Sensors in Breast Cancer: Let the Fates Decide. J Mol Endocrinol. 2020. Epub 2020/03/27. doi: 10.1530/JME-19-0274. PubMed PMID: 32209723.

29. Wallace AD, Cao Y, Chandramouleeswaran S, Cidlowski JA. Lysine 419 targets human glucocorticoid receptor for proteasomal degradation. Steroids. 2010;75(12):1016-23. Epub 2010/07/14. doi: 10.1016/j.steroids.2010.06.015. PubMed PMID: 20619282; PubMed Central PMCID: PMCPMC2926287.

30. Hua G, Paulen L, Chambon P. GR SUMOylation and formation of an SUMO-SMRT/NCoR1-HDAC3 repressing complex is mandatory for GC-induced IR nGRE-mediated transrepression. Proc Natl Acad Sci U S A. 2016;113(5):E626-34. Epub 2015/12/30. doi: 10.1073/pnas.1522821113. PubMed PMID: 26712002; PubMed Central PMCID: PMCPMC4747746.

31. Ito K, Yamamura S, Essilfie-Quaye S, Cosio B, Ito M, Barnes PJ, et al. Histone deacetylase 2-mediated deacetylation of the glucocorticoid receptor enables NF-kappaB suppression. J Exp Med. 2006;203(1):7-13. Epub 2005/12/29. doi: 10.1084/jem.20050466. PubMed PMID: 16380507; PubMed Central PMCID: PMCPMC2118081.

32. Webster JC, Jewell CM, Bodwell JE, Munck A, Sar M, Cidlowski JA. Mouse glucocorticoid receptor phosphorylation status influences multiple functions of the receptor protein. J Biol Chem. 1997;272(14):9287-93. Epub 1997/04/04. doi: 10.1074/jbc.272.14.9287. PubMed PMID: 9083064.

33. Galliher-Beckley AJ, Williams JG, Cidlowski JA. Ligand-independent phosphorylation of the glucocorticoid receptor integrates cellular stress pathways with nuclear receptor signaling. Mol Cell Biol. 2011;31(23):4663-75. Epub 2011/09/21. doi: 10.1128/MCB.05866-11. PubMed PMID: 21930780; PubMed Central PMCID: PMCPMC3232926.

34. Neal CL, Yao J, Yang W, Zhou X, Nguyen NT, Lu J, et al. 14-3-3zeta overexpression defines high risk for breast cancer recurrence and promotes cancer cell survival. Cancer Res. 2009;69(8):3425-32. Epub 2009/03/26. doi: 10.1158/0008-5472.CAN-08-2765. PubMed PMID: 19318578; PubMed Central PMCID: PMCPMC2671640.

35. Xu J, Acharya S, Sahin O, Zhang Q, Saito Y, Yao J, et al. 14-3-3zeta turns TGF-beta's function from tumor suppressor to metastasis promoter in breast cancer by contextual changes of Smad partners from p53 to Gli2. Cancer Cell. 2015;27(2):177-92. Epub 2015/02/12. doi: 10.1016/j.ccell.2014.11.025. PubMed PMID: 25670079; PubMed Central PMCID: PMCPMC4325275.

36. Wu W, Chaudhuri S, Brickley DR, Pang D, Karrison T, Conzen SD. Microarray analysis reveals glucocorticoid-regulated survival genes that are associated with inhibition of apoptosis in breast epithelial cells. Cancer Res. 2004;64(5):1757-64. Epub 2004/03/05. doi: 10.1158/0008-5472.can-03-2546. PubMed PMID: 14996737.

37. Mendoza MC, Er EE, Blenis J. The Ras-ERK and PI3K-mTOR pathways: cross-talk and compensation. Trends Biochem Sci. 2011;36(6):320-8. Epub 2011/05/03. doi: 10.1016/j.tibs.2011.03.006. PubMed PMID: 21531565; PubMed Central PMCID: PMCPMC3112285.

38. Serfas MS, Tyner AL. Brk, Srm, Frk, and Src42A form a distinct family of intracellular Src-like tyrosine kinases. Oncol Res. 2003;13(6-10):409-19. Epub 2003/05/03. doi: 10.3727/096504003108748438. PubMed PMID: 12725532.

39. Regan Anderson TM, Ma SH, Raj GV, Cidlowski JA, Helle TM, Knutson TP, et al. Breast Tumor Kinase (Brk/PTK6) Is Induced by HIF, Glucocorticoid Receptor, and PELP1-Mediated Stress Signaling in Triple-Negative Breast Cancer. Cancer Res. 2016;76(6):1653-63. Epub 2016/01/31. doi: 10.1158/0008-5472.CAN-15-2510. PubMed PMID: 26825173; PubMed Central PMCID: PMCPMC4794366.

40. Regan Anderson TM, Peacock DL, Daniel AR, Hubbard GK, Lofgren KA, Girard BJ, et al. Breast tumor kinase (Brk/PTK6) is a mediator of hypoxia-associated breast cancer progression. Cancer Res. 2013;73(18):5810-20. Epub 2013/08/10. doi: 10.1158/0008-5472.CAN-13-0523. PubMed PMID: 23928995; PubMed Central PMCID: PMCPMC3820501.

41. Ostrander JH, Daniel AR, Lofgren K, Kleer CG, Lange CA. Breast tumor kinase (protein tyrosine kinase 6) regulates heregulin-induced activation of ERK5 and p38 MAP kinases in breast cancer cells. Cancer Res. 2007;67(9):4199-209. Epub 2007/05/08. doi: 10.1158/0008-5472.CAN-06-3409. PubMed PMID: 17483331.

42. Peng M, Emmadi R, Wang Z, Wiley EL, Gann PH, Khan SA, et al. PTK6/BRK is expressed in the normal mammary gland and activated at the plasma membrane in breast tumors. Oncotarget. 2014;5(15):6038-48. Epub 2014/08/26. doi: 10.18632/oncotarget.2153. PubMed PMID: 25153721; PubMed Central PMCID: PMCPMC4171611.

43. Hong E, Shin J, Kim HI, Lee ST, Lee W. Solution structure and backbone dynamics of the non-receptor protein-tyrosine kinase-6 Src homology 2 domain. J Biol Chem. 2004;279(28):29700-8. Epub 2004/04/02. doi: 10.1074/jbc.M313185200. PubMed PMID: 15056653.

44. Zheng Y, Wang Z, Bie W, Brauer PM, Perez White BE, Li J, et al. PTK6 activation at the membrane regulates epithelial-mesenchymal transition in prostate cancer. Cancer Res. 2013;73(17):5426-37. Epub 2013/07/17. doi:

10.1158/0008-5472.CAN-13-0443. PubMed PMID: 23856248; PubMed Central PMCID: PMCPMC3766391.

45. Tsui T, Miller WT. Cancer-Associated Mutations in Breast Tumor Kinase/PTK6 Differentially Affect Enzyme Activity and Substrate Recognition. Biochemistry. 2015;54(20):3173-82. doi: 10.1021/acs.biochem.5b00303.

46. Mathur PS, Gierut JJ, Guzman G, Xie H, Xicola RM, Llor X, et al. Kinase-Dependent and -Independent Roles for PTK6 in Colon Cancer. Mol Cancer Res. 2016;14(6):563-73. Epub 2016/03/18. doi: 10.1158/1541-7786.MCR-15-0450. PubMed PMID: 26983689; PubMed Central PMCID: PMCPMC4912439.

47. Harvey AJ, Pennington CJ, Porter S, Burmi RS, Edwards DR, Court W, et al. Brk protects breast cancer cells from autophagic cell death induced by loss of anchorage. Am J Pathol. 2009;175(3):1226-34. Epub 2009/08/08. doi: 10.2353/ajpath.2009.080811. PubMed PMID: 19661439; PubMed Central PMCID: PMCPMC2731141.

48. Irie HY, Shrestha Y, Selfors LM, Frye F, Iida N, Wang Z, et al. PTK6 regulates IGF-1-induced anchorage-independent survival. PLoS One. 2010;5(7):e11729. Epub 2010/07/30. doi: 10.1371/journal.pone.0011729. PubMed PMID: 20668531; PubMed Central PMCID: PMCPMC2909213.

49. Chen HY, Shen CH, Tsai YT, Lin FC, Huang YP, Chen RH. Brk activates rac1 and promotes cell migration and invasion by phosphorylating paxillin. Mol Cell Biol. 2004;24(24):10558-72. Epub 2004/12/02. doi: 10.1128/MCB.24.24.10558-10572.2004. PubMed PMID: 15572663; PubMed Central PMCID: PMCPMC533963.

50. Castro NE, Lange CA. Breast tumor kinase and extracellular signal-regulated kinase 5 mediate Met receptor signaling to cell migration in breast cancer cells. Breast Cancer Res. 2010;12(4):R60. Epub 2010/08/07. doi: 10.1186/bcr2622. PubMed PMID: 20687930; PubMed Central PMCID: PMCPMC2949652.

51. Peng M, Ball-Kell SM, Tyner AL. Protein tyrosine kinase 6 promotes ERBB2-induced mammary gland tumorigenesis in the mouse. Cell Death Dis. 2015;6:e1848. Epub 2015/08/08. doi: 10.1038/cddis.2015.210. PubMed PMID: 26247733; PubMed Central PMCID: PMCPMC4558503.

52. Crews ST. Control of cell lineage-specific development and transcription by bHLH-PAS proteins. Genes Dev. 1998;12(5):607-20. Epub 1998/04/16. doi: 10.1101/gad.12.5.607. PubMed PMID: 9499397.

53. Peters JM, Wiley LM. Evidence that murine preimplantation embryos express aryl hydrocarbon receptor. Toxicol Appl Pharmacol. 1995;134(2):214-21. Epub 1995/10/01. doi: 10.1006/taap.1995.1186. PubMed PMID: 7570597.

54. Ma Q, Whitlock JP, Jr. The aromatic hydrocarbon receptor modulates the Hepa 1c1c7 cell cycle and differentiated state independently of dioxin. Mol Cell Biol. 1996;16(5):2144-50. Epub 1996/05/01. doi: 10.1128/mcb.16.5.2144. PubMed PMID: 8628281; PubMed Central PMCID: PMCPMC231202.

55. Hanahan D, Weinberg RA. Hallmarks of cancer: the next generation. Cell. 2011;144(5):646-74. Epub 2011/03/08. doi: 10.1016/j.cell.2011.02.013. PubMed PMID: 21376230.

56. Hushka LJ, Williams JS, Greenlee WF. Characterization of 2,3,7,8-tetrachlorodibenzofuran-dependent suppression and AH receptor pathway gene expression in the developing mouse mammary gland. Toxicol Appl Pharmacol. 1998;152(1):200-10. Epub 1998/10/17. doi: 10.1006/taap.1998.8508. PubMed PMID: 9772216.

57. Schmidt JV, Bradfield CA. Ah receptor signaling pathways. Annu Rev Cell Dev Biol. 1996;12:55-89. Epub 1996/01/01. doi: 10.1146/annurev.cellbio.12.1.55. PubMed PMID: 8970722.

58. Dalton TP, Puga A, Shertzer HG. Induction of cellular oxidative stress by aryl hydrocarbon receptor activation. Chem Biol Interact. 2002;141(1-2):77-95. Epub 2002/09/06. doi: 10.1016/s0009-2797(02)00067-4. PubMed PMID: 12213386.

59. Zhao M, Howard EW, Parris AB, Guo Z, Zhao Q, Yang X. Alcohol promotes migration and invasion of triple-negative breast cancer cells through activation of p38 MAPK and JNK. Mol Carcinog. 2017;56(3):849-62. Epub 2016/08/18. doi: 10.1002/mc.22538. PubMed PMID: 27533114.

60. Nanda R, Stringer-Reasor EM, Saha P, Kocherginsky M, Gibson J, Libao B, et al. A randomized phase I trial of nanoparticle albumin-bound paclitaxel with or without mifepristone for advanced breast cancer. Springerplus. 2016;5(1):947. Epub 2016/07/08. doi: 10.1186/s40064-016-2457-1. PubMed PMID: 27386391; PubMed Central PMCID: PMCPMC4929099.

61. Ritch SJ, Brandhagen BN, Goyeneche AA, Telleria CM. Advanced assessment of migration and invasion of cancer cells in response to mifepristone therapy using double fluorescence cytochemical labeling. BMC Cancer. 2019;19(1):376. Epub 2019/04/25. doi: 10.1186/s12885-019-5587-3. PubMed PMID: 31014286; PubMed Central PMCID: PMCPMC6480622.

62. Qiu L, Levine K, Gajiwala KS, Cronin CN, Nagata A, Johnson E, et al. Small molecule inhibitors reveal PTK6 kinase is not an oncogenic driver in breast cancers. PLOS ONE. 2018;13(6):e0198374. doi: 10.1371/journal.pone.0198374.

63. Yu JH, Kim H. Oxidative stress and cytokines in the pathogenesis of pancreatic cancer. J Cancer Prev. 2014;19(2):97-102. Epub 2014/10/23. doi:

10.15430/JCP.2014.19.2.97. PubMed PMID: 25337577; PubMed Central PMCID: PMCPMC4204162.

64. Taylor CA, Zheng Q, Liu Z, Thompson JE. Role of p38 and JNK MAPK signaling pathways and tumor suppressor p53 on induction of apoptosis in response to Ad-eIF5A1 in A549 lung cancer cells. Mol Cancer. 2013;12:35. Epub 2013/05/04. doi: 10.1186/1476-4598-12-35. PubMed PMID: 23638878; PubMed Central PMCID: PMCPMC3660295.

65. Mansouri A, Ridgway LD, Korapati AL, Zhang Q, Tian L, Wang Y, et al. Sustained activation of JNK/p38 MAPK pathways in response to cisplatin leads to Fas ligand induction and cell death in ovarian carcinoma cells. J Biol Chem. 2003;278(21):19245-56. Epub 2003/03/15. doi: 10.1074/jbc.M208134200. PubMed PMID: 12637505.

66. Huang G, Shi LZ, Chi H. Regulation of JNK and p38 MAPK in the immune system: signal integration, propagation and termination. Cytokine. 2009;48(3):161-9. Epub 2009/09/11. doi: 10.1016/j.cyto.2009.08.002. PubMed PMID: 19740675; PubMed Central PMCID: PMCPMC2782697.

67. Jovicic MJ, Lukic I, Radojcic M, Adzic M, Maric NP. Modulation of c-Jun N-terminal kinase signaling and specific glucocorticoid receptor phosphorylation in the treatment of major depression. Med Hypotheses. 2015;85(3):291-4. Epub 2015/06/09. doi: 10.1016/j.mehy.2015.05.015. PubMed PMID: 26052031; PubMed Central PMCID: PMCPMC4549182.

68. Tienchaiananda P, Nipondhkit W, Maneenil K, Sa-Nguansai S, Payapwattanawong S, Laohavinij S, et al. A randomized, double-blind, placebo-controlled study evaluating the efficacy of combination olanzapine, ondansetron and dexamethasone for prevention of chemotherapy-induced nausea and vomiting in patients receiving doxorubicin plus cyclophosphamide. Ann Palliat Med. 2019;8(4):372-80. Epub 2019/09/11. doi: 10.21037/apm.2019.08.04. PubMed PMID: 31500422.

69. DeRose YS, Gligorich KM, Wang G, Georgelas A, Bowman P, Courdy SJ, et al. Patient-derived models of human breast cancer: protocols for in vitro and in vivo applications in tumor biology and translational medicine. Curr Protoc Pharmacol. 2013;Chapter 14:Unit14 23. Epub 2013/03/05. doi: 10.1002/0471141755.ph1423s60. PubMed PMID: 23456611; PubMed Central PMCID: PMCPMC3630511.

70. Gao J, Aksoy BA, Dogrusoz U, Dresdner G, Gross B, Sumer SO, et al. Integrative analysis of complex cancer genomics and clinical profiles using the cBioPortal. Sci Signal. 2013;6(269):pl1. Epub 2013/04/04. doi: 10.1126/scisignal.2004088. PubMed PMID: 23550210; PubMed Central PMCID: PMCPMC4160307.

71. Cerami E, Gao J, Dogrusoz U, Gross BE, Sumer SO, Aksoy BA, et al. The cBio cancer genomics portal: an open platform for exploring multidimensional cancer genomics data. Cancer Discov. 2012;2(5):401-4. Epub 2012/05/17. doi: 10.1158/2159-8290.CD-12-0095. PubMed PMID: 22588877; PubMed Central PMCID: PMCPMC3956037.

72. Pereira B, Chin SF, Rueda OM, Vollan HK, Provenzano E, Bardwell HA, et al. The somatic mutation profiles of 2,433 breast cancers refines their genomic and transcriptomic landscapes. Nat Commun. 2016;7:11479. Epub 2016/05/11. doi: 10.1038/ncomms11479. PubMed PMID: 27161491; PubMed Central PMCID: PMCPMC4866047.

73. Kim D, Langmead B, Salzberg SL. HISAT: a fast spliced aligner with low memory requirements. Nat Methods. 2015;12(4):357-60. Epub 2015/03/10. doi: 10.1038/nmeth.3317. PubMed PMID: 25751142; PubMed Central PMCID: PMCPMC4655817.

74. Love MI, Huber W, Anders S. Moderated estimation of fold change and dispersion for RNA-seq data with DESeq2. Genome Biol. 2014;15(12):550. Epub 2014/12/18. doi: 10.1186/s13059-014-0550-8. PubMed PMID: 25516281; PubMed Central PMCID: PMCPMC4302049.

75. Chen Z, Lan X, Wu D, Sunkel B, Ye Z, Huang J, et al. Ligand-dependent genomic function of glucocorticoid receptor in triple-negative breast cancer. Nat Commun. 2015;6:8323. Epub 2015/09/17. doi: 10.1038/ncomms9323. PubMed PMID: 26374485; PubMed Central PMCID: PMCPMC4573460.

76. Swinstead EE, Miranda TB, Paakinaho V, Baek S, Goldstein I, Hawkins M, et al. Steroid Receptors Reprogram FoxA1 Occupancy through Dynamic Chromatin Transitions. Cell. 2016;165(3):593-605. Epub 2016/04/12. doi: 10.1016/j.cell.2016.02.067. PubMed PMID: 27062924; PubMed Central PMCID: PMCPMC4842147.

77. Nagy A, Lanczky A, Menyhart O, Gyorffy B. Validation of miRNA prognostic power in hepatocellular carcinoma using expression data of independent datasets. Sci Rep. 2018;8(1):9227. Epub 2018/06/17. doi: 10.1038/s41598-018-27521-y. PubMed PMID: 29907753; PubMed Central PMCID: PMCPMC6003936.

78. Aguirre-Gamboa R, Gomez-Rueda H, Martinez-Ledesma E, Martinez-Torteya A, Chacolla-Huaringa R, Rodriguez-Barrientos A, et al. SurvExpress: an online biomarker validation tool and database for cancer gene expression data using survival analysis. PLoS One. 2013;8(9):e74250. Epub 2013/09/26. doi: 10.1371/journal.pone.0074250. PubMed PMID: 24066126; PubMed Central PMCID: PMCPMC3774754.

79. El Ayachi I, Fatima I, Wend P, Alva-Ornelas JA, Runke S, Kuenzinger WL, et al. The WNT10B Network Is Associated with Survival and Metastases in

Chemoresistant Triple-Negative Breast Cancer. Cancer Res. 2019;79(5):982-93. Epub 2018/12/20. doi: 10.1158/0008-5472.CAN-18-1069. PubMed PMID: 30563890.

80. Foulkes WD, Smith IE, Reis-Filho JS. Triple-negative breast cancer. N Engl J Med. 2010;363(20):1938-48. doi: 10.1056/NEJMra1001389. PubMed PMID: 21067385.

81. Skor MN, Wonder EL, Kocherginsky M, Goyal A, Hall BA, Cai Y, et al. Glucocorticoid receptor antagonism as a novel therapy for triple-negative breast cancer. Clin Cancer Res. 2013;19(22):6163-72. doi: 10.1158/1078-0432.CCR-12-3826.

82. Kach J, Conzen SD, Szmulewitz RZ. Targeting the glucocorticoid receptor in breast and prostate cancers. Sci Transl Med. 2015;7(305):305ps19. Epub 2015/09/18. doi: 10.1126/scitranslmed.aac7531. PubMed PMID: 26378243; PubMed Central PMCID: PMCPMC4807967.

83. Wu W, Pew T, Zou M, Pang D, Conzen SD. Glucocorticoid receptor-induced MAPK phosphatase-1 (MPK-1) expression inhibits paclitaxel-associated MAPK activation and contributes to breast cancer cell survival. J Biol Chem. 2005;280(6):4117-24. Epub 2004/12/14. doi: 10.1074/jbc.M411200200. PubMed PMID: 15590693.

84. Anbalagan M, Rowan BG. Estrogen receptor alpha phosphorylation and its functional impact in human breast cancer. Mol Cell Endocrinol. 2015;418 Pt 3:264-72. Epub 2015/01/20. doi: 10.1016/j.mce.2015.01.016. PubMed PMID: 25597633.

85. Knutson TP, Truong TH, Ma S, Brady NJ, Sullivan ME, Raj G, et al. Posttranslationally modified progesterone receptors direct ligand-specific expression of breast cancer stem cell-associated gene programs. J Hematol Oncol. 2017;10(1):89. Epub 2017/04/18. doi: 10.1186/s13045-017-0462-7. PubMed PMID: 28412963; PubMed Central PMCID: PMCPMC5392969.

86. Regan Anderson TM, Ma S, Perez Kerkvliet C, Peng Y, Helle TM, Krutilina RI, et al. Taxol Induces Brk-dependent Prosurvival Phenotypes in TNBC Cells through an AhR/GR/HIF-driven Signaling Axis. Mol Cancer Res. 2018;16(11):1761-72. doi: 10.1158/1541-7786.MCR-18-0410.

87. Tonsing-Carter E, Hernandez KM, Kim CR, Harkless RV, Oh A, Bowie KR, et al. Glucocorticoid receptor modulation decreases ER-positive breast cancer cell proliferation and suppresses wild-type and mutant ER chromatin association. Breast Cancer Res. 2019;21(1):82. Epub 2019/07/26. doi: 10.1186/s13058-019-1164-6. PubMed PMID: 31340854; PubMed Central PMCID: PMCPMC6651939.

88. van Zijl F, Krupitza G, Mikulits W. Initial steps of metastasis: cell invasion and endothelial transmigration. Mutat Res. 2011;728(1-2):23-34. Epub 2011/05/25. doi: 10.1016/j.mrrev.2011.05.002. PubMed PMID: 21605699; PubMed Central PMCID: PMCPMC4028085.

89. Jiang WG, Sanders AJ, Katoh M, Ungefroren H, Gieseler F, Prince M, et al. Tissue invasion and metastasis: Molecular, biological and clinical perspectives. Semin Cancer Biol. 2015;35 Suppl:S244-S75. Epub 2015/04/14. doi: 10.1016/j.semcancer.2015.03.008. PubMed PMID: 25865774.

90. Quail DF, Joyce JA. Microenvironmental regulation of tumor progression and metastasis. Nat Med. 2013;19(11):1423-37. Epub 2013/11/10. doi: 10.1038/nm.3394. PubMed PMID: 24202395; PubMed Central PMCID: PMCPMC3954707.

91. Ding MJ, Su KE, Cui GZ, Yang WH, Chen L, Yang M, et al. Association between transforming growth factor-beta1 expression and the clinical features of triple negative breast cancer. Oncol Lett. 2016;11(6):4040-4. Epub 2016/06/18. doi: 10.3892/ol.2016.4497. PubMed PMID: 27313737; PubMed Central PMCID: PMCPMC4888107.

92. Bhola NE, Balko JM, Dugger TC, Kuba MG, Sanchez V, Sanders M, et al. TGF-beta inhibition enhances chemotherapy action against triple-negative breast cancer. J Clin Invest. 2013;123(3):1348-58. Epub 2013/02/09. doi: 10.1172/JCI65416. PubMed PMID: 23391723; PubMed Central PMCID: PMCPMC3582135.

93. Xu X, Zhang L, He X, Zhang P, Sun C, Xu X, et al. TGF-beta plays a vital role in triple-negative breast cancer (TNBC) drug-resistance through regulating stemness, EMT and apoptosis. Biochem Biophys Res Commun. 2018;502(1):160-5. Epub 2018/05/25. doi: 10.1016/j.bbrc.2018.05.139. PubMed PMID: 29792857.

94. Massague J. TGFbeta in Cancer. Cell. 2008;134(2):215-30. Epub 2008/07/30. doi: 10.1016/j.cell.2008.07.001. PubMed PMID: 18662538; PubMed Central PMCID: PMCPMC3512574.

95. Yu L, Hebert MC, Zhang YE. TGF-beta receptor-activated p38 MAP kinase mediates Smad-independent TGF-beta responses. EMBO J. 2002;21(14):3749-59. Epub 2002/07/12. doi: 10.1093/emboj/cdf366. PubMed PMID: 12110587; PubMed Central PMCID: PMCPMC126112.

96. Iriondo O, Liu Y, Lee G, Elhodaky M, Jimenez C, Li L, et al. TAK1 mediates microenvironment-triggered autocrine signals and promotes triple-negative breast cancer lung metastasis. Nat Commun. 2018;9(1):1994. Epub 2018/05/20. doi: 10.1038/s41467-018-04460-w. PubMed PMID: 29777109; PubMed Central PMCID: PMCPMC5959931.

97. Lee H, Bai W. Regulation of estrogen receptor nuclear export by ligand-induced and p38-mediated receptor phosphorylation. Mol Cell Biol. 2002;22(16):5835-45. Epub 2002/07/26. PubMed PMID: 12138194; PubMed Central PMCID: PMCPMC133965.

98. Khandrika L, Lieberman R, Koul S, Kumar B, Maroni P, Chandhoke R, et al. Hypoxia-associated p38 mitogen-activated protein kinase-mediated androgen receptor activation and increased HIF-1alpha levels contribute to emergence of an aggressive phenotype in prostate cancer. Oncogene. 2009;28(9):1248-60. Epub 2009/01/20. doi: 10.1038/onc.2008.476. PubMed PMID: 19151763; PubMed Central PMCID: PMCPMC2651999.

99. Fietz ER, Keenan CR, Lopez-Campos G, Tu Y, Johnstone CN, Harris T, et al. Glucocorticoid resistance of migration and gene expression in a daughter MDA-MB-231 breast tumour cell line selected for high metastatic potential. Sci Rep. 2017;7:43774. Epub 2017/03/07. doi: 10.1038/srep43774. PubMed PMID: 28262792; PubMed Central PMCID: PMCPMC5338339.

100. Coser KR, Chesnes J, Hur J, Ray S, Isselbacher KJ, Shioda T. Global analysis of ligand sensitivity of estrogen inducible and suppressible genes in MCF7/BUS breast cancer cells by DNA microarray. Proc Natl Acad Sci U S A. 2003;100(24):13994-9. Epub 2003/11/12. doi: 10.1073/pnas.2235866100. PubMed PMID: 14610279; PubMed Central PMCID: PMCPMC283534.

101. Bahhnassy A, Mohanad M, Shaarawy S, Ismail MF, El-Bastawisy A, Ashmawy AM, et al. Transforming growth factor-β, insulin-like growth factor I/insulin-like growth factor I receptor and vascular endothelial growth factor-A: prognostic and predictive markers in triple-negative and non-triple-negative breast cancer. Mol Med Rep. 2015;12(1):851-64. doi: 10.3892/mmr.2015.3560.

102. Ivanovic V, Dedovic-Tanic N, Milovanovic Z, Lukic S, Nikolic S, Baltic V, et al. Case with triple-negative breast cancer shows overexpression of both cFOS and TGF-beta1 in node-positive tissue. Per Med. 2016;13(6):523-30. Epub 2016/11/01. doi: 10.2217/pme-2016-0032. PubMed PMID: 29754549.

103. Beviglia L, Kramer RH. HGF induces FAK activation and integrin-mediated adhesion in MTLn3 breast carcinoma cells. Int J Cancer. 1999;83(5):640-9. Epub 1999/10/16. doi: 10.1002/(sici)1097-0215(19991126)83:5<640::aid-ijc13>3.0.co;2-d. PubMed PMID: 10521801.

104. Recio JA, Merlino G. Hepatocyte growth factor/scatter factor activates proliferation in melanoma cells through p38 MAPK, ATF-2 and cyclin D1. Oncogene. 2002;21(7):1000-8. doi: 10.1038/sj.onc.1205150.

105. Duzgun SA, Yerlikaya A, Zeren S, Bayhan Z, Okur E, Boyaci I. Differential effects of p38 MAP kinase inhibitors SB203580 and SB202190 on growth and migration of human MDA-MB-231 cancer cell line. Cytotechnology.

2017;69(4):711-24. Epub 2017/04/11. doi: 10.1007/s10616-017-0079-2. PubMed PMID: 28393288; PubMed Central PMCID: PMCPMC5507849.

106. Dontu G, Abdallah WM, Foley JM, Jackson KW, Clarke MF, Kawamura MJ, et al. In vitro propagation and transcriptional profiling of human mammary stem/progenitor cells. Genes Dev. 2003;17(10):1253-70. Epub 2003/05/21. doi: 10.1101/gad.1061803. PubMed PMID: 12756227; PubMed Central PMCID: PMCPMC196056.

107. Pan X, Chen Z, Huang R, Yao Y, Ma G. Transforming growth factor beta1 induces the expression of collagen type I by DNA methylation in cardiac fibroblasts. PLoS One. 2013;8(4):e60335. Epub 2013/04/06. doi: 10.1371/journal.pone.0060335. PubMed PMID: 23560091; PubMed Central PMCID: PMCPMC3613378.

108. Shi N, Guo X, Chen SY. Olfactomedin 2, a novel regulator for transforming growth factor-beta-induced smooth muscle differentiation of human embryonic stem cell-derived mesenchymal cells. Mol Biol Cell. 2014;25(25):4106-14. Epub 2014/10/10. doi: 10.1091/mbc.E14-08-1255. PubMed PMID: 25298399; PubMed Central PMCID: PMCPMC4263453.

109. Zhou J, Shao Z, Kerkela R, Ichijo H, Muslin AJ, Pombo C, et al. Serine 58 of 14-3-3zeta is a molecular switch regulating ASK1 and oxidant stress-induced cell death. Mol Cell Biol. 2009;29(15):4167-76. Epub 2009/05/20. doi: 10.1128/MCB.01067-08. PubMed PMID: 19451227; PubMed Central PMCID: PMCPMC2715813.

110. Leehy KA, Regan Anderson TM, Daniel AR, Lange CA, Ostrander JH. Modifications to glucocorticoid and progesterone receptors alter cell fate in breast cancer. J Mol Endocrinol. 2016;56(3):R99-R114. Epub 2016/02/03. doi: 10.1530/JME-15-0322. PubMed PMID: 26831511.

111. Beck CA, Estes PA, Bona BJ, Muro-Cacho CA, Nordeen SK, Edwards DP. The steroid antagonist RU486 exerts different effects on the glucocorticoid and progesterone receptors. Endocrinology. 1993;133(2):728-40. Epub 1993/08/01. doi: 10.1210/endo.133.2.8344212. PubMed PMID: 8344212.

112. Daniel AR, Lange CA. Protein kinases mediate ligand-independent derepression of sumoylated progesterone receptors in breast cancer cells. Proc Natl Acad Sci U S A. 2009;106(34):14287-92. Epub 2009/08/27. doi: 10.1073/pnas.0905118106. PubMed PMID: 19706513; PubMed Central PMCID: PMCPMC2732858.

113. Razavi P, Chang MT, Xu G, Bandlamudi C, Ross DS, Vasan N, et al. The Genomic Landscape of Endocrine-Resistant Advanced Breast Cancers. Cancer Cell. 2018;34(3):427-38 e6. Epub 2018/09/12. doi: 10.1016/j.ccell.2018.08.008. PubMed PMID: 30205045.

114. Humphreys JM, Piala AT, Akella R, He H, Goldsmith EJ. Precisely ordered phosphorylation reactions in the p38 mitogen-activated protein (MAP) kinase cascade. J Biol Chem. 2013;288(32):23322-30. Epub 2013/06/08. doi: 10.1074/jbc.M113.462101. PubMed PMID: 23744074; PubMed Central PMCID: PMCPMC3743502.

115. Huang CY, Ferrell JE, Jr. Ultrasensitivity in the mitogen-activated protein kinase cascade. Proc Natl Acad Sci U S A. 1996;93(19):10078-83. Epub 1996/09/17. doi: 10.1073/pnas.93.19.10078. PubMed PMID: 8816754; PubMed Central PMCID: PMCPMC38339.

116. Seong HA, Manoharan R, Ha H. Coordinate Activation of Redox-Dependent ASK1/TGF-beta Signaling by a Multiprotein Complex (MPK38, ASK1, SMADs, ZPR9, and TRX) Improves Glucose and Lipid Metabolism in Mice. Antioxid Redox Signal. 2016;24(8):434-52. Epub 2015/10/01. doi: 10.1089/ars.2015.6325. PubMed PMID: 26421442.

117. Tobiume K, Matsuzawa A, Takahashi T, Nishitoh H, Morita K, Takeda K, et al. ASK1 is required for sustained activations of JNK/p38 MAP kinases and apoptosis. EMBO Rep. 2001;2(3):222-8. Epub 2001/03/27. doi: 10.1093/embo-reports/kve046. PubMed PMID: 11266364; PubMed Central PMCID: PMCPMC1083842.

118. Bergamaschi A, Frasor J, Borgen K, Stanculescu A, Johnson P, Rowland K, et al. 14-3-3zeta as a predictor of early time to recurrence and distant metastasis in hormone receptor-positive and -negative breast cancers. Breast Cancer Res Treat. 2013;137(3):689-96. Epub 2012/12/29. doi: 10.1007/s10549-012-2390-0. PubMed PMID: 23271328; PubMed Central PMCID: PMCPMC3632437.

119. Petrvalska O, Kosek D, Kukacka Z, Tosner Z, Man P, Vecer J, et al. Structural Insight into the 14-3-3 Protein-dependent Inhibition of Protein Kinase ASK1 (Apoptosis Signal-regulating kinase 1). J Biol Chem. 2016;291(39):20753-65. Epub 2016/08/16. doi: 10.1074/jbc.M116.724310. PubMed PMID: 27514745; PubMed Central PMCID: PMCPMC5034064.

120. West DC, Kocherginsky M, Tonsing-Carter EY, Dolcen DN, Hosfield DJ, Lastra RR, et al. Discovery of a glucocorticoid receptor (GR) activity signature using selective GR antagonism in ER-negative breast cancer. Clinical Cancer Research. 2018:clincanres.2793.017. doi: 10.1158/1078-0432.CCR-17-2793.

121. Regan Anderson TM, Ma S, Perez Kerkvliet C, Peng Y, Helle TM, Krutilina RI, et al. Taxol Induces Brk-dependent Prosurvival Phenotypes in TNBC Cells through an AhR/GR/HIF–driven Signaling Axis. Molecular Cancer Research. 2018. doi: 10.1158/1541-7786.MCR-18-0410.

122. Regan Anderson TM, Peacock DL, Daniel AR, Hubbard GK, Lofgren KA, Girard BJ, et al. Breast tumor kinase (Brk/PTK6) is a mediator of hypoxia-

associated breast cancer progression. Cancer Research. 2013:canres.0523.2013. doi: 10.1158/0008-5472.CAN-13-0523.

123. Ostrander JH, Daniel AR, Lofgren K, Kleer CG, Lange CA. Breast Tumor Kinase (Protein Tyrosine Kinase 6) Regulates Heregulin-Induced Activation of ERK5 and p38 MAP Kinases in Breast Cancer Cells. Cancer Research. 2007;67(9):4199. doi: 10.1158/0008-5472.CAN-06-3409.

124. Castro NE, Lange CA. Breast tumor kinase and extracellular signal-regulated kinase 5 mediate Met receptor signaling to cell migration in breast cancer cells. Breast Cancer Research. 2010;12(4):R60. doi: 10.1186/bcr2622.

125. Shen C-H, Chen H-Y, Lin M-S, Li F-Y, Chang C-C, Kuo M-L, et al. Breast Tumor Kinase Phosphorylates p190RhoGAP to Regulate Rho and Ras and Promote Breast Carcinoma Growth, Migration, and Invasion. Cancer Research. 2008;68(19):7779. doi: 10.1158/0008-5472.CAN-08-0997.

126. Lofgren KA, Ostrander JH, Housa D, Hubbard GK, Locatelli A, Bliss RL, et al. Mammary gland specific expression of Brk/PTK6 promotes delayed involution and tumor formation associated with activation of p38 MAPK. Breast Cancer Research. 2011;13(5):R89. doi: 10.1186/bcr2946.

127. Pereira DM, Gomes SE, Borralho PM, Rodrigues CMP. MEK5/ERK5 activation regulates colon cancer stem-like cell properties. Cell Death Discovery. 2019;5(1):68. doi: 10.1038/s41420-019-0150-1.

128. Kamalati T, Jolin HE, Mitchell PJ, Barker KT, Jackson LE, Dean CJ, et al. Brk, a breast tumor-derived non-receptor protein-tyrosine kinase, sensitizes mammary epithelial cells to epidermal growth factor. J Biol Chem. 1996;271(48):30956-63. Epub 1996/11/29. doi: 10.1074/jbc.271.48.30956. PubMed PMID: 8940083.

129. Ostrander JH, Daniel AR, Lange CA. Brk/PTK6 signaling in normal and cancer cell models. Curr Opin Pharmacol. 2010;10(6):662-9. doi: 10.1016/j.coph.2010.08.007. PubMed PMID: 20832360.

130. Brauer PM, Tyner AL. Building a better understanding of the intracellular tyrosine kinase PTK6 — BRK by BRK. Biochimica et Biophysica Acta (BBA) - Reviews on Cancer. 2010;1806(1):66-73. doi: https://doi.org/10.1016/j.bbcan.2010.02.003.

131. Mitchell PJ, Sara EA, Crompton MR. A novel adaptor-like protein which is a substrate for the non-receptor tyrosine kinase, BRK. Oncogene. 2000;19(37):4273-82. doi: 10.1038/sj.onc.1203775. PubMed PMID: 10980601.

132. Qiu H, Miller WT. Role of the Brk SH3 domain in substrate recognition. Oncogene. 2004;23(12):2216-23. doi: 10.1038/sj.onc.1207339.

133. Qiu H, Zappacosta F, Su W, Annan RS, Miller WT. Interaction between Brk kinase and insulin receptor substrate-4. Oncogene. 2005;24(36):5656-64. doi: 10.1038/sj.onc.1208721.

134. Zheng Y, Tyner AL. Context-specific protein tyrosine kinase 6 (PTK6) signalling in prostate cancer. European Journal of Clinical Investigation. 2013;43(4):397-404. doi: 10.1111/eci.12050.

135. Aguirre-Gamboa R, Gomez-Rueda H, Martínez-Ledesma E, Martínez-Torteya A, Chacolla-Huaringa R, Rodriguez-Barrientos A, et al. SurvExpress: An Online Biomarker Validation Tool and Database for Cancer Gene Expression Data Using Survival Analysis. PLOS ONE. 2013;8(9):e74250. doi: 10.1371/journal.pone.0074250.

136. Anders CK, Carey LA. Biology, metastatic patterns, and treatment of patients with triple-negative breast cancer. Clinical breast cancer. 2009;9 Suppl 2(Suppl 2):S73-S81. doi: 10.3816/CBC.2009.s.008. PubMed PMID: 19596646.

137. Nguyen DX, Bos PD, Massague J. Metastasis: from dissemination to organ-specific colonization. Nature reviews Cancer. 2009;9(4):274-84. Epub 2009/03/25. doi: 10.1038/nrc2622. PubMed PMID: 19308067.

138. Finisguerra V, Prenen H, Mazzone M. Preclinical and clinical evaluation of MET functions in cancer cells and in the tumor stroma. Oncogene. 2016;35(42):5457-67. doi: 10.1038/onc.2016.36.

139. Garcia-Mata R, Boulter E, Burridge K. The 'invisible hand': regulation of RHO GTPases by RHOGDIs. Nat Rev Mol Cell Biol. 2011;12(8):493-504. Epub 2011/07/23. doi: 10.1038/nrm3153. PubMed PMID: 21779026; PubMed Central PMCID: PMCPMC3260518.

140. Foucquier J, Guedj M. Analysis of drug combinations: current methodological landscape. Pharmacology research & perspectives. 2015;3(3):e00149. Epub 2015/07/15. doi: 10.1002/prp2.149. PubMed PMID: 26171228; PubMed Central PMCID: PMCPMC4492765.

141. Zhong Z, Yeow WS, Zou C, Wassell R, Wang C, Pestell RG, et al. Cyclin D1/cyclin-dependent kinase 4 interacts with filamin A and affects the migration and invasion potential of breast cancer cells. Cancer Res. 2010;70(5):2105-14. Epub 2010/02/25. doi: 10.1158/0008-5472.CAN-08-1108. PubMed PMID: 20179208; PubMed Central PMCID: PMCPMC2917898.

142. Wingate H, Puskas A, Duong M, Bui T, Richardson D, Liu Y, et al. Low molecular weight cyclin E is specific in breast cancer and is associated with mechanisms of tumor progression. Cell Cycle. 2009;8(7):1062-8. Epub 2009/03/24. doi: 10.4161/cc.8.7.8119. PubMed PMID: 19305161; PubMed Central PMCID: PMCPMC2692060.

143. Helbig G, Christopherson KW, 2nd, Bhat-Nakshatri P, Kumar S, Kishimoto H, Miller KD, et al. NF-kappaB promotes breast cancer cell migration and metastasis by inducing the expression of the chemokine receptor CXCR4. J Biol Chem. 2003;278(24):21631-8. Epub 2003/04/12. doi: 10.1074/jbc.M300609200. PubMed PMID: 12690099.

144. Sutherland RL, Musgrove EA. Cyclins and breast cancer. J Mammary Gland Biol Neoplasia. 2004;9(1):95-104. Epub 2004/04/15. doi: 10.1023/B:JOMG.0000023591.45568.77. PubMed PMID: 15082921.

145. Joyce D, Albanese C, Steer J, Fu M, Bouzahzah B, Pestell RG. NF-kappaB and cell-cycle regulation: the cyclin connection. Cytokine & growth factor reviews. 2001;12(1):73-90. Epub 2001/04/20. doi: 10.1016/s1359-6101(00)00018-6. PubMed PMID: 11312120.

146. Safe S, Lee SO, Jin UH. Role of the aryl hydrocarbon receptor in carcinogenesis and potential as a drug target. Toxicol Sci. 2013;135(1):1-16. Epub 2013/06/19. doi: 10.1093/toxsci/kft128. PubMed PMID: 23771949; PubMed Central PMCID: PMCPMC3748760.

147. Veldhoen M, Hirota K, Westendorf AM, Buer J, Dumoutier L, Renauld JC, et al. The aryl hydrocarbon receptor links TH17-cell-mediated autoimmunity to environmental toxins. Nature. 2008;453(7191):106-9. Epub 2008/03/26. doi: 10.1038/nature06881. PubMed PMID: 18362914.

148. Androutsopoulos VP, Tsatsakis AM, Spandidos DA. Cytochrome P450 CYP1A1: wider roles in cancer progression and prevention. BMC Cancer. 2009;9:187. Epub 2009/06/18. doi: 10.1186/1471-2407-9-187. PubMed PMID: 19531241; PubMed Central PMCID: PMCPMC2703651.

149. D'Amato NC, Rogers TJ, Gordon MA, Greene LI, Cochrane DR, Spoelstra NS, et al. A TDO2-AhR signaling axis facilitates anoikis resistance and metastasis in triple-negative breast cancer. Cancer research. 2015;75(21):4651-64. Epub 2015/09/11. doi: 10.1158/0008-5472.CAN-15-2011. PubMed PMID: 26363006.

150. Pragyan P, Kesharwani SS, Nandekar PP, Rathod V, Sangamwar AT. Predicting drug metabolism by CYP1A1, CYP1A2, and CYP1B1: insights from MetaSite, molecular docking and quantum chemical calculations. Mol Divers. 2014;18(4):865-78. Epub 2014/07/17. doi: 10.1007/s11030-014-9534-6. PubMed PMID: 25028215.

151. Minsavage GD, Park SK, Gasiewicz TA. The aryl hydrocarbon receptor (AhR) tyrosine 9, a residue that is essential for AhR DNA binding activity, is not a phosphoresidue but augments AhR phosphorylation. J Biol Chem. 2004;279(20):20582-93. Epub 2004/02/24. doi: 10.1074/jbc.M312977200. PubMed PMID: 14978034.

152. Sachs N, de Ligt J, Kopper O, Gogola E, Bounova G, Weeber F, et al. A Living Biobank of Breast Cancer Organoids Captures Disease Heterogeneity. Cell. 2018;172(1-2):373-86.e10. Epub 2017/12/12. doi: 10.1016/j.cell.2017.11.010. PubMed PMID: 29224780.

153. Goel RK, Lukong KE. Tracing the footprints of the breast cancer oncogene BRK - Past till present. Biochimica et biophysica acta. 2015;1856(1):39-54. Epub 2015/05/23. doi: 10.1016/j.bbcan.2015.05.001. PubMed PMID: 25999240.

154. Morlacchi P, Robertson FM, Klostergaard J, McMurray JS. Targeting SH2 domains in breast cancer. Future medicinal chemistry. 2014;6(17):1909-26. Epub 2014/12/17. doi: 10.4155/fmc.14.120. PubMed PMID: 25495984; PubMed Central PMCID: PMCPMC4339284.

155. Stoker AW. Protein tyrosine phosphatases and signalling. J Endocrinol. 2005;185(1):19-33. Epub 2005/04/09. doi: 10.1677/joe.1.06069. PubMed PMID: 15817824.

156. Unwin RD, Sternberg DW, Lu Y, Pierce A, Gilliland DG, Whetton AD. Global effects of BCR/ABL and TEL/PDGFRbeta expression on the proteome and phosphoproteome: identification of the Rho pathway as a target of BCR/ABL. J Biol Chem. 2005;280(8):6316-26. Epub 2004/12/01. doi: 10.1074/jbc.M410598200. PubMed PMID: 15569670.

157. Lin Y, Mallen-St Clair J, Wang G, Luo J, Palma-Diaz F, Lai C, et al. p38 MAPK mediates epithelial-mesenchymal transition by regulating p38IP and Snail in head and neck squamous cell carcinoma. Oral Oncol. 2016;60:81-9. Epub 2016/08/18. doi: 10.1016/j.oraloncology.2016.06.010. PubMed PMID: 27531877.

158. Strippoli R, Benedicto I, Foronda M, Perez-Lozano ML, Sanchez-Perales S, Lopez-Cabrera M, et al. p38 maintains E-cadherin expression by modulating TAK1-NF-kappa B during epithelial-to-mesenchymal transition. J Cell Sci. 2010;123(Pt 24):4321-31. Epub 2010/11/26. doi: 10.1242/jcs.071647. PubMed PMID: 21098640.

159. Cargnello M, Roux PP. Activation and function of the MAPKs and their substrates, the MAPK-activated protein kinases. Microbiology and molecular biology reviews : MMBR. 2011;75(1):50-83. Epub 2011/03/05. doi: 10.1128/mmbr.00031-10. PubMed PMID: 21372320; PubMed Central PMCID: PMCPMC3063353.

160. Shimada T, Fujii-Kuriyama Y. Metabolic activation of polycyclic aromatic hydrocarbons to carcinogens by cytochromes P450 1A1 and 1B1. Cancer science. 2004;95(1):1-6. Epub 2004/01/15. doi: 10.1111/j.1349-7006.2004.tb03162.x. PubMed PMID: 14720319.

161. Androutsopoulos VP, Spyrou I, Ploumidis A, Papalampros AE, Kyriakakis M, Delakas D, et al. Expression profile of CYP1A1 and CYP1B1 enzymes in

colon and bladder tumors. PLoS One. 2013;8(12):e82487. Epub 2013/12/21. doi: 10.1371/journal.pone.0082487. PubMed PMID: 24358191; PubMed Central PMCID: PMCPMC3864999.

162. Rodriguez M, Potter DA. CYP1A1 regulates breast cancer proliferation and survival. Mol Cancer Res. 2013;11(7):780-92. Epub 2013/04/12. doi: 10.1158/1541-7786.Mcr-12-0675. PubMed PMID: 23576571; PubMed Central PMCID: PMCPMC3720830.

163. Xu XL, Ye YL, Wu ZM, He QM, Tan L, Xiao KH, et al. Overexpression of PTK6 predicts poor prognosis in bladder cancer patients. J Cancer. 2017;8(17):3464-73. Epub 2017/11/21. doi: 10.7150/jca.21318. PubMed PMID: 29151930; PubMed Central PMCID: PMCPMC5687160.

164. Ishida M, Mikami S, Kikuchi E, Kosaka T, Miyajima A, Nakagawa K, et al. Activation of the aryl hydrocarbon receptor pathway enhances cancer cell invasion by upregulating the MMP expression and is associated with poor prognosis in upper urinary tract urothelial cancer. Carcinogenesis. 2010;31(2):287-95. Epub 2009/09/17. doi: 10.1093/carcin/bgp222. PubMed PMID: 19755661.

165. O'Donnell EF, Kopparapu PR, Koch DC, Jang HS, Phillips JL, Tanguay RL, et al. The aryl hydrocarbon receptor mediates leflunomide-induced growth inhibition of melanoma cells. PLoS One. 2012;7(7):e40926. Epub 2012/07/21. doi: 10.1371/journal.pone.0040926. PubMed PMID: 22815870; PubMed Central PMCID: PMCPMC3398955.

166. Kodama T, Shimizu N, Yoshikawa N, Makino Y, Ouchida R, Okamoto K, et al. Role of the glucocorticoid receptor for regulation of hypoxia-dependent gene expression. J Biol Chem. 2003;278(35):33384-91. Epub 2003/06/18. doi: 10.1074/jbc.M302581200. PubMed PMID: 12810720.

167. Sato S, Shirakawa H, Tomita S, Tohkin M, Gonzalez FJ, Komai M. The aryl hydrocarbon receptor and glucocorticoid receptor interact to activate human metallothionein 2A. Toxicol Appl Pharmacol. 2013;273(1):90-9. Epub 2013/09/03. doi: 10.1016/j.taap.2013.08.017. PubMed PMID: 23994556; PubMed Central PMCID: PMCPMC6301017.

168. Prudnikova TY, Rawat SJ, Chernoff J. Molecular pathways: targeting the kinase effectors of RHO-family GTPases. Clin Cancer Res. 2015;21(1):24-9. Epub 2014/10/23. doi: 10.1158/1078-0432.CCR-14-0827. PubMed PMID: 25336694; PubMed Central PMCID: PMCPMC4286478.

169. Igea A, Nebreda AR. The Stress Kinase p38alpha as a Target for Cancer Therapy. Cancer Res. 2015;75(19):3997-4002. Epub 2015/09/18. doi: 10.1158/0008-5472.CAN-15-0173. PubMed PMID: 26377941.

170. Safe S, Cheng Y, Jin UH. The Aryl Hydrocarbon Receptor (AhR) as a Drug Target for Cancer Chemotherapy. Current opinion in toxicology. 2017;2:24-9. Epub 2017/05/02. doi: 10.1016/j.cotox.2017.01.012. PubMed PMID: 28459113; PubMed Central PMCID: PMCPMC5407490.

171. Yisireyili M, Wulamu W, Aili A, Li Y, Alimujiang A, Aipire A, et al. Chronic restraint stress induces esophageal fibrosis with enhanced oxidative stress in a murine model. Exp Ther Med. 2019;18(2):1375-83. Epub 2019/07/19. doi: 10.3892/etm.2019.7669. PubMed PMID: 31316626; PubMed Central PMCID: PMCPMC6601379.

172. Kang H, Kim H, Lee S, Youn H, Youn B. Role of Metabolic Reprogramming in Epithelial(-)Mesenchymal Transition (EMT). Int J Mol Sci. 2019;20(8). Epub 2019/04/28. doi: 10.3390/ijms20082042. PubMed PMID: 31027222; PubMed Central PMCID: PMCPMC6514888.

173. Guda MR, Asuthkar S, Labak CM, Tsung AJ, Alexandrov I, Mackenzie MJ, et al. Targeting PDK4 inhibits breast cancer metabolism. Am J Cancer Res. 2018;8(9):1725-38. Epub 2018/10/17. PubMed PMID: 30323966; PubMed Central PMCID: PMCPMC6176187.

174. Perez Kerkvliet C, Dwyer AR, Diep CH, Oakley RH, Liddle C, Cidlowski JA, et al. Glucocorticoid receptors are required effectors of TGFbeta1-induced p38 MAPK signaling to advanced cancer phenotypes in triple-negative breast cancer. Breast Cancer Res. 2020;22(1):39. Epub 2020/05/03. doi: 10.1186/s13058-020-01277-8. PubMed PMID: 32357907.

175. Hoffman JA, Papas BN, Trotter KW, Archer TK. Single-cell RNA sequencing reveals a heterogeneous response to Glucocorticoids in breast cancer cells. Commun Biol. 2020;3(1):126. Epub 2020/03/15. doi: 10.1038/s42003-020-0837-0. PubMed PMID: 32170217; PubMed Central PMCID: PMCPMC7070043.

Appendices

Contribution by author in Chapter 3:

Carlos Perez Kerkvliet

- Execution of the experimental design, analysis and interpretation of data for the following figures: Figures 3.1A-D, 3.2A-D, 3.3A-E, 3.4A-F, 3.5A-G, 3.6, 3.7A-E, 3.8A-F, 3.9A-C, 3.10A-H, 3.11A-F, 3.12A-F, 3.13E, 3.14, 3.15, 3.16A-F, 3.17, Tables 3.1, 3.2, 3.3 and 3.4.
- Drafted and revised the manuscript/publication.

Amy R. Dwyer

- Execution of the experimental design of Figure 3.5H, Figure 3.13A-D

Caroline Diep

- Execution and experimental design of Figure 3.16D.

Robert H. Oakley

- Provided support with RNA-Seq data analysis.

Christopher Liddle

- Provided support with RNA-Seq data analysis.

John A. Cidlowski

- Provided support with RNA-Seq data analysis.
- Revision of the publication/manuscript.

Carol A. Lange

- Conception and assistance in the experimental design studies.
- Assistance in the interpretation and analysis of data.
- Revision of the publication/manuscript.

Contribution by author in Chapter 4:

Carlos Perez Kerkvliet

- Experimental design, analysis and interpretation of data Figure 4.1A-B, Figure 4.3A,B,D, Figure 4.4A-C, Figure 4.5C-D, Figure 4.8A,C,D, Figure 4.9D and Table 4.1.
- Drafted and revised the submitted manuscript with focus on introduction, results and discussion.

Amy R. Dwyer

- Experimental design, analysis and interpretation of data Figure 4.3C,E,F, Figure 4.8B,E-F.
- Drafted and revised the submitted manuscript with focus on methods and results section.
- Critical revision of the manuscript for content.

Raisa I. Kurtilina

- Assisted in the experimental design and execution of Figure 4.1C-J, Figure 4.2, Figure 4.6, Figure 4.7 and Table 4.2.

Hilaire C. Playa

- Assisted in the experimental design and execution of Figure 4.1C-J, Figure 4.2, Figure 4.6, Figure 4.7 and Table 4.2.

Deanna N. Parke

- Assisted in the experimental design and execution of Figure 4.1C-J, Figure 4.2, Figure 4.6, Figure 4.7 and Table 4.2.

Warner A. Thomas

- Assisted in the experimental design and execution of Figure 4.1C-J, Figure 4.2, Figure 4.6, Figure 4.7 and Table 4.2.

Branden A. Smeester

- Assistance in the creation of models for Figure 4.3F.

Tiffany N. Seagroves

- Conception and assistance in the experimental design studies
- Assistance in the interpretation and analysis of data
- Revision of the publication/manuscript

Carol A. Lange

- Conception and assistance in the experimental design studies
- Assistance in the interpretation and analysis of data
- Revision of the publication/manuscript